UNIVERSITÄTSKLINIKUM HAMBURG-EPPENDORF

I. Medizinische Klinik und Poliklinik und
Institut für Biochemie und Molekulare Zellbiologie

An investigation into the immunometabolic control of brown and white adipose tissue by efferocytic macrophages

Dissertation
zur Erlangung des Doktorgrades PhD an der Medizinischen Fakultät
der Universität Hamburg.

vorgelegt von:
Simon Meyer aus Hamburg

Hamburg 2025

Betreuer:in / Gutachter:in der Dissertation: **Prof. Dr. Jörg Heeren**

Gutachter:in der Dissertation: **Prof. Dr. Nicola Gagliani**

Vorsitz der Prüfungskommission: **Prof. Dr. Jörg Heeren**

Mitglied der Prüfungskommission: **Prof. Dr. Nicola Gagliani**

Mitglied der Prüfungskommission: **Prof. Dr. Hartmut Schlüter**

Datum der mündlichen Prüfung: **29.09.2025**

Table of Contents

1. Introduction

1.1 Efferocytosis

1.1.1 From smelling to digestion

Tissue homeostasis and the resolution of inflammation critically depend on the timely and efficient clearance of apoptotic cells -a process known as *efferocytosis* [1], [2]. At the center of this vital function are macrophages, professional phagocytes. Macrophages can detect, engulf, and degrade apoptotic cells in a manner that is generally immunologically silent or even actively anti-inflammatory [3]. Unlike classical phagocytosis, which usually refers to the clearance of pathogens and often involves inflammatory signaling, efferocytosis requires a tightly regulated multi-step process that facilitates efficient uptake and prevents the release of intracellular contents from dying cells, which could otherwise drive inflammation or autoimmunity [4], [5].

Apoptotic cells are characterized by a series of well-defined morphological and biochemical changes, including cell shrinkage, chromatin condensation, membrane blebbing, and the externalization of phosphatidylserine on the outer leaflet of the plasma membrane [6], [7]. These features distinguish apoptotic cells from healthy cells or cells undergoing other types of cell death such as necrosis or proptosis and serve as essential cues for their recognition and removal by phagocytes [8], [9]. Notably, the process by which apoptotic cells are recognized and cleared can vary depending on the cell type undergoing apoptosis, the stimulus triggering cell death, and the tissue environment [10]. However, there are also many conserved features.

The process of efferocytosis usually begins with the so-called “smell phase”. During apoptosis, cells can release soluble molecules which include metabolites [11], nucleotides [12], [13], lipids [14], [15], and chemokines [16]. These molecules are often referred to as “find-me” signals and can attract phagocytes as well as prepare them for engulfment. This can happen through modulation of the cytoskeleton or the digestion machinery within the phagocyte, but also by altering the expression of receptors involved in the recognition of apoptotic cells [17], [18], [19]. One prominent example of a find me signal is CX3CL1/fractalkine. During apoptosis CX3CL1, is released rapidly from apoptotic lymphocytes, via caspase- and *Bcl-2*-regulated mechanisms to attract macrophages. Effective chemotaxis of macrophages to apoptotic lymphocytes is thereby critically dependent on macrophage fractalkine receptor, CX3CR1 [16].

The next step in efferocytosis is the recognition phase which determines whether apoptotic cells will be efficiently cleared or left to undergo secondary necrosis [10]. Phosphatidylserine on the outer leaflet of the apoptotic cell membrane serves as a universal “eat-me” signal and is sensed by a diverse set of receptors on macrophages referred to as efferocytosis receptors. These receptors

can either bind directly to phosphatidylserine (e.g TIM4 or stabilin-2) [20], [21] or indirectly via soluble bridging molecules. Key examples of these phosphatidylserine bridging molecules are GAS6 (Growth arrest-specific 6) and Protein S, which simultaneously bind to phosphatidylserine and to members of the TAM family of receptor kinases [22]. TYRO3, AXL, and MERTK are the name giving members of this family, from which MERTK is widely expressed in tissue-resident macrophages and was shown to be essential in the recognition and uptake of apoptotic cells in both homeostatic and inflammatory settings [23], [24].

In the case of the TAM receptors, it is well understood that ligand binding induces dimerization and autophosphorylation, triggering downstream signaling pathways such as PI3K/Akt signaling and RAC1 activation [22]. RAC1 in particular is then able to mediate cytoskeletal dynamics necessary for the next step of efferocytosis, apoptotic cell engulfment [25]. During apoptotic cell engulfment, rapid polymerization of F-actin at the contact site between the macrophage and the apoptotic cell (synapse) drives the extension of the phagocytic cup around the target. Once the apoptotic cell is fully engulfed, the macrophage membrane seals off the apoptotic cell body to form a phagosome or efferosome [26].

The last step of efferocytosis is the digestion phase. Here the efferosome undergoes a maturation process involving sequential fusion with intracellular organelles: First the GTPase RAB5 is recruited to efferosomes and remains bound following the release from the plasma membrane. Then RAB5 mediates the fusion of the efferosome with early endosomes, starting the acidification of the efferosome. Shortly after this, RAB5 is exchanged for RAB7, with RAB7 then mediating the fusion of late endosomes and lysosomes to the efferosome [27], [28]. Moreover. through effectors such as RILP and ORPL1, active RAB7 also coordinates the movement of lysosomes along microtubules and mediates their fusion with the efferosome [29], [30], [31]. This generates a highly hydrolytic environment that activates lysosomal proteases to degrade the apoptotic cell [26]. Also unlike phagocytosis, the efferosome maturation pathway also involves RAB17, which directs the degraded contents from the efferosome away from antigen presenting pathways [32].

Importantly, changes in inflammatory conditions, tissue injury or other stressors can influence the process of macrophage efferocytosis as well as macrophage efferocytosis receptor expression to better suit the altered environment and functional demand. For example, IFN-γ and tumor necrosis factor-alpha (TNF-α) have been shown to downregulate MERTK expression while IL10 can help to upregulate MERTK through STAT3 signaling [33], [34]. AXL, on the other hand is often upregulated specifically in response to inflammatory stimuli such as type I interferons or LPS [33], [35]. The expression of efferocytosis receptors on macrophages is also strongly impacted by efferocytosis itself, yet this will be discussed in **1.1.2.**

Of note, many of the key findings discussed in this paragraph were made in mice and not humans. Although the consensus in the field is that the efferocytosis machinery appears to be largely conserved between humans and mice there are several notable differences. These include for example differential effects of aging on *Tim4* and *Mertk* expression and the lesser role of adenosine and inosine sensing in human macrophages [36].

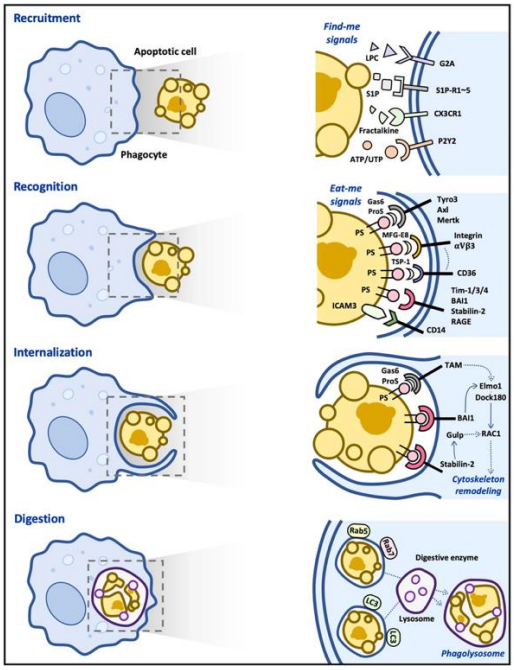

Figure 1: Molecular basis of efferocytosis from Moon et al 2023 *[37].*

1.1.2 Downstream consequences of efferocytosis

Engagement of efferocytosis receptors already leads to downstream signaling within macrophages, modulating their inflammatory response. Crucially, upon recognition of apoptotic cells both AXL and MERTK can directly suppress the production of pro-inflammatory cytokines such as TNF-α and interleukin-1β (IL1β) by inhibiting NF-κB signaling [38], [39]. In addition, fusion of the phagosome with the lysosomes leads to the controlled release of a diverse set of molecules into the cytosol of macrophages. Increased lipid substrate abundance following efferocytosis for example has been shown to increase oxidative phosphorylation within the macrophages leading to an increase in the NAD^+/NADH ratio. This triggers the sirtuin family protein, SIRT1, ultimately helping in the induction of IL10 release post efferocytosis [40]. Following the degradation of the apoptotic cell, the concentration of cholesterol within macrophages sharply rises as well [41]. Accumulation of cholesterol esters as lipid droplets in the ER of "foamy" macrophages is thereby implicated in the progression of atherosclerosis and is thought to be driven by efferocytosis of other macrophages within the atherosclerotic lesions [42], [43]. One of the major mechanisms on how cholesterol accumulation in phagocytes is prevented is the rapid upregulation of *Abca1* which facilitates export of cytosolic cholesterol towards lipid-poor apolipoprotein A1 to form HDL [44]. Surprisingly, early induction of *Abca1* during efferocytosis does not require the canonical LXR-mediated pathway but is mediated by a BAI1-ELMO1-Dock180-Rac1 signaling module [41]. Nonetheless, *Abca1* regulation by LXR might be relevant after prolonged exposure of apoptotic cells [3].

Possibly the most important switch by which macrophage efferocytosis impacts macrophage biology is nuclear receptor signaling. Nuclear receptors are a superfamily of ligand-activated transcription factors that sense lipid metabolites and induce gene expression responses. Several nuclear receptors are now known to be activated during efferocytosis, including liver X receptors (LXRα/β), peroxisome proliferator-activated receptors (PPARγ, PPARδ, and to a lesser extent PPARα), retinoid X receptors (RXRs), glucocorticoid receptor (GR), and the nuclear receptor subfamily 4 group A (NR4A1) [45], [46], [47], [48], [49]. PPARγ and PPARδ for example can be activated by fatty acid derivatives that can enter the phagocyte through efferocytosis, regulating the transcription of genes involved in lipid metabolism, mitochondrial function, cytokine production and apoptotic cell recognition [50]. Similarly, oxysterols derived from the breakdown of the apoptotic cell membrane have been shown to cause the activation of liver-X receptors (LXRs) α/β, which strongly induce the expression of *Abca1* and *Mertk* forming a positive feedback loop for efferocytosis [45], [51]. The importance of nuclear receptor signaling for efferocytosis is further highlighted by the fact that mice, defective in either LXR and PPARγ signaling, show severe impairments in their ability to efficiently perform efferocytosis [52], [53].

Importantly many of the described signaling pathways intersect with other signaling pathways such as STAT- or ERK-signaling, to profoundly reshape macrophage biology [54], [55]. After apoptotic cell ingestion, LXR and PPAR signaling can synergize with these pathways to facilitate the polarization

of macrophages towards anti-inflammatory or tissue-remodeling phenotypes [56]. These phenotypes in turn are coupled to the secretion of IL10 and TGFβ therefore actively contributing to a pro-resolving cytokine environment [57], [58].

The exact response of macrophages to apoptotic cells thereby depends on both the type of apoptotic cell, as well as other environmental cues present at the time. For example, efferocytosis of apoptotic neutrophils can induce a tissue remodeling phenotype in macrophages depending upon concomitant sensing of IL4 [59]. In a similar setting, sensing of apoptotic hepatocytes was able to promote a more immunosuppressive, tolerogenic phenotype, while efferocytosis of apoptotic thymocytes only slightly altered the macrophage response to IL4 [59], [60]. While anti-inflammatory and tissue-remodeling phenotypes often overlap, markers such as ARG1, YM1, and RELM-α are closely associated with wound healing functions [61]. RELM-α promotes angiogenesis by enhancing VEGF production [62] and both macrophage ARG1 and YM1 have reported roles in extracellular matrix deposition and reorganization [63], [64].

Nonetheless, terms such as *anti-inflammatory* and *tissue remodeling* macrophages are often used interchangeably, particularly outside the field of macrophage immunology, along with labels like *alternatively activated* or *M2* macrophages, due to changing trends in terminology and overlapping marker gene expression.

Finally, efferocytosis has also been shown to enhance macrophage proliferation to help resolve tissue injury. In particular nucleotides, derived from the hydrolysis of apoptotic cell DNA, activate a DNA-PKcs-mTORC2/Rictor pathway that increases Myc to promote non-inflammatory macrophage proliferation [65]. Of note, non-inflammatory macrophage proliferation thereby stands in contrast to inflammatory macrophage accumulation which usually occurs in settings of acute inflammation or settings where efferocytosis is impaired [10], [66].

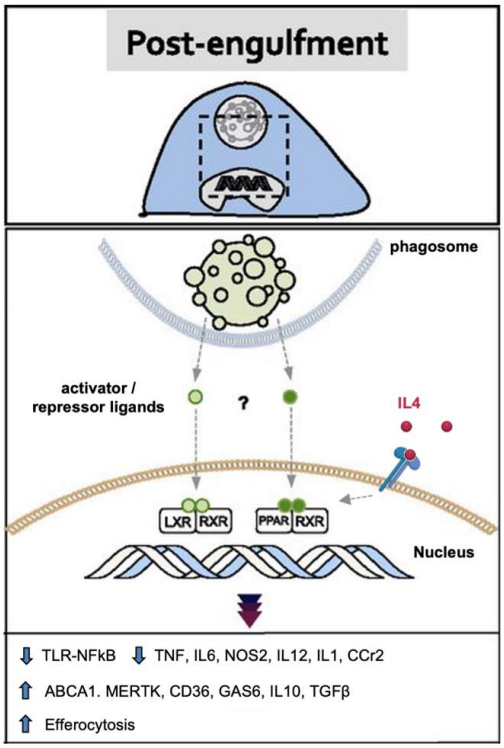

Figure 2: Immunomodulatory roles of efferocytosis signals post engulfment
(adapted from Elliott et al., 2017 [67])

1.1.3 Efferocytosis in the clinic

Dysregulation of efferocytosis is considered causative in numerous pathological conditions including atherosclerosis, systemic lupus erythematosus, multiple sclerosis and diabetes Type 1 and Type 2 [42], [68], [69]. For this reason, serious attempts have been made to target parts of the efferocytosis machinery for therapeutical purposes and current opportunities are actively discussed [19]. Moreover, several therapies targeting efferocytosis are already used in the clinic with many more that either indirectly affect efferocytosis or that have an effect on efferocytosis besides their believed main mechanism of action.

An excellent example of a therapy that harnesses the anti-inflammatory effect of apoptotic cells is 'extracorporeal photopheresis' (ECP) which is widely used to dampen inflammation in systemic lupus erythematosus, arthritis, and in particular during organ or bone marrow transplantation [70]. During ECP, the leukocytes from a patient are removed, treated with UVA light to induce cell death (possibly along with other medication), and then reintroduced into the patient. This approach has been highly beneficial in dampening overall inflammation and in improving graft acceptance when the recipient was exposed to donor apoptotic cells [71]. Still, it is unclear how ECP functions in

detail, and data are lacking on what kind of cell death is induced by the treatment and in which population of cells.

Targeting the TAM family of efferocytosis receptors is of particular interest in oncology since the immunosuppressive capacity of these receptors can potentially dampen anti-tumor immunity. Downregulation or blockage of MERTK activity has shown benefits in breast cancer [72], [73], non-small lung cell carcinoma [74], leukemia [75], glioblastoma [76] and also in other cancer settings [77], [78], [79]. In leukemia MERTK dependent efferocytosis has also been shown to affect the expression of inhibitory immune checkpoint molecules such as PD-L1 [80]. On the other hand, in an inflammation-driven tumorigenesis model, blocking efferocytosis by *Axl* and *Mertk* deletion has been linked to the progression of intestinal adenoma [81]. Given this, combining efferocytosis-targeted therapies with conventional treatments such as chemotherapy but also immune checkpoint inhibition may in the future enhance therapeutic efficacy.

A number of clinically used molecules have been reported to directly or indirectly affect efferocytic capacity. For instance, PPARγ agonist pioglitazone, commonly used in the treatment of diabetes type 2, enhanced the clearance of apoptotic neutrophils, and normalized the course of peritonitis in a mouse model of chronic granulomatous disease [82]. It is therefore unclear to what extent effects on efferocytosis contribute to any of the clinical benefits mediated by these compounds. Pro-resolving lipid mediators such as resolvins, protectins, and maresins -derived from omega-3 fatty acids- have also demonstrated potent capacity to stimulate efferocytosis and accelerate resolution of inflammation in preclinical models. These agents are being explored as adjuncts to standard therapies in chronic inflammatory diseases and tissue injury [83].

One of the most commonly used medications known to directly affect the expression of efferocytosis receptors are Glucocorticoids. Glucocorticoids are widely used anti-inflammatory agents and can upregulate *Mertk* expression in myeloid cells through engagement of the glucocorticoid receptor [49]. Glucocorticoids possibly mimic signaling that would physiologically occur upon efferocytosis, utilizing the feedforward nature of the process. However, the contribution of efferocytosis regulation to the clinically relevant effects of glucocorticoids is poorly understood.

Another extremely popular class of drugs with off-target effects on efferocytosis are statins. Commonly used for hypercholesterolemia, statins have been shown to promote a pro-resolving macrophage phenotype and improve efferocytic function through modulation of the RhoA-ROCK signaling pathway, shifting the balance between Rac-1 and RhoA [84], [85], [86]. This effect has been shown to contribute to plaque stabilization in atherosclerosis [87].

Since cholesterol accumulation within macrophages is part of the pathology in atherosclerosis [42], strategies targeting LXR signaling within macrophages have also been tried. Besides their effect on cholesterol efflux, these approaches could hold great promise also in treating many other diseases that could benefit from higher MERTK expression and greater efferocytosis capacity. Indeed, multiple studies in murine models have demonstrated that treatment with synthetic LXR agonists, such as GW3965 and T0901317 can significantly inhibit the development and progression of atherosclerotic lesions [88], [89] and GW3965 has been directly shown to enhance efferocytosis [53]. However, targeting these multifunctional nuclear receptors has suffered from the same challenges as many other strategies targeting efferocytosis, significantly slowing clinical translation. Challenges include the complexity of the involved pathways, substantial off target and side effects and balancing macrophage function to ensure also sufficient anti-cancer and anti-infection effects [90]. Therefore, therapies that selectively enhance efferocytosis in a controlled manner are needed. In addition, therapeutic intervention could benefit from effective delivery strategies that selectively target macrophages while minimizing systemic exposure to non-target tissues. Identifying novel pathways involved in the regulation of macrophage efferocytosis could also provide novel targets to enhance the efficacy and safety of future therapies.

1.2 Adipose tissue

1.2.1 Adipose tissue biology

Adipose tissue is an extraordinarily flexible and heterogeneous organ that regulates many aspects of whole-body physiology. Adipose tissue is defined by the presence of specialized lipid handling cells called adipocytes, which function as the body's primary energy reservoir, but can also act as endocrine cells or a source of heat [91]. Physiologic stimuli can induce dramatic alterations in adipose tissue metabolism, structure, and phenotype and limitations to this plasticity can cause diminished or aberrant responses and drive the progression of cardiometabolic disease along with other pathological consequences of obesity [92]. Classically, adipose tissue is thereby categorized into white adipose tissue (WAT) and brown adipose tissue (BAT), each with distinct physiological roles and properties [93], [94].

WAT is the primary organ for energy storage in both mice and humans, storing energy in the form of triglycerides (TAGs) within adipocyte lipid droplets [93]. Major WAT depots in humans are located subcutaneously and viscerally, with visceral fat residing in the abdominal cavity around internal organs [95]. Similarly, in mice, subcutaneous fat is located in the inguinal region (inguinal WAT, ingWAT) near the hind limbs, and visceral fat is found near the gonads (gonadal WAT, gWAT) [96]. There are notable sex differences in fat distribution in humans; females are more likely to accumulate subcutaneous fat, while males tend to store more visceral fat [97]. Estrogen plays a key role in mediating these differences [98]. In mice, fat accumulation is also sex- and strain-dependent. For example, in the commonly used C57BL/6 mouse strain, female mice tend to gain less fat mass compared to males, even under high-calorie diets, and often do not reach the levels of adiposity necessary to model certain pathologies [99]. The same is true for many mice of other genetic backgrounds [100], [101], [102]. Consequently, male mice of the C57BL/6 genetic backgrounds are often preferred in metabolic studies, perpetuating a gender bias and a strain bias in metabolic science [103]. Moreover, distinct adipose depots differ in their associations with health outcomes. Subcutaneous fat is generally linked with higher insulin sensitivity, while visceral fat is associated with insulin resistance and increased secretion of pro-inflammatory cytokines such as interleukin-6 (IL6) and TNF-α [104], [105], [106], [107].

In contrast to WAT, BAT specializes in energy expenditure through non-shivering thermogenesis (NST), a process that dissipates energy from nutrients as heat. This thermogenic function is mainly mediated by the uncoupling protein 1 (UCP1), a protein almost exclusively expressed in BAT [94]. Within mitochondria-rich brown adipocytes, UCP1 is located in the inner mitochondrial membrane and increases its conductance by effectively operating as an H^+ carrier activated by long chain fatty acids. This leads to BAT mitochondria generating heat rather than ATP during thermogenic activation [108]. This process is so efficient in generating heat that BAT thermogenesis can increase systemic

energy expenditure by a significant fraction which can be captured by methods such as indirect calorimetry [109].

In mice, the largest and most studied BAT depot is the interscapular BAT (iBAT), located in the dorsal back between the shoulder blades. Other BAT depots in mice include subscapular BAT, deep cervical BAT (deep in the dorsal neck between the scapula and the head), mediastinal BAT (around the aorta within the thoracic cavity), and perirenal BAT. Recent studies have also identified novel BAT depots in the pelvic and lower abdominal regions of mice [110]. As heat loss is also a function of the surface-to-volume ratio, small organisms like mice tend to have more active and more pronounced BAT depots [94]. Corresponding to this notion, human infants possess significantly more BAT compared to adults. In neonates, BAT constitutes about 5% of body mass and is primarily located in regions such as the interscapular area, neck, axillae, and around major blood vessels [111]. Nonetheless, around the year 2009 four groups independently reported that active BAT was present in adults and could be activated via cold exposure [112], [113], [114], [115]. Indeed, moderate cold stimulation is sufficient to augment glucose uptake into BAT in humans, accompanied by enhanced fatty acid oxidation and increased energy expenditure [116], [117], [118]. Uptake of glucose tracers such as (18)F-fluorodeoxyglucose as measured by positron-emission tomography is thereby currently considered the gold standard for measuring BAT activity in humans and has helped to identify human BAT-depots, especially in the supraclavicular and paravertebral areas [119]. Importantly, increased BAT mass has been correlated with improved health outcomes in humans, such as lower blood glucose and triglyceride levels, as well as a lower prevalence of type 2 diabetes [112], [114], [115], [117], [120], [121], [122], [123]. These findings have spurred further research into the field of human brown fat, with a particular focus on increasing energy expenditure by enhancing NST.

Beyond the typical classification of white and brown adipose tissue, a continuum of intermediate adipocyte phenotypes exists [91]. Prolonged energy surplus [124], exposure to warm environmental temperatures, and aging [125] are known to induce "whitening" of brown adipose tissue, a process characterized by a more white-like phenotype in brown adipocytes [126]. Conversely, under certain physiological or pharmacological stimuli - such as chronic cold exposure or β-adrenergic stimulation - WAT has shown the potential to undergo "browning", giving rise to beige (or "brite") adipocytes. These beige adipocytes display many of the metabolic benefits of brown adipocytes, including the expression of UCP1 and therefore the ability to perform NST [127], [128], [129]. The discovery that beige adipocytes can emerge within WAT depots in adult humans has garnered considerable attention, particularly given that humans typically possess a much larger volume of white fat relative to classical BAT [127], [130].

In general BAT in adult humans, even within classical depots, exhibits certain morphological features that are more similar to WAT than to murine BAT [131]. This discrepancy is thought to

result from chronic overnutrition and reduced thermogenic demand due to the thermally regulated environments typical of modern human lifestyles [132]. Consequently, caution must be exercised when extrapolating findings from murine classical BAT to human BAT. One strategy to mitigate this translational gap involves prolonged exposure of mice to thermoneutrality (TN; ~30°C for mice) and high-fat diets (HFDs). This has been shown to produce a more human-like BAT phenotype in mice and has therefore been termed the "humanization" of murine adipose tissue [131] . Nonetheless, despite notable differences between brown-like (beige) and white adipocytes, several key regulatory pathways, governing fundamental adipocyte functions, are highly conserved across these cell types and between species such as humans and mice. This conservation is particularly evident in the mechanisms controlling energy storage and lipolysis, as well as in the principal signaling pathways that activate NST [91], [127].

1.2.2 Regulation of energy storage and release in adipose tissue

During periods of energy surplus, such as the postprandial state, elevated levels of glucose and lipids - primarily in the form of circulating lipoproteins like chylomicrons - are present in the bloodstream [133]. High levels of glucose thereby stimulate insulin secretion from pancreatic β-cells, which is sensed by peripheral tissues, including adipose tissue [134], [135]. In response to increased insulin, adipocytes but also skeletal muscle enhance glucose uptake, primarily through the insulin-stimulated translocation of the glucose transporter GLUT4 to the plasma membrane [136]. Once inside adipocytes, glucose is converted to glycerol-3-phosphate, serving as a backbone for triacylglycerol (TAG) synthesis in a process termed de novo lipogenesis (DNL) [137]. In WAT, DNL is primarily stimulated by insulin and carbohydrate intake and is largely mediated by carbohydrate response element-binding protein (ChREBP), which transcriptionally upregulates key lipogenic enzymes such as acetyl-CoA carboxylase (ACC) and fatty acid synthase (FASN) [138]. Interestingly, ChREBP dependent DNL has been shown to be critical for whitening of BAT in response to thermoneutrality [139], but DNL has also been shown to occur during cold exposure, potentially providing fatty acids as fuel for BAT thermogenesis [140], [141], [142].

Concurrently, insulin suppresses the breakdown of stored TAGs and modulates the activity of lipoprotein lipase, an enzyme critical for hydrolyzing fatty acids from circulating lipoproteins [143]. In response to high blood glucose, insulin is released and leads to the localization of lipoprotein lipase to the luminal side of capillary endothelial cells. There it is anchored by the protein GPIHBP1 which facilitates its action [143], [144], [145], [146]. Interestingly short-term cold exposure or acute β3-adrenergic receptor (β3AR) stimulation can also result in secretion of insulin as a response to higher levels of circulating non-esterified fatty acids (NEFAs). Subsequent sensing of insulin by brown adipocytes and corresponding lipid uptake was shown to be critical for BAT for thermogenesis [147].

In addition to the control via insulin signaling, LPL expression and activity in BAT is also strongly modulated by cold exposure enabling rapid uptake of lipids from the circulation into BAT [144]. The precise mechanism of how exactly liberated fatty acids cross the endothelial barrier in blood vessels and then find their way into adipocytes is thereby not entirely understood. What is understood, is that the fatty acid translocase CD36 is crucial for this process, and emerging evidence highlights a key role for endothelial cells, particularly during cold exposure [148]. Similar to GLUT4, CD36 translocation to the plasma membrane is insulin-responsive and CD36 is transcriptionally regulated by cold exposure and PPARγ [148], [149], [150]. Of note, CD36 is also known to be highly expressed in macrophages in a PPARγ dependent manner and is implicated in efferocytosis via its function as a scavenger receptor [151], [152].

Lipolysis acts as a functional counterbalance to lipogenesis and energy storage and involves the breakdown of TAGs stored in adipocyte lipid droplets into free fatty acids (FFAs) and glycerol. This process primarily occurs under conditions of low to moderate insulin levels, such as fasting to provide energy during periods of negative energy balance [153]. Lipolysis has also been shown to occur upon cold exposure and is essential for BAT thermogenesis by activating UCP1 and by providing fuel for fatty acid oxidation [94], [108]. Cold exposure therefore provides a setting where DNL, lipid uptake as well as lipolysis are induced simultaneously, proving that these processes are not necessarily mutually exclusive.

The key regulatory mechanism of lipolysis in both white and brown adipocytes is adrenergic stimulation via the sympathetic nervous system (SNS), particularly through the release of norepinephrine (NE). Upon conditions such as a negative energy balance or cold exposure, SNS activity increases selectively within adipose tissue, prompting the local release of NE from sympathetic nerve terminals into the adipose microenvironment [153]. Among the 3 β-adrenergic receptor (β-AR) subtypes, the β3-AR is the predominant receptor expressed in murine brown and white adipocytes and was shown to be essential in regulating lipolysis and thermogenesis [154]. In contrast, in humans, both the β1-AR and the β2-AR have been proposed to regulate human lipolysis and thermogenesis [155], [156] and there is controversy whether there is a significant physiological role for the β3-AR in human adipocytes. However, recent studies have shown that β3-AR does play a functional role in human brown/beige adipocytes [157] and new β3 selective agonists have been shown to have effects in humans [129].

Binding of NE to G protein-coupled adrenergic receptors activates adenylyl cyclases, while prolonged or repeated stimulation can lead to internalization of these receptors [158]. Crucially, adenylyl cyclase activation will lead to elevated intracellular cyclic AMP (cAMP) levels. This increase in cAMP activates protein kinase A (PKA), a central mediator of lipolytic signaling [153]. PKA then phosphorylates multiple downstream effectors, including hormone-sensitive lipase (HSL) and perilipin-1, a lipid droplet-associated protein [159], [160]. PKA-mediated phosphorylation of perilipin induces conformational changes that allow active lipases such as phosphorylated HSL

(pHSL) to access the lipid core and simultaneously releases comparative gene identification-58 (CGI-58) [161]. CGI-58 is a coactivator of adipose triglyceride lipase, which catalyzes the first and rate-limiting step in TAG hydrolysis, producing diacylglycerols (DAGs) and FFAs [162]. In the next step HSL then catalyzes the conversion of DAGs to monoacylglycerols (MAGs), releasing additional FFAs [159]. In mice, PKA enhances HSL activity through phosphorylation at serine residues Ser563 and Ser660 [163] but also several additional pathways have been shown to modulate HSL activity. Of note, AMP-activated protein kinase signaling has been demonstrated to inhibit HSL activity through phosphorylation at Ser565 [164]. The ratio of pHSL at Ser563 or Ser660 to total HSL is frequently used as a biochemical readout for lipolytic activity due to the availability of site-specific antibodies and the direct connection of phosphorylation at these sites to β-adrenergic signaling [163], [165]. The final step of lipolysis is catalyzed by monoacylglycerol lipase (MGL), which hydrolyzes MAGs into glycerol and FFAs, completing the TAG catabolic pathway [166].

Importantly, despite species-specific differences in adrenergic receptor expression, these lipolytic mechanisms are widely assumed to be conserved across species with most rodent HSL phosphorylation sites having known human analogs [167].

In the past, attempts have been made to clinically enhance lipolysis in adipose tissue with the goal of developing therapeutic interventions for obesity and related metabolic diseases. Still, despite some promising results in preclinical models, clinical applications remain under investigation due to concerns about adverse effects such as inducing tachycardia, insulin resistance or other cardiometabolic events [168], [169], [170], [171]. A major challenge thereby remains the less favorable adrenergic receptor profile in human adipose tissue compared to that of mice [172]. For this reason, pathways evading adrenergic receptors are under intense investigation to possibly achieve more adipose tissue specific effects in humans. Still, inducing the release of fatty acids into the bloodstream without increasing energy expenditure might carry additional risks. This highlights the potential of approaches that simultaneously increase lipolysis and energy expenditure, through for example induction of NST.

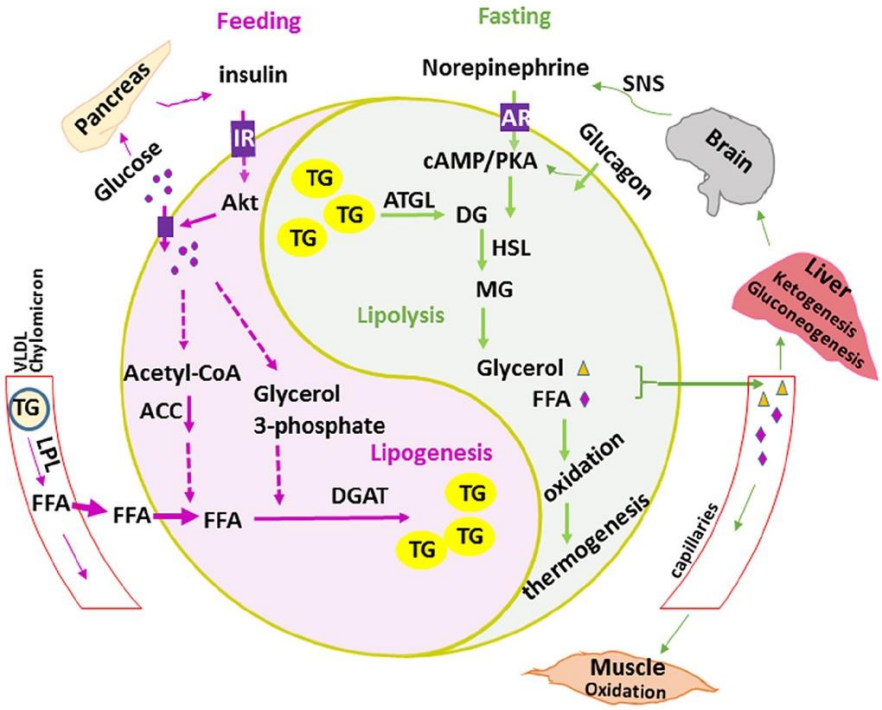

Figure 3: Lipid metabolism and mobilization in adipose tissue after Luo and Liu, 2016 [173].
AR, adrenergic receptor; cAMP, cyclic adenosine monophosphate; IR, insulin receptor; PKA, protein kinase A.

1.2.3 Regulation of non-shivering thermogenesis and thermogenic differentiation

Activation of NST in adipocytes shares several regulatory mechanisms with lipolysis. However, these pathways are differentially activated across adipose tissue depots. In mice, BAT and inguinal white adipose tissue can induce both lipolysis and thermogenic gene expression, whereas gonadal/visceral white adipocytes, despite arguably being more sensitive to lipolytic stimuli [174], are very resistant to browning and UCP1 expression [175]. Interestingly, in humans, some reports describe an opposing pattern, with visceral fat expressing higher levels of thermogenic marker genes [176]. This heterogeneity between adipocytes is attributed to, among other things, differences in sympathetic innervation and to adipocyte lineage effects [177], [178], [179], [180]. Like lipolysis, NST is predominantly regulated by SNS signaling [94]. Cold exposure activates sensory neurons, prompting the release of NE from sympathetic nerve terminals within adipose depots. NE then binds to β-adrenergic receptors, activating adenylyl cyclase and increasing cyclic AMP levels, which in turn activates PKA. As a consequence, PKA not only phosphorylates proteins that facilitate lipolysis but also modulates thermogenic gene transcription [94].

A key event for NST induction is PKA-mediated phosphorylation of cAMP response element-binding protein (CREB), which can bind to the promotor region of UCP1 to enhance its expression [181].

Furthermore CREB can also bind to the promotor of *Ppargc1a*, (encoding PGC-1α), a described master regulator of mitochondrial biogenesis and UCP1, to also enhance its expression [182]. In addition, PKA activates p38 MAPK, which further induces PGC1α transcription via ATF2 and directly phosphorylates PGC1α, increasing its stability and coactivator activity [183]. The combined action of CREB, ATF2, and PGC1*α* will lead to an increase in UCP1 expression and to an increase in mitochondrial biogenesis. Moreover, PGC-1α will also interact with other transcription factors such as PPARγ and PRDM16 to further enhance UCP1 transcription [184]. Of note, lipolysis also assists in NST by providing fatty acids not only as fuel but also as ligands for PPARγ and UCP1 activation [94], [185]. In addition to these adipocyte intrinsic pathways, thyroid hormone has also been shown to increase UCP1 levels. Sympathetic stimulation strongly increases deiodinase type 2 (*Dio2*) expression in brown adipocytes, leading to higher local T3 availability, amplifying UCP1 transcription through thyroid hormone receptor β [186], [187].

Although these pathways play a dominant role in both brown and beige adipocytes, there are also key differences in NST regulation between brown and beige adipocytes. Constitutively active, lineage-specific enhancer activity allows brown adipocytes to maintain constantly high levels of thermogenic protein expression such as UCP1 as well as high mitochondria content. In contrast, beige adipocytes require continuous stimulation, such as chronic NE exposure, to maintain thermogenic competence [188]. Additionally, besides the pathways described above, there are also many other signaling events that can regulate NST in adipocytes, varying in importance between BAT and WAT. Finally, there are also UCP1 independent thermogenic pathways, most notable futile cycles, whose relative importance appears to be especially large in beige fat, particularly in UCP1-negative beige adipocytes [189].

Both brown and beige adipocytes hold significant therapeutic potential due to their capacity to burn excess energy and secrete beneficial signaling molecules. However, as with efforts to induce lipolysis, previous research has largely focused on β3-adrenergic receptor agonists and PPARγ agonists, which have yielded unsatisfactory clinical results [190]. Nonetheless, the relative complexity in the regulation of NST may offer advantages by presenting a wider array of targets that allow for greater specificity and potentially fewer side effects.

Also in recent years, there has been growing interest in the crosstalk between adipocytes and other cell types within - and beyond - the adipose tissue. In particular, endothelial and immune cells have shown promising potential in regulating and enhancing the thermogenic activity of brown and beige fat [148], [191]. Furthermore, in order to sustain thermogenic activity, extensive tissue remodeling needs to occur in adipose tissue which inevitably involves other cell types. These remodeling processes include changes in extracellular matrix deposition [192], [193], [194], angiogenesis [195] and sympathetic innervation [196]. Macrophages in particular have a reported role in all of these processes. Moreover the substantial metabolic stress induced by an increased thermogenic

activity and remodeling could potentially cause an inflammatory response, if not properly controlled by macrophages [192].

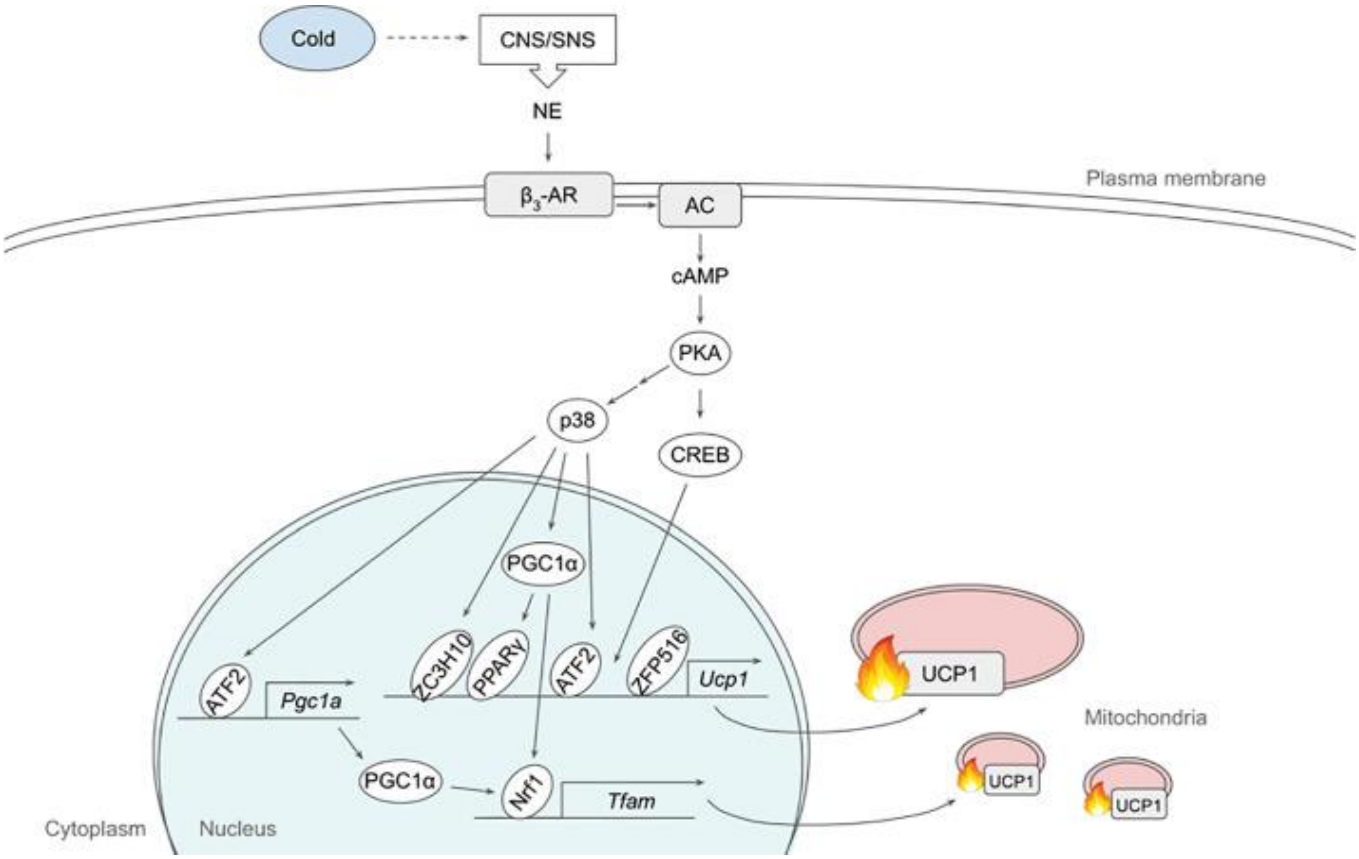

Figure 4: Schematic model of β3-adrenergic signaling pathway that promotes thermogenesis in adipocytes after Tabuchi and Sul, 2021. *[197].* β3-AR, β3-adrenergic receptor; CNS, central nervous system; CREB, cAMP response-element binding protein; ETC, electron transport chain; FFA, free fatty acid; IRF4, interferon regulatory factor 4; NE, norepinephrine; NRF1, nuclear respiratory factor 1; PGC1α, peroxisome proliferator activated receptor γ coactivator α; PKA, protein kinase A; PPARγ, peroxisome proliferator activated receptor γ; SNS sympathetic nervous system; TCA, tricarboxylic acid; TFAM, mitochondrial transcription factor A; UCP1, uncoupling protein 1; ZC3H10, zinc finger CCCH-type containing 10; ZFP516, zinc finger protein 516

1.2.4 Macrophages in adipose tissue dysfunction, remodeling and activation

Immune cells play a pivotal role in regulating adipose tissue physiology, with adipose tissue macrophages (ATMs) constituting the most abundant immune cell population in both lean and obese states [198]. Residing primarily within the stromal vascular fraction, ATMs adapt dynamically to local metabolic and immunological cues [199]. ATMs have been shown to play a dual role in

human health: while essential for tissue homeostasis and remodeling under physiological conditions, they can also drive chronic inflammation and tissue dysfunction when dysregulated [199]. In lean individuals, adipose tissue is thought to be populated predominantly by anti-inflammatory macrophages, which release cytokines, such as TGFβ and IL10 and contribute to extracellular matrix remodeling and maintenance of insulin sensitivity [199], [200], [201], [202]. However, in the context of chronic caloric excess and adipose tissue expansion, there is a profound phenotypic shift towards classically activated, pro-inflammatory macrophages [203]. These cells are recruited from circulating monocytes and accumulate around necrotic adipocytes to form crown-like structures, a hallmark of inflamed adipose tissue [204]. Pro-inflammatory ATMs have been shown to release TNF-α, IL6, and IL1β, which perpetuate local inflammation and can disrupt insulin signaling pathways [203], [204], [205], [206], [207], [208]. The persistence of these crown-like structures has been suggested to be due to the failure of macrophages to efficiently clear dying adipocytes, possibly due to a diminished capacity for efferocytosis. The accumulation of cellular debris and necrotic adipocytes is then thought to sustain and amplify local inflammation [203], [204]. Fitting this narrative, pro-inflammatory macrophages have been shown to be significantly impaired in their efferocytosis capacity in various settings [209], [210]. As such, therapeutic strategies aimed at restoring ATM efferocytosis may offer novel avenues for improving adipose tissue health and treating metabolic diseases such as type 2 diabetes (see also **1.1.3**).

Emerging evidence indicates that macrophage phenotypes in adipose tissue are also more nuanced than the traditional pro- vs anti-inflammatory dichotomy, comprising a spectrum of complex activation states. For instance, subsets such as metabolically activated or TREM2^{+} lipid-associated macrophages (LAMs) have been identified in both human and murine models of obesity that can comprise a significant fraction of total macrophages and can also be found in crown-like structures [211], [212]. Obese mice lacking the expression of TREM2 and therefore lacking LAMs, have more classically inflammatory macrophages in adipose tissue and exhibit worsened metabolic outcomes such as increased insulin resistance [211]. The high lipid-handling capacity of LAMs might thereby represent a response to lipids from apoptotic adipocytes, either supporting or compensating the reduced capacity for classical efferocytosis.

This idea is supported by Reinisch and colleagues, who recently showed that the emergence of LAMs in murine visceral adipose tissue in response to an intermittent fasting regiment was critically dependent on the ability of adipocytes to undergo p53 dependent apoptosis [213]. Moreover, their findings highlight that significant cell death can also accompany adipose tissue catabolic activation and shrinkage. Interestingly, increases in CLS were observed only in visceral fat, with minimal LAM recruitment in ingWAT and iBAT [213]. These depot-specific differences underscore the distinct responses of adipose tissue depots to metabolic stress and suggest that local signals may regulate macrophage capacity for apoptotic cell clearance.

In the BAT, LAM cells have been shown to regulate brown to white fat conversion by scavenging damaged lipids and mitochondria from metabolically overloaded brown adipocytes via CD36 [214]. Also via CD36, BAT macrophages have been shown to scavenge adipocyte-derived extracellular vesicles containing damaged mitochondria, thus contributing to efficient thermogenesis in BAT [215]. Accumulated evidence also shows an association between thermogenic activation of BAT and ingWAT and anti-inflammatory macrophage polarization through for example C-X-C motif chemokine ligand 14 (CXCL14) and meteorin-like signaling [200], [216], [217]. Furthermore, it was shown that IL4 is secreted by eosinophils in iBAT and ingWAT in response to cold exposure, likely contributing to this polarization [218], [219].

Anti-inflammatory macrophages have also been shown to influence tissue innervation through various pathways. A relatively recent study then showed that in subcutaneous WAT during cold exposure, "M2-like" macrophages specifically secrete Slit guidance ligand 3 to enhance the local SNS activation *via* the ROBO1 receptor [220]. Consistent with this positive effect of macrophages on local adrenergic tone, an independent study found that IL25-induced alternative macrophage activation increased outgrowth of sympathetic nerves in subcutaneous WAT [221].

An inhibitory effect of macrophages on SNS in adipose tissue has also been shown by Wolf et. al. in 2017 [222]. Here Plexin A4 overexpression in *Mecp2*-deleted CX3CR1^{+} macrophages resulted in decreased outgrowth of Semaphorin 6A-positive sympathetic axons. Interestingly, *Mecp2*-expressing macrophages were found to be insignificant in coordinating the responsiveness to acute thermogenic stimulation and instead were linked to sustaining sympathetic innervation and adaptive thermogenesis at levels necessary for homeostasis [222]. In 2024 Yadav et al. also showed that MAFB in macrophages regulates cold-induced neuronal density in brown adipose tissue by preventing inflammatory macrophage accumulation [223].

In addition to indirect effects on thermogenesis by influencing SNS activity and remodelling, also direct effects have been reported. A subset of cholinergic adipose macrophages was identified ,that secrete acetylcholine to directly and selectively activate beige fat thermogenesis upon cold exposure. Interestingly, the authors showed that these cholinergic adipose macrophages are regulated via NE, specifically through the β_2 adrenergic receptor [224], [225]. BAT macrophages have also been discussed to support thermogenesis directly by producing NE themselves [226], although this notion has been challenged [227]. Finally, CX3CR1^{+} sympathetic neuron associated macrophages (SAMs) have been shown to scavenge and metabolize NE, thereby controlling energy expenditure [228].

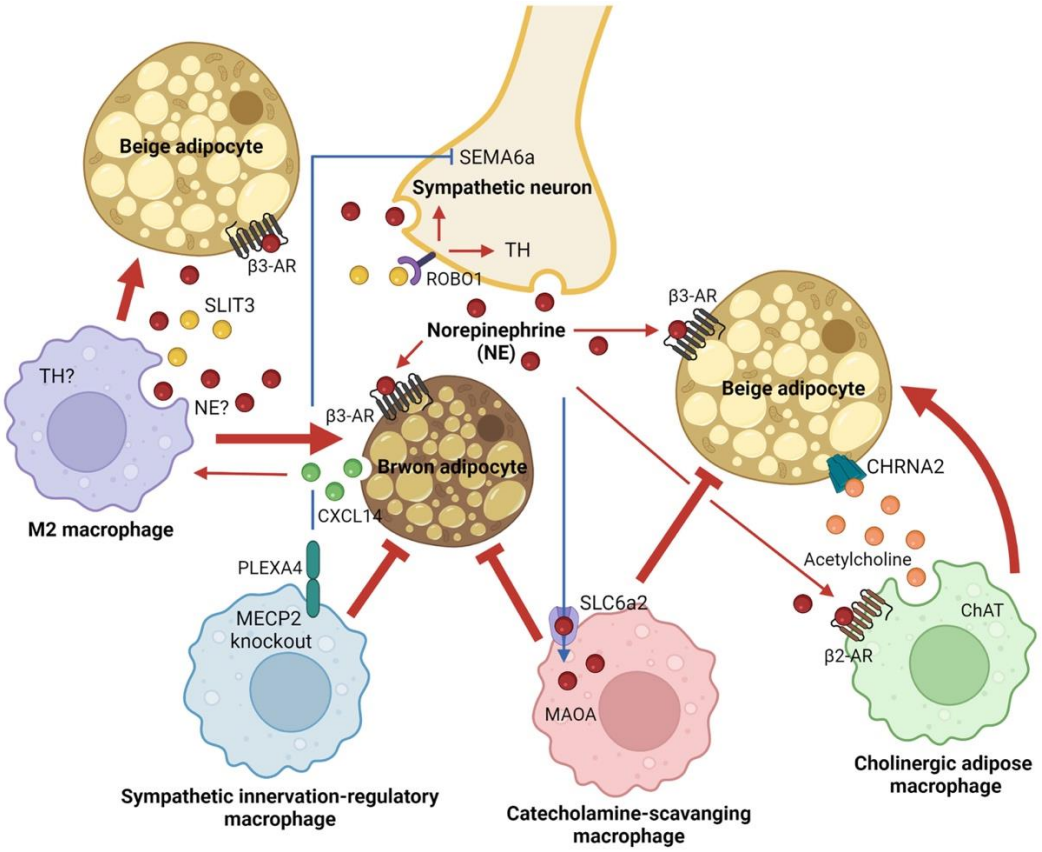

Figure 5: Adipose tissue macrophage-mediated adaptive thermogenesis in brown and beige adipocytes after Rahman and Jun 2022. *[200]. AR, adrenergic receptor; ChAT, choline acetyltransferase; CHRNA2, neuronal acetylcholine receptor subunit alpha 2; CXCL14, C-X-C motif chemokine ligand 14; MAOA, monoamine oxidase A; MECP2, methyl-CpG binding protein 2; NE, norepinephrine; PLEXA4, plexin A4; ROBO1, roundabout guidance receptor 1; SEMA6a, semaphoring 6a; SLC6a2, solute carrier family 6 member 2; SLIT3, slit guidance ligand 3; TH, tyrosine hydroxylase.*

2. Aims of the study

Macrophages have been shown to play a central role in tissue remodeling and resolution of inflammation, largely through their capacity for efferocytosis, which not only removes dying cells but also triggers an anti-inflammatory and tissue remodeling phenotype in macrophages [2], [59], [65].

Cold stress induces extensive structural remodeling in adipose tissue, characterized by increased vascularization [195], enhanced innervation [196] and alterations to the extracellular matrix [192], [193], [194]. Moreover, cold stress is also associated with a profound shift towards an anti-inflammatory polarization in adipose tissue macrophage [192], [229], [230].

Adipose tissue macrophages in particular (ATMs) are recognized as critical mediators of metabolic health and tissue adaptation [191], [208], yet the contribution of efferocytosis to these functions remains incompletely understood.

In this study, we employed cold exposure to trigger intense thermogenic remodeling of adipose tissue, allowing us to investigate the role of macrophage efferocytosis in this adaptive process. We thereby had two distinct aims:

1. Elucidate how macrophage efferocytosis is regulated during thermogenic activation of adipose tissue and identify factors involved in this regulation.

2. Investigate the role of macrophage efferocytosis in brown and white adipose tissue thermogenic remodelling.

Throughout this thesis we put an emphasis on brown adipose tissue as it is the main thermogenic organ in mice responding to cold exposure.

3. Results

3.1 Adrenergic signaling impacts macrophage efferocytosis *in vivo* and *in vitro*

3.1.1 Adipose tissue macrophages from cold exposed mice show increased efferocytic capacity for apoptotic cells

During catabolic activation of adipose tissue and particularly in response to cold exposure, substantial amounts of NE are released locally, initiating lipolysis and/or NST [94] (see also **1.1.2** and **1.1.3**). If the stimulus persists, the adipose tissue undergoes extensive remodeling, which can include changes in vascularization, innervation, extracellular matrix composition as well as recruitment of adipose tissue progenitors and immune cells [92]. These adaptive processes are necessary to sustain novel metabolic requirements and prevent adipose tissue dysfunction [192], [231]. Macrophage-mediated efferocytosis thereby has an established role in tissue remodeling by clearing apoptotic cells, preventing excessive inflammation and expanding the pool of pro-resolving macrophages [2], [65] (see also **1.1.2** and **1.2.2**). To assess whether the efferocytic capacity of ATMs is altered during cold exposure, we developed an ex vivo efferocytosis assay. For this, ATMs from wild-type mice housed either at TN (30°C) or exposed to cold (6°C for 24 h) were isolated by CD11b-based magnetic bead separation and were co-incubated with freshly isolated pre-labeled apoptotic thymocytes for 1.5 hours. The efferocytic capacity of ATMs was quantified by flow cytometry, measuring the percentage of $CD11b^{+}F4/80^{+}$ macrophages positive for the apoptotic cell dye (aT-dye). To account for non-specific binding, each macrophage sample was split into two wells: one incubated with apoptotic thymocytes at 37°C (Uptake) and the other incubated on ice (Binding).

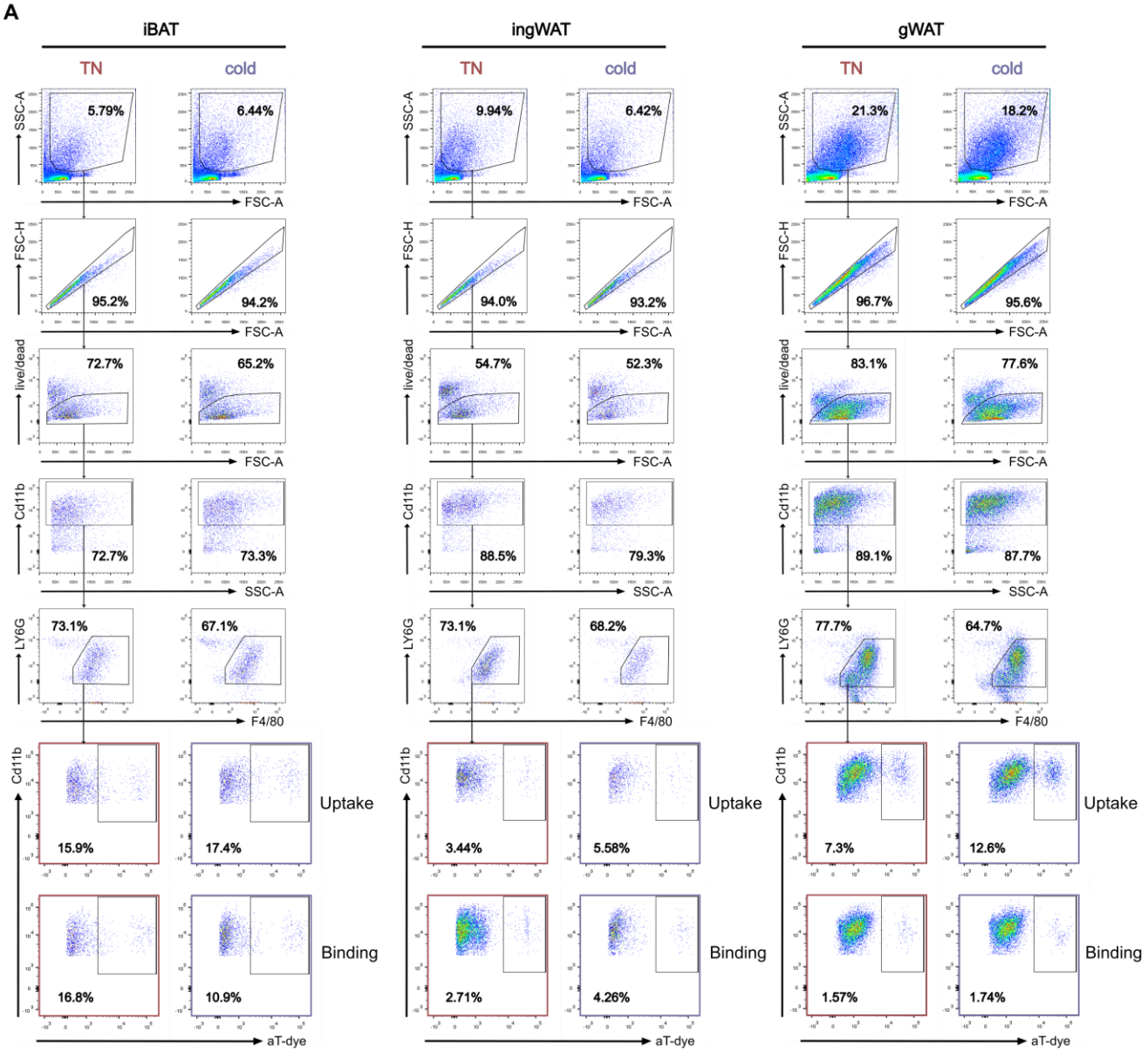
A
iBAT
ingWAT
gWAT
TN
cold
SSC-A
FSC-A
FSC-H
live/dead
Cd11b
LY6G
F4/80
aT-dye
Uptake
Binding
5.79%
6.44%
9.94%
6.42%
21.3%
18.2%
95.2%
94.2%
94.0%
93.2%
96.7%
95.6%
72.7%
65.2%
54.7%
52.3%
83.1%
77.6%
72.7%
73.3%
88.5%
79.3%
89.1%
87.7%
73.1%
67.1%
73.1%
68.2%
77.7%
64.7%
15.9%
17.4%
3.44%
5.58%
7.3%
12.6%
16.8%
10.9%
2.71%
4.26%
1.57%
1.74%

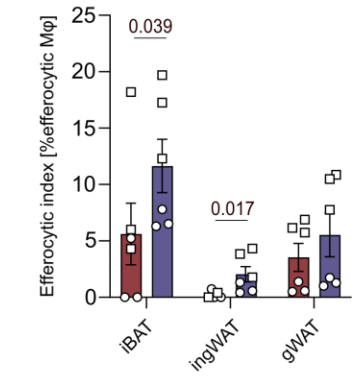
B
Efferocytic index [%efferocytic Mφ]
25
20
15
10
5
0
0.039
0.017
iBAT
ingWAT
gWAT

Figure 6: Cold exposure increases the efferocytosis capacity of brown adipose tissue macrophages. Gating strategy (**A**) and pooled results of 2 independent *ex vivo* efferocytosis assays (**B**), comparing the efferocytosis capacity of $Cd11b^+$ ATMs from mice kept at thermoneutral housing conditions or exposed to cold (6°C) for 24h. Apoptosis enriched thymocytes were incubated with macrophages for 1.5h and efferocytic capacity assessed by flow cytometry. Each dot represents macrophages isolated from a pool of 3 mice and results from the same experiments are indicated by the same symbol (circles vs. squares). n=6. Mean±SEMs; Mann-Whitney tests.

The frequency of $CD11b^+F4/80^+$ iBAT macrophages engulfing pre-labeled apoptotic thymocytes was significantly higher in cold housed mice compared to controls kept at TN. Similarly, the efferocytic capacity of ingWAT macrophages increased under cold conditions, although the overall frequency of efferocytic cells remained low (1–4%). The efferocytic capacity of gWAT macrophages was not significantly changed in cold housed mice. Among all depots, iBAT macrophages exhibited the highest efferocytic activity on average under both TN and cold conditions (**Figure *6*, A and B**). These findings suggest that cold exposure promotes efferocytic capacity in ATMs through an unknown stimulus.

3.1.2 β2 adrenergic stimulation induces efferocytosis of apoptotic cells in BMDMs *in vitro*

To identify if secreted factors from cold-activated adipose tissue may underlie the enhanced efferocytic capacity of ATMs observed in **Figure 6**, we employed an *in vitro* system using bone marrow–derived macrophages (BMDMs) stimulated with conditioned media from NE-pretreated primary murine brown adipocytes. Adipocytes were treated with 1 µM NE for 24 hours, after which the entire supernatant was transferred to the BMDMs for another 24 hours. As outlined in **1.2.3**, NE is a key mediator of thermogenic activation in adipose tissue and NE is widely used to activate primary adipocytes *in vitro*. The effects of conditioned media from untreated (untreated adip.sn) and NE-stimulated adipocytes (NE-cond adip.sn) on BMDM efferocytosis are shown in **Figure 7.**

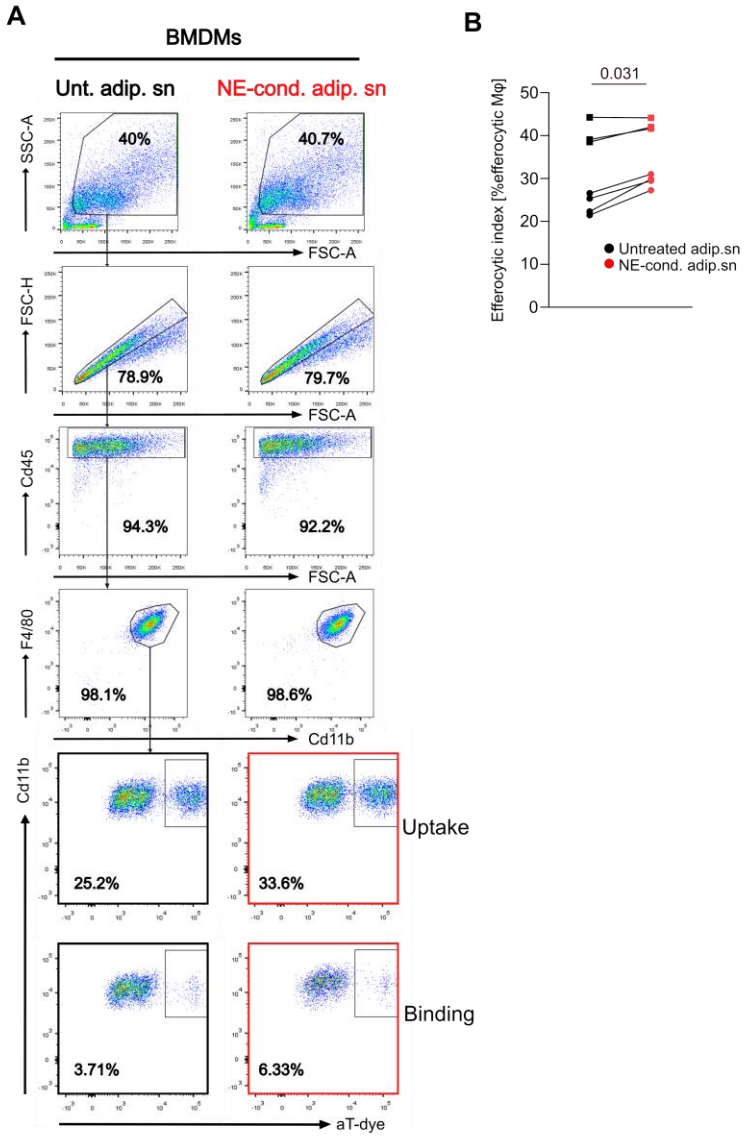

Figure 7: Treatment with NE-conditioned adipocyte supernatant increases the efferocytosis capacity of BMDMs. Gating strategy (**A**) and efferocytosis assay results (**B**) for BMDMs isolated from wild-type mice treated for 24h with supernatant of primary brown adipocytes incubated with or without 1 µM NE for 24h beforehand. Apoptosis enriched thymocytes were incubated with BMDMs for 45 minutes. The amount of apoptotic cell dye (aT dye) within macrophages was assessed by flow cytometry. Each datapoint represents BMDMs from one mouse. Results are a pool of two independent experiments. n=7. Mean±SEMs. Wilcoxon test.

Treatment with NE-conditioned adipocyte supernatant for 24h significantly enhanced the efferocytic capacity of BMDMs for apoptotic thymocytes, mirroring *in vivo* findings following cold exposure (**Figure 7**). However, the specific factors driving the effects *in vivo* and *in vitro* remained unclear as activated adipocytes are known to release various immunologically active molecules [232].

In search for factors promoting efferocytosis, we next tried direct beta-adrenergic stimulation of BMDMs. Surprisingly, direct treatment of BMDMs with NE or other β2-agonistic substances induced efferocytosis to the same extent as the NE conditioned adipocyte supernatant**,** suggesting that β2-adrenergic signaling in macrophages can potentially account for the observed effects shown in

Figure 7 and **3.1.1** (**Figure 8**). Therefore, further investigation on the effects of β2-signaling on macrophages was necessary.

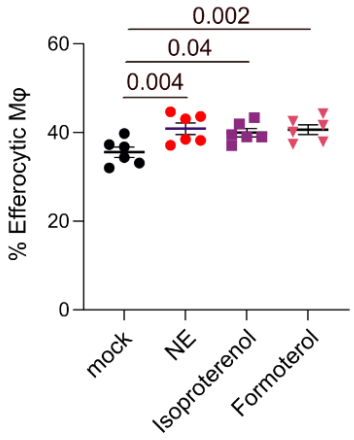

Figure 8: Stimulation of BMDM with β2 adrenergic substances induces efferocytosis of apoptotic thymocytes in vitro. Efferocytosis capacity of BMDMs isolated from wild-type mice treated with 1 μM NE, 1 μM Isoprotenerol, or 1 μM Formoterol for 24h assessed via efferocytosis. Each datapoint represents BMDMs from one mouse. n=6. Mean±SEMs. Friedman test.

3.1.3 Axl and Mertk expression contributes to increased efferocytic capacity of BMDMs after adrenergic stimulation

To further investigate the molecular mechanism by which Beta2-agonism induces efferocytosis, we analyzed the transcriptional response of BMDMs to NE stimulation, as NE is the natural stimulus released upon cold-treatment. BMDMs were treated with NE for 24 hours, followed by bulk RNA sequencing. NE-stimulation markedly altered the BMDM transcriptome, with over 500 genes upregulated and more than 300 downregulated. The 200 most significantly upregulated genes after 24 hours of NE-treatment are shown in **Figure 9** with respective key genes with known connection to either thermogenesis or efferocytosis highlighted.

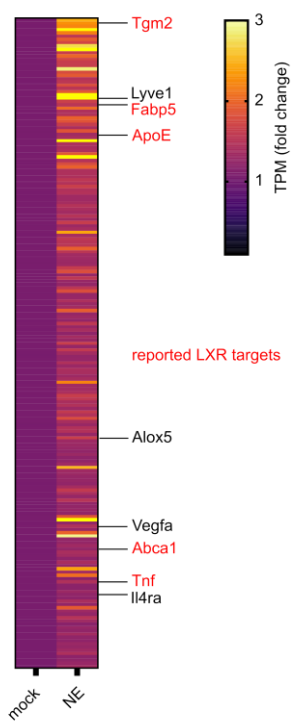

Figure 9: Transcriptional changes induced by 24h of NE treatment in wild-type BMDMs. Heatmap of the 200 most significantly upregulated genes in BMDMs isolated from wild-type mice after 24h treatment with 1 μM NE. Selected genes based on established roles in thermogenesis or efferocytosis are annotated. n=3. TPM=Transcripts Per Million.

The IL4 receptor (IL4ra), along with genes involved in angiogenesis (e.g., *Vegfa*), extracellular matrix binding (e.g., *Lyve1*), and lipid metabolism (e.g., *Alox5*), were among the most significantly upregulated. Notably, several LXR target genes - including *Tgm2*, *Fabp5*, *ApoE*, *Abca1*, and *Tnf* - were also upregulated 24 hours after NE treatment (**Figure 9**). As described in **1.1.2**, LXR is a key regulator of efferocytosis, modulating the expression of genes involved in cholesterol efflux (e.g., *Abca1*) and promoting the expression of efferocytosis receptors, particularly the receptor tyrosine kinase *Mertk* [45].

To investigate whether regulation of the LXR downstream target *Mertk* contributes to the observed effects of NE on efferocytosis, we assessed mRNA expression of *Mertk* and its structurally related receptor *Axl* using RT-qPCR in BMDMs upon NE stimulation. Using flow cytometry, we also evaluated MERTK protein levels in NE-stimulated BMDMs genetically lacking the β2-adrenergic receptor, as well as in control BMDMs. Notably, the β2-receptor is the most highly expressed adrenergic receptor on macrophages, including BMDMs [225]. BMDMs were differentiated from *Adrβ2*$^{+/+}$ and *Adrβ2*$^{-/-}$ mice, the latter genetically lacking β2-adrenergic receptor expression in all cells. Along with MERTK expression, we simultaneously assessed efferocytic activity in these BMDMs.

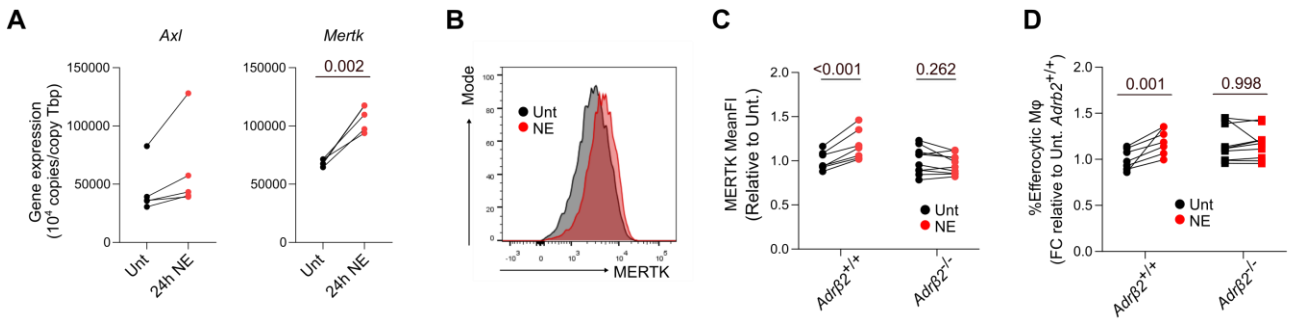

Figure 10: NE induced the expression of *Axl* and *Mertk* in BMDMs on RNA and protein level in an Adrβ2 dependent manner. (**A**) Normalized gene expressions of *Axl* and *Mertk* in BMDMs isolated from wild-type mice after treatment with 1 μM NE for 24h. Each datapoint represents BMDMs from one mouse. Mean±SEMs. n=5. Paired t-tests; (**B**) Representative histogram as well as quatification of mean fluorescence intensity (MFI) for MERTK (**C**) and efferocytosis capacity for apoptotic thymocytes (**D**) in BMDMs isolated from female *Adrβ2*$^{+/+}$ and *Adrβ2*$^{-/-}$ mice with and without treatment with 1 μM NE for 24h. Each datapoint represents BMDMs from one mouse. Results are a pool of two independent experiments. n=7/10. Mean±SEMs. 2-Way ANOVA. For gating strategies for Cd11b^{+}F4/80^{+} macrophages refer to Figure 7.

Treatment of wild-type BMDMs with NE increased mRNA expression of the efferocytic receptors *Axl* and *Mertk* (**Figure 10, A**). This was accompanied by a corresponding rise in surface MERTK protein levels, (**Figure 10, B and C**) as well as by an increased efferocytic capacity in *Adrβ2*$^{+/+}$ BDMDs (**Figure 10, D**). In contrast, NE failed to significantly enhance MERTK protein expression (**Figure 10, C**) or efferocytosis (**Figure 10, D**) in BMDMs lacking the β2-adrenergic receptor (*Adrβ2*$^{-/-}$ mice). These findings strengthen the link between adrenergic β2-signaling and efferocytosis and highlight AXL and MERTK as potential mediators of this interaction.

To determine whether β2-mediated regulation of *Axl* and *Mertk* contributes directly to efferocytosis, we then provided apoptotic thymocytes to BMDMs differentiated from either *Csf1r-Cre*$^{-}$*Axl*$^{f/f}$*Mertk*$^{f/f}$ or *Csf1r-Cre*$^{+}$*-Axl*$^{f/f}$*Mertk*$^{f/f}$ mice. BMDMs derived from *Csf1r-Cre*$^{+}$ mice lack expression of *Axl* and *Mertk*. Efferocytic capacity was then assessed between untreated and NE-stimulated conditions and across genotypes. Pooled results from two independent experiments are shown in **Figure 11**.

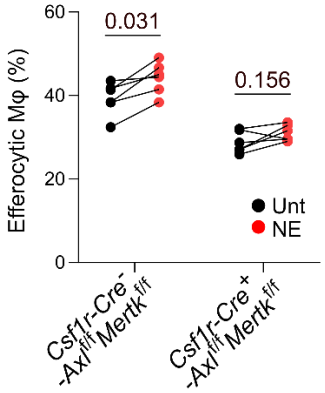

Figure 11: Loss of *Axl* and *Mertk* expression renders BMDMs less able to upregulate efferocytosis in response to NE treatment. Efferocytosis capacity for apoptotic thymocytes of BMDMs isolated from *Csf1r-Cre⁻ Axl$^{f/f}$Mertk$^{f/f}$* and *Csf1r-Cre⁺Axl$^{f/f}$Mertk$^{f/f}$* BMDMs with and without treatment with 1 μM NE for 24h. Each datapoint represents BMDMs from one mouse. Results are a pool of two independent experiments. For the gating strategy refer to **Figure 7**. n=6. Mean±SEMs. 2-Way ANOVA.

NE failed to significantly enhance the efferocytic capacity in *Csf1r-Cre⁺-Axlf^{f}Mertk$^{f/f}$* BMDMs, with only a trend towards higher efferocytosis being observable (**Figure 11**). These findings strongly suggest that AXL and MERTK contribute to the NE-mediated enhancement of BMDMs efferocytic capacity. However, it remains unclear whether the increased efferocytosis observed in ATMs upon cold exposure (see **3.1.1**) also involves changes in AXL and MERTK expression. Similarly, whether NE can directly induce AXL and MERTK expression *in vivo* has yet to be determined.

3.1.4 Expression of efferocytic receptors is induced in adipose tissue macrophages by cold exposure

To assess whether cold-induced efferocytosis in ATMs, as described in **3.1.1**, is accompanied by upregulation of efferocytic receptors, we analyzed the surface expression of MERTK and classical efferocytic receptors, including the class B scavenger receptor CD36 and the phosphatidylserine receptor TIM4 on iBAT and ingWAT macrophages using flow cytometry. Wild-type mice housed at TN were compared with those exposed to cold for 1 or 7 days. Flow cytometry analysis also included markers of macrophage phenotype and Ki67 staining to assess proliferative activity and was carried out by **Dr. Imke Liebold**. gWAT macrophages were excluded from this analysis, because gWAT does not undergo cold-induced thermogenic remodeling (see also **1.2.3**). Quantitative results and representative dot plots are presented in **Figure 12**.

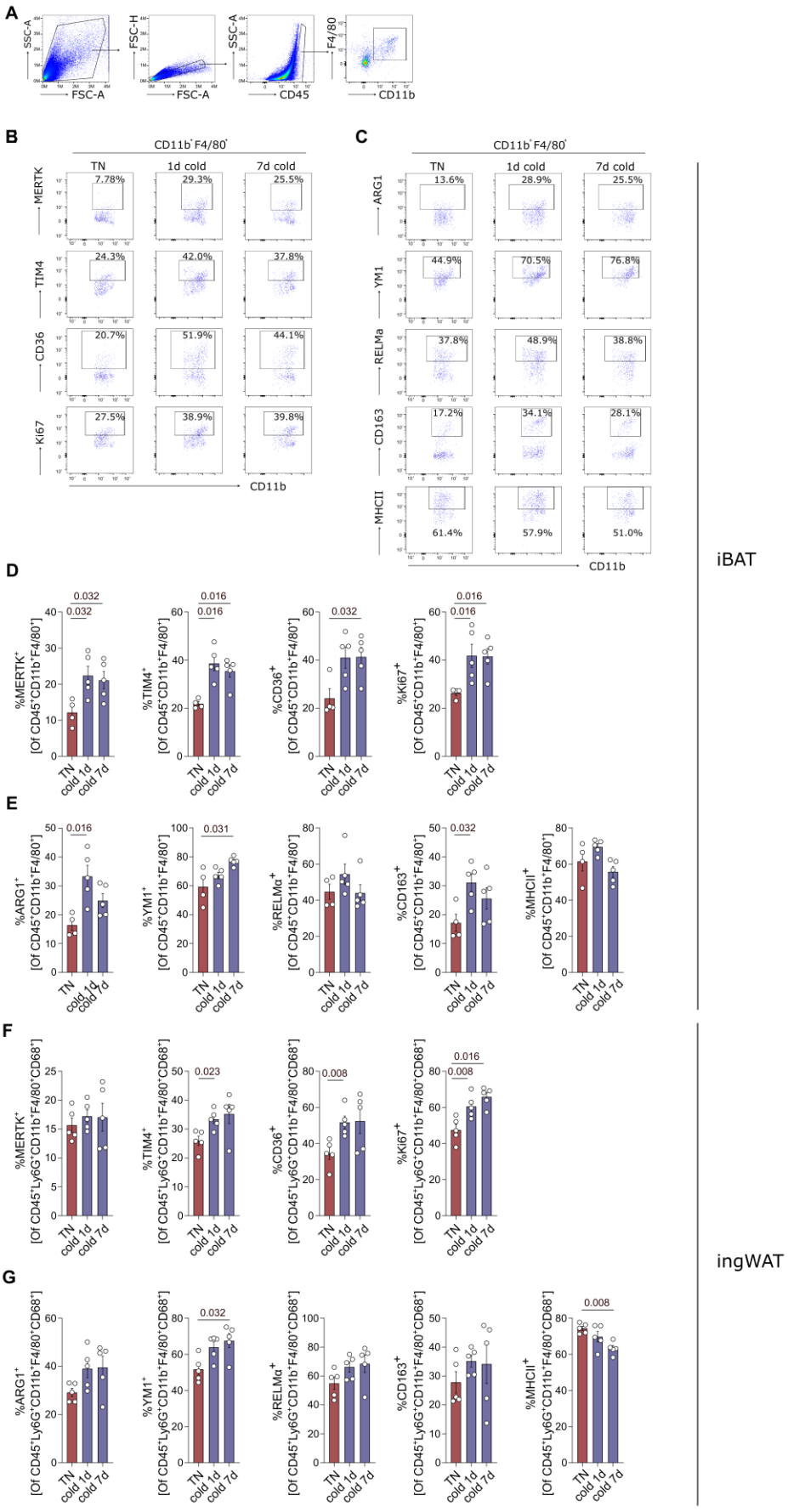

Figure 12: Cold exposure induces efferocytosis receptor expression including MERTK in iBAT and ingWAT macrophages. Flow cytometry results showing gating strategy (**A**) as well as representative dotplots for stainings of efferocytosis receptors (**B**) and markers of macrophage polarisation (**C**) on iBAT macrophages isolated from wild-type mice kept at thermoneutral housing conditions (TN, 30°C) with or without cold exposure (6°C) for 1 day or 7 days. (**C**); Frequency of iBAT macrophages expressing selected efferocytosis receptors or selected pro- or anti-inflammatory molecules (**E**). Each datapoint represents one mouse. n=4/5. Mean±SEMs. Mann-Whitney test; (**F**+**G**) Same as for D and E but for ingWAT macrophages. Each datapoint corresponds to one mouse. n=5. Mean±SEMs. Mann-Whitney tests.

We observed a higher frequency of efferocytic receptor expressing iBAT $CD11b^+F4/80^+$ macrophages upon cold exposure, including a higher frequency of CD36, TIM4 and MERTK expressing cells (**Figure 12, D**). Furthermore, cold exposure resulted in higher frequencies of iBAT macrophages expressing the anti-inflammatory markers ARG1 and YM1 and resulted in higher frequencies of $Ki67^+$ BAT macrophages, indicating increased macrophage proliferation *in vivo* [233] (**Figure 12, E**). Differences in efferocytic receptor and anti-inflammatory marker expression thereby seemed to be independent of the duration of cold exposure. These results show that higher efferocytic capacity in iBAT macrophages of cold exposed mice coincides also with higher expression of efferocytic receptors and show an anti-inflammatory and proliferative macrophage phenotype following cold exposure. These observations are consistent with the reported effects of efferocytosis on macrophage phenotype as well as with the concept of efferocytosis-induced proliferation, a process aiming at expanding the pool of resolving macrophages [65].

Largely, the same results as observed for iBAT macrophages were also observed for ingWAT $CD11b^+F4/80^+LY6G^+CD68^+$ macrophages with the notable exception of MERTK induction. IngWAT of cold exposed mice had a higher frequency of CD36, TIM4, ARG1, YM1 and Ki67 expressing macrophages, indicating that also in ingWAT cold exposure can induce an efferocytic signature in macrophages (**Figure 12, F and G**). The frequency of MHC2+ ingWAT macrophages was also reduced after 7d of cold exposure consistent with a more anti-inflammatory macrophage phenotype (**Figure 12, G**) [234], [235]. It is unclear if the lack of MERTK induction on ingWAT macrophages represents a real biological difference between the depots or whether this difference is due to technical limitations. Overall, cold-induced changes were generally more pronounced in iBAT macrophages compared to ingWAT, consistent with findings in section **3.1.1**. This supports the idea that NE, which is more abundant in the highly innervated iBAT, may drive efferocytosis more robustly in iBAT than in ingWAT.

Next, we assessed *Mertk* mRNA expression in $Cd11b^+$ cells enriched from iBAT, ingWAT, and gWAT of mice housed under thermoneutral conditions or exposed to cold for 24 hours. For the enrichment, magnetic $Cd11b^+$ microbeads were used and **Jennifer Witt** carried out the actual experiment. Consistent with the idea that macrophages represent the largest immune cell population in adipose tissue [236], the majority of $Cd11b^+$ cells obtained using this method are expected to be ATMs**.**

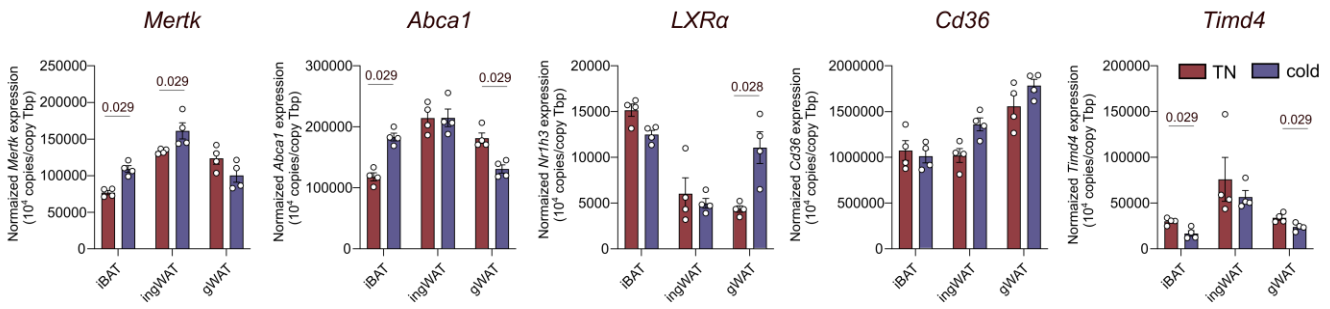

Figure 13: Cold exposure induces RNA expression of *Mertk* and the *LXR* downstream target *Abca1* in iBAT and ingWAT macrophages in vivo. Normalized RNA expression of selected genes in MACS sorted Cd11b$^+$ cells isolated from adipose tissue of wild-type mice kept under thermoneutral (30°C, TN) housing conditions or exposed to cold (6°C) for 1d. Gene expression was assessed by RT-qPCR. Each point corresponds to a pool of five mice. n=4. Mean±SEMs. Mann-Whitney tests.

We observed a significantly higher *Mertk* mRNA expression in CD11b$^+$ cells from iBAT and ingWAT, but not from gWAT, following 24 hours of cold exposure (**Figure 13**). These findings align with surface expression data of MERTK shown in **Figure 12**, reinforcing the association between cold exposure and the upregulation of efferocytosis receptors in ATMs. Furthermore, results shown in **Figure 13** also support a depot-specific response in the magnitude of *Mertk* induction by cold, with iBAT Cd11b$^+$ exhibiting a more pronounced induction compared to ingWAT Cd11b$^+$ cells (**Figure 13**). Again, this difference might be linked to differences in sympathetic innervation and local NE levels. Interestingly, the well-established LXR target gene *Abca1* was also higher in iBAT CD11b$^+$ cells, consistent with activation of LXR signaling within ATMs in response to increased NE sensing during cold exposure. mRNA levels of the relevant LXR isoform itself remained unchanged in iBAT and ingWAT CD11b$^+$ cells but were elevated in gWAT CD11b$^+$ cells (**Figure 13**). mRNA levels of *Axl* and *Cd36* were not significantly changed in CD11b$^+$ cells of cold housed mice, while *Timd4* was significantly downregulated (**data not shown**, **Figure 13**). This contrasted with protein expression patterns presented in **Figure 12**, suggesting that mRNA and protein levels may not be linearly correlated. Nonetheless, when focusing on *Mertk* and *Abca1* induction, these findings align with surface expression data and also *in vitro* data from **3.1.3**, reinforcing the association between cold exposure, LXR signaling and the upregulation of MERTK in ATMs.

3.1.5 Efferocytosis can be induced by NE *in vivo*

Given the impact of NE on efferocytic macrophages *in vitro,* we next sought to determine whether NE could also directly act as a trigger of efferocytosis *in vivo*. For this, we injected wild-type mice subcutaneously with NaCl or NE at 1 mg/kg bodyweight twice, 12h and 30 minutes before analysis. Afterwards the rate of efferocytic ATMs was determined by an *ex vivo* efferocytosis assay as in **3.1.1**. In addition to the usual Cd11b and F4/80 staining, macrophages were stained against CX3CR1 as

well as LY6C for further phenotypical characterization. CX3CR1 thereby is reportedly expressed on sympathetic associated macrophages and has an established role in the chemotaxis towards apoptotic cells, while LY6C is commonly used to discriminate between resident and infiltrating macrophages [228], [237].

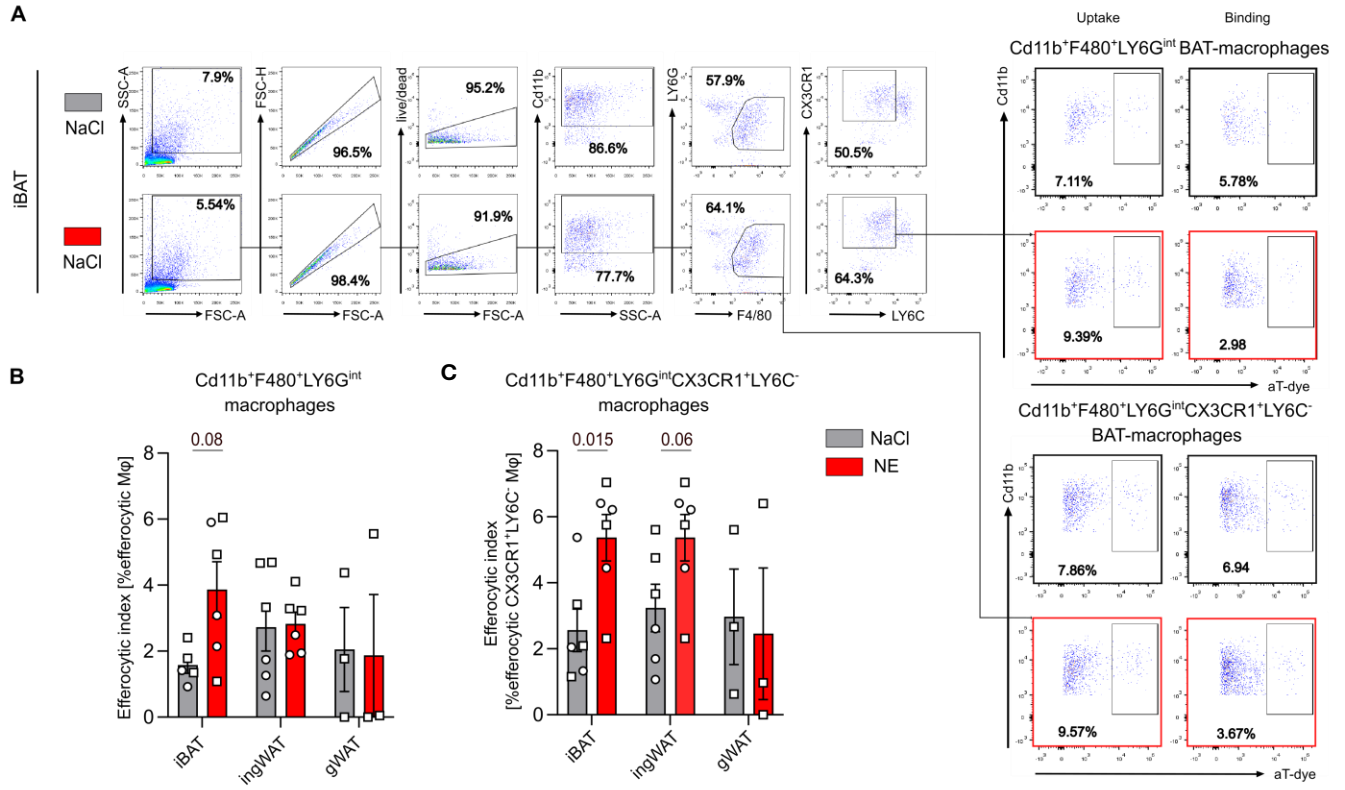

Figure 14: Injection of NE directly increases efferocytosis in CX3CR1^{+}LY6C^{-} iBAT macrophages in vivo. Gating strategy (**A**) and pooled results of 2 independent ex vivo efferocytosis assays, comparing the efferocytosis capacity of Cd11b^{+}MACS + adherence purified Cd11b^{+}F4/80^{+} (**B**) and Cd11b^{+}F4/80^{+}CX3CR1^{+}LY6C^{-} (**C**) ATMs between male wild-type mice injected subcutaneously with either NaCl or NE at 1mg/kg bodyweight 12h and 30 minutes before analysis. During the experiment mice were kept at room temperature. Efferocytosis assays were carried out as described for **Figure 6**. Each dot represents a pool of 3 mice. n=6. Mean±SEMs; Mann-Whitney tests.

NE treatment resulted in higher efferocytosis in iBAT macrophages, with minimal effects observed on total ingWAT or gWAT macrophages (**Figure 14, B**). Notably, further analysis of CX3CR1^{+}LY6C^{-} macrophages revealed significantly higher efferocytotic capacity of iBAT ATMs upon NE-injection, with a trend towards higher efferocytic capacity observable for ingWAT macrophages (**Figure 14, C**). CX3CR1^{+}LY6C^{-} macrophages comprised 25–75% of total iBAT macrophages, and this frequency remained unchanged with cold exposure (**data not shown**). Furthermore, when focusing on CX3CR1^{+}LY6C^{-} macrophages, also a trend towards higher efferocytic capacity could be observed for ingWAT macrophages.

Collectively, these findings suggest that adrenergic signaling can promote efferocytosis not only *in vitro* but also *in vivo*. Furthermore, the effect of NE provides a possible explanation for the effects of cold exposure on macrophage efferocytosis. It remains to be determined whether BAT macrophages are intrinsically more responsive to NE or whether the observed effects are due to limitations in experimental design. The same goes for CX3CR1^{+}LY6C^{-} ATMs vs LY6C^{+} cells.

3.2 Cold activated brown adipose tissue shows signs of cell death and releases IL4

3.2.1 Signs of cellular stress and apoptosis in mouse brown adipose tissue upon cold exposure

Induction of efferocytic receptors is typically triggered by the need to clear damaged cells, thereby preventing the development of a detrimental inflammatory response. Given the increased expression of efferocytic receptors observed following NE treatment, we next assessed whether this was associated with an accumulation of dying cells upon cold exposure. To assess signs of apoptosis in BAT upon thermogenic remodelling, we analyzed markers of cell stress and apoptosis in murine BAT from mice housed at thermoneutral or cold conditions for 24h on mRNA level. For this, we performed RNA sequencing of mature adipocytes (mAdipocytes) and stromal vascular fraction (SVF) which revealed alterations in many genes involved in apoptosis regulation. Key candidate genes, including the pro-apoptotic *Bax* and its anti-apoptotic counterpart *Bcl-2*, were validated by RT-qPCR of iBAT mRNA. Additionally, BAX protein levels were compared between thermoneutral kept and cold-exposed mice.

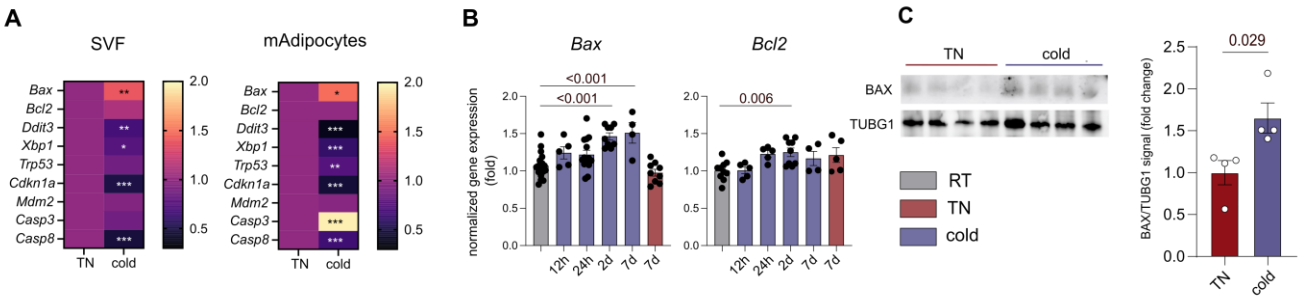

Figure 15: Signs of apoptosis in iBAT of mice housed under cold conditions. (**A**) Normalized expression of selected apoptosis related genes on mRNA level by 2 days of cold exposure (6°C) in iBAT mature adipocyte (mAdipocyte) or stromal vascular fraction (SVF) of male wild-type mice after two weeks of acclimatization to thermoneutral (30°C, TN) housing conditions. mRNA levels were assessed by bulk RNA-Sequencing and are displayed as heatmaps. n=3. *padj ≤ 0.05; **padj ≤ 0.01; ***padj ≤ 0.001. Data analysis was carried out by **Dr. Lorenz Adlung**; (**B**) Normalized mRNA levels of *Bax* and *Bcl2* assessed by RT-qPCR in iBAT of wild-type mice exposed to room temperature, TN or cold for different durations. Each dot represents one mouse. n=4-18. Mean±SEMs. Unpaired t-tests; (**C**) Protein levels of BAX (~21 kDa) and γTubulin (TUBG1, ~51 kDa) in iBAT of male wild-type mice kept at TN or exposed to cold for 1d assessed by western blotting. Each dot represents one mouse. n=4. Mean±SEMs. Mann-Whitney test

As previously mentioned, the expression of several genes involved in apoptosis regulation was altered by cold exposure. For example, the expression of the executioner Caspase 3 was markedly upregulated in the mature adipocyte fraction (**Figure 15, A**). Strikingly, *Bax* mRNA levels were also significantly increased in both the mature adipocyte and stromal vascular fractions of murine BAT. In contrast, *Bcl2* expression remained unchanged in the RNA-seq analysis (**Figure 15, A**). *Bax* (Bcl-2-associated X protein) has been established as a potent inducer of apoptosis by permeabilizing the mitochondrial outer membrane, leading to the activation of downstream caspases, while *Bcl-2* (B-cell lymphoma 2) acts as an anti-apoptotic protein by inhibiting the function of BAX. The balance between *Bax* and *Bcl-2* levels has been shown to determine cell fate, with a higher *Bax*/*Bcl-2* ratio favoring apoptosis and a lower ratio promoting cell survival [238]. RT-qPCR confirmed the cold-induced upregulation of *Bax* mRNA in BAT and additionally revealed a modest but significant regulation of *Bcl2* (**Figure 15, B**). The upregulation of *Bax* mRNA thereby suggests enhanced pro-apoptotic signaling, whereas the modest increase in *Bcl2* may reflect a compensatory anti-apoptotic response aimed at limiting cell death. Correspondingly, an increase in BAX protein was observed in BAT lysates after 24 hours of cold exposure, although overall protein levels remained low under both conditions (**Figure 15, C**). Together, these findings suggest that thermogenic activation may act as a mild apoptotic trigger in otherwise healthy BAT.

3.2.2 Cytokine release from mouse adipose tissue upon cold exposure

Given the importance of the coincident detection of dying cells and anti-inflammatory cytokines, such as IL4 in shaping macrophage function and phenotype [59], we compared cytokine release from BAT and ingWAT explants between mice kept at control conditions (room temperature) and mice exposed to cold (6°C for 24h). After organ harvest, adipose tissue explants were placed in cell culture media and cytokine levels in the supernatant were analyzed 4h later using a Legendplex multiplex cytokine detection kit. The cytokine detection was thereby carried out with the help of **Dr. Stephanie Leyk.**

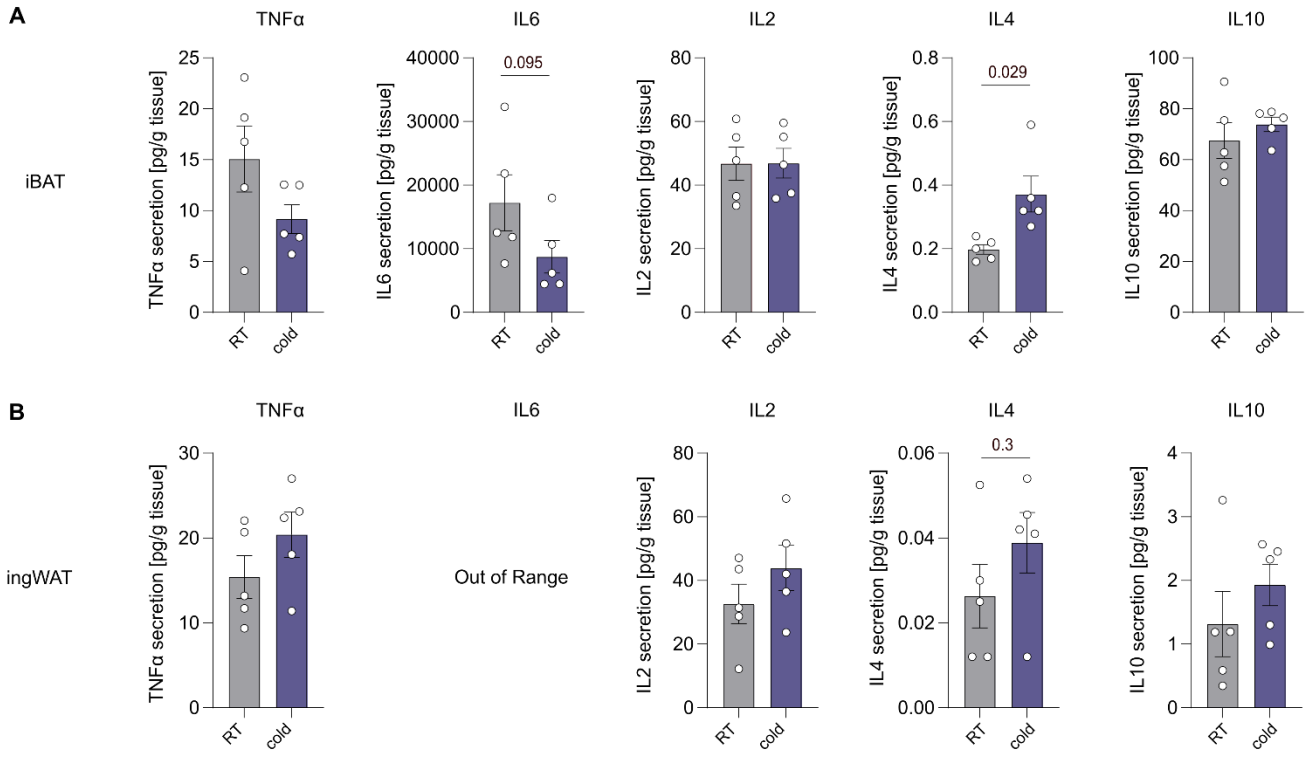

Figure 16: Cold exposure induces a more anti-inflammatory cytokine profile characterized by higher IL4 concentrations in iBAT and ingWAT explants. Cytokine levels in supernatants of iBAT (**A**) and ingWAT (**B**) explants from male wild-type mice kept at room temperature of exposed to cold for 1d after 4h of incubation as assessed by LEGENDplex analysis. Each dot represents one mouse. n=5. Mean±SEMs. Mann-Whitney tests

In this experimental setting, thermogenic activation by cold was associated with a significantly higher release of IL4 from BAT explants and a weak trend towards increased IL4 release from ingWAT explants (**Figure 16, A and B**). Higher release of IL4 in iBAT and ingWAT upon cold-treatment has also been previously reported [226]. Additionally, the secretion of the pro-inflammatory cytokine IL6 tended to be lower, at least in BAT explants (**Figure 16, A**). These observations are consistent

with the results presented in **Figure 12**, indicating a shift towards a more anti-inflammatory environment, particularly in cold-exposed BAT. Moreover, together with the findings presented in **Figure 15**, these results suggest that the conditions necessary for macrophage-driven tissue remodeling via efferocytosis may be present in thermogenically activated adipose tissue: (1) expression of efferocytosis receptors by macrophages, (2) presence of apoptotic cells, and (3) an anti-inflammatory cytokine milieu characterized by elevated IL4 levels.

3.3 The role of AXL/MERTK dependent efferocytosis in adipose tissue plasticity and activation

3.3.1 Mice lacking *Axl* and *Mertk* expression and kept on standard diet show no major problems in dealing with cold challenge

The next key question to address was whether AXL/MERTK-dependent efferocytosis plays a significant role in adipose tissue biology and adaptation. To investigate this, we used mice lacking *Axl* and *Mertk* expression specifically in macrophages (*Csf1r*-Cre^{+}-*Axl*$^{f/f}$*Mertk*$^{f/f}$), alongside their littermate controls (*Csf1r*-Cre^{-}-*Axl*$^{f/f}$*Mertk*$^{f/f}$). To induce tissue remodeling as well as high levels of NE in adipose tissue, we used various settings of cold exposure and focused mostly on ingWAT and especially iBAT. These depots were selected based on prior findings (**3.1** and **3.2**) and their high degree of sympathetic innervation, which likely results in higher NE concentrations during cold exposure. Since young *Csf1r*-Cre^{+}-*Axl*$^{f/f}$*Mertk*$^{f/f}$ mice exhibit no gross abnormalities under standard housing conditions [239], [240], our first experiment compared gene expression profiles in iBAT between *Csf1r-Cre*$^{-}$-Axl$^{f/f}$*Mertk*$^{f/f}$ and *Csf1r-Cre*$^{+}$-*Axl*$^{f/f}$*Mertk*$^{f/}$ mice after a 24-hour cold (6°C) challenge. Control mice maintained at RT (22°C) were also included. Moreover, rectal temperature was measured to test whether mice were able to defend their body temperature against the cold. A drop in body temperature in *Csf1r-Cre*$^{+}$-*Axl*$^{f/f}$*Mertk*$^{f/f}$ mice would indicate impaired BAT thermogenesis due to the absence of *Axl*- and *Mertk*-expressing macrophages in BAT. The results of this experiment are presented in **Figure 17**.

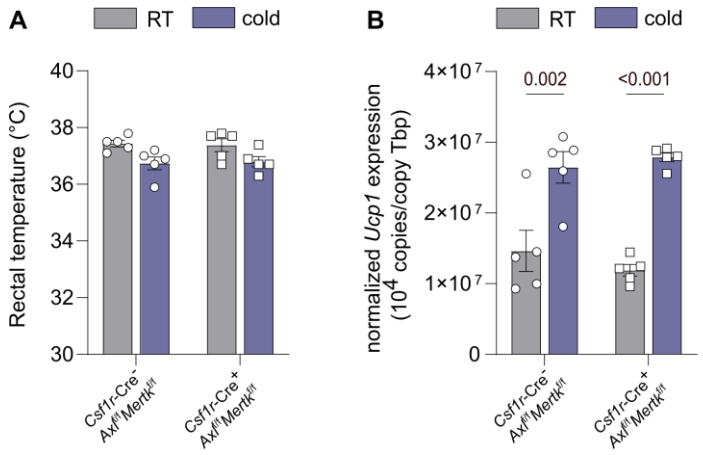

Figure 17: No difference in rectal temperature or UCP1 RNA expression between *Csf1r-Cre*$^{-}$*-Axl*$^{f/f}$*Mertk*$^{f/f}$ and *Csf1r-Cre*$^{+}$*-Axl*$^{f/f}$*Mertk*$^{f/f}$ mice at room temperature or after 1 day of cold exposure. Rectal temperature (**A**, Physitemp rectal thermometer, Cat# BAT-12 t) and UCP1 RNA expression in iBAT (**B**) of male *Csf1r*-Cre^{-}-*Axl*$^{f/f}$*Mertk*$^{f/f}$ and *Csf1r*-Cre^{+}-*Axl*$^{f/f}$*Mertk*$^{f/f}$ mice at room temperature or after 1 day of cold exposure. Each datapoint corresponds to one mouse. n=5. Mean±SEMs. 2-Way ANOVAs.

No significant differences were observed in rectal temperature (**Figure 17, A**) or cold-induced *Ucp1* expression in BAT (**Figure 17, B**) between *Csf1r*-Cre^{-}-*Axl*$^{f/f}$*Mertk*$^{f/f}$ and *Csf1r*-Cre^{+}-*Axl*$^{f/f}$*Mertk*$^{f/f}$ mice. Similarly, there were no genotype-dependent differences in the expression of other thermogenic, inflammatory, or apoptosis-related genes, or in adipose tissue depot weights (**data not shown**).

Based on these findings, we adopted an alternative experimental design: mice were housed under thermoneutral conditions (30°C) for two weeks, followed by a four-day cold exposure. This approach aimed to fully suppress baseline BAT thermogenesis and induce a greater change in NE levels once cold exposure begins. Furthermore, the extended cold exposure aimed to provide more time for potential effects of *Axl*- and *Mertk*-deficiency in macrophages to emerge. After the experiment, BAT gene expression was again analyzed via RT-qPCR, and macrophage polarization was assessed by flow cytometry.

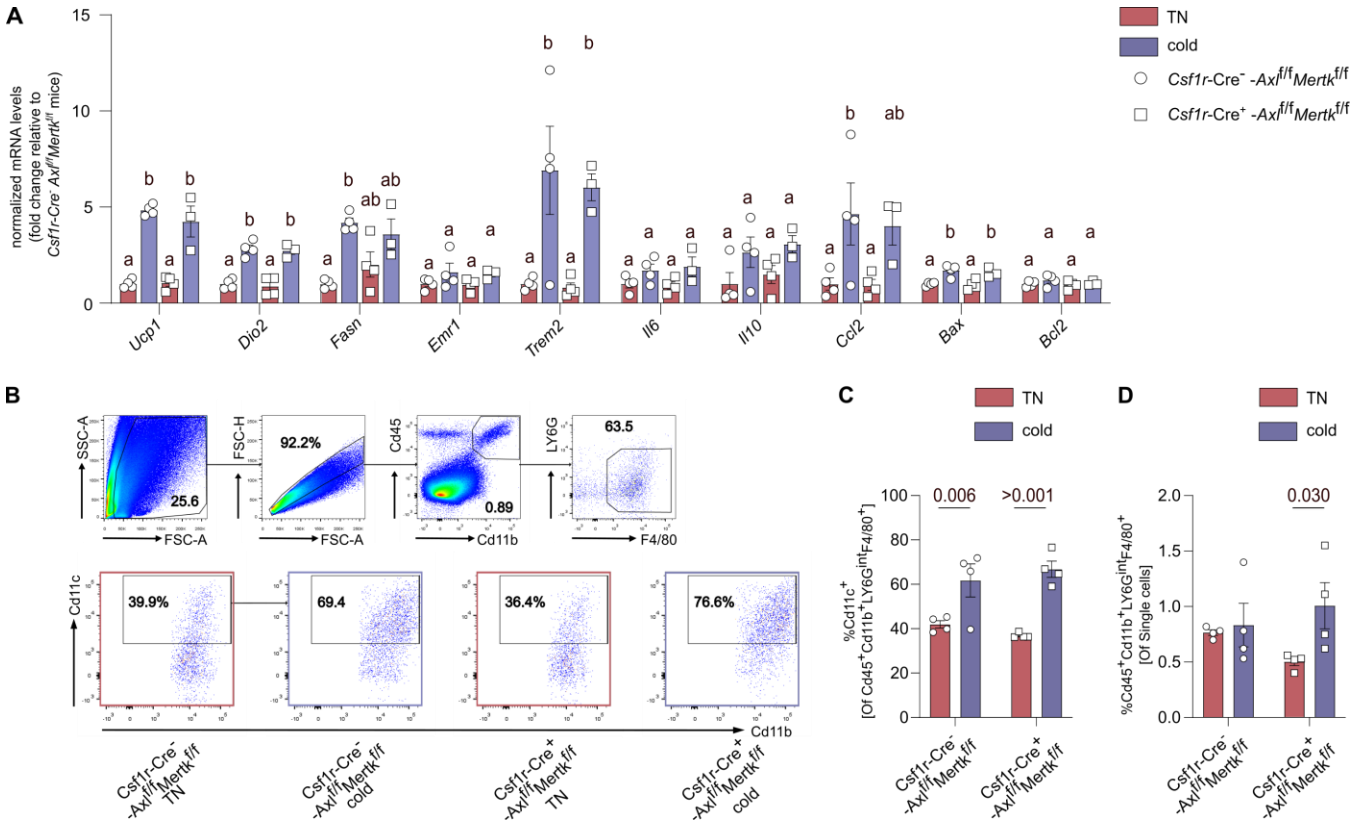

Figure 18: Switch from thermoneutral housing to cold housing induces the presence of lipid associated macrophages in iBAT of both *Csf1r-Cre⁻-Axl$^{f/f}$Mertk$^{f/f}$* and *Csf1r-Cre⁺-Axl$^{f/f}$Mertk$^{f/f}$* mice. (**A**) RNA expression of selected genes related to non-shivering thermogenesis, inflammation or apoptosis assessed by RT-qPCR in iBAT of male *Csf1r-Cre⁻-Axl$^{f/f}$ Mertk$^{f/f}$* and *Csf1r-Cre⁺-Axl$^{f/f}$ Mertk$^{f/f}$*mice after 2 weeks of thermoneutral housing (30°C) with and without additional 4 days of cold housing (6°C). Each datapoint corresponds to one mouse. n=4. Mean±SEMs. Mann-Whitney tests; Gating strategy and representative dotplots (**B**) together with corresponding quantifications of Cd11c⁺ cells among all Cd45⁺Cd11b⁺Ly6G^{int}F4/80⁺ macrophages (**C**) and Cd45⁺Cd11b⁺Ly6G^{int}F4/80⁺ among all cells (**D**) in iBAT of male *Csf1r-Cre⁻-Axl$^{f/f}$ Mertk$^{f/f}$* and *Csf1r-Cre⁺-Axl$^{f/f}$* Mertk$^{f/f}$ mice after 2 weeks of thermoneutral housing with and without additional 4 days of cold housing. Each datapoint in C and D corresponds to one mouse. n=4. Mean±SEMs. Mann-Whitney tests. 2-Way ANOVA.

Cold exposure strongly induced thermogenic gene expression in the BAT of both *Csf1r-Cre⁻-Axl$^{f/f}$Mertk$^{f/f}$* and *Csf1r-Cre⁺-Axl$^{f/f}$Mertk$^{f/f}$* mice, along with increased mRNA levels of *Trem2*, a known marker and transcriptional regulator of LAM identity (**Figure 18, A**) [211]. However, no genotype-dependent differences in gene expression were observed in either iBAT (**Figure 18, A**) or ingWAT (**data not shown**). These findings were supported by flow cytometry, which revealed higher

frequencies of Cd45^{+}Ly6G^{int}CD11b^{+}F4/80^{+}CD11c^{+} macrophages in BAT of cold-housed *Csf1r-Cre*$^{-}$-*Axl*$^{f/f}$*Mertk*$^{f/f}$ and *Csf1r-Cre*$^{+}$-*Axl*$^{f/f}$*Mertk*$^{f/f}$ mice (**Figure 18, B and C**). CD11c is a surface marker associated with both LAM identity and pro-inflammatory identity in macrophages and is linked to insulin resistance and metabolic syndrome [241], [242]. The increase of Cd11c^{+} macrophages in BAT occurred independently of genotype (**Figure 18, B**), and no other genotype-specific differences in macrophage polarization were detected (**data not shown**). Interestingly, slightly but significantly higher frequencies of CD45^{+}LY6G^{int}CD11b^{+}F4/80^{+} among all cells were observed only in *Csf1r-Cre*$^{+}$-*Axl*$^{f/f}$*Mertk*$^{f/f}$ mice (**Figure 18, C**). This suggests a potential, albeit modest, genotype-dependent macrophage infiltration into BAT upon cold exposure, possibly mediated by the lack of *Axl* and *Mertk* expression in ATMs. Interestingly, an increased *Trem2* expression in BAT was not observed when mice were transferred from RT to cold housing as in the previous experiment (**data not shown**). Given that LAM recruitment in adipose tissue is often associated with tissue stress and apoptosis [213], these findings suggest that transitioning from TN to cold might impose a significantly greater physiological challenge to BAT compared to transitioning from RT. Therefore, we adapted thermoneutral housing as our standardized baseline condition for the following experiments. Nonetheless the obtained data also indicates that AXL/MERTK-dependent efferocytosis is not immediately required for normal BAT function during these comparatively simple cold challenges.

Major adaptive responses often require the cessation of stressors for efficient tissue remodeling and resolution [187]. Furthermore, repeated metabolic stressors can have cumulative effects on tissue integrity and remodeling, as recently demonstrated by Reinisch and colleagues [164]. We therefore adapted a third experimental setup in which *Csf1r-Cre*$^{-}$-*Axl*$^{f/f}$*Mertk*$^{f/f}$ and *Csf1r-Cre*$^{+}$-*Axl*$^{f/f}$*Mertk*$^{f/f}$ mice were first adapted to thermoneutral housing for two weeks, before they were subjected to two consecutive but individual cold challenges (4 and 2.5 days) separated by a 3-day re-adaptation period. A scheme of the experimental design can be found in **Figure 19**. Throughout the study, energy expenditure was continuously monitored by using the Sable System®, which additionally assessed respiratory exchange ratio, food intake, and locomotor activity for each mouse. Furthermore, at the end of the experiment, a final injection of CL316,243 - a β3-selective adrenergic agonist - was administered at thermoneutral temperature. This allowed for the measurement of thermogenic adipocyte-driven energy expenditure [243], distinct from whole-body thermogenesis during cold exposure. Results of energy expenditure measurements are shown in **Figure 19**.

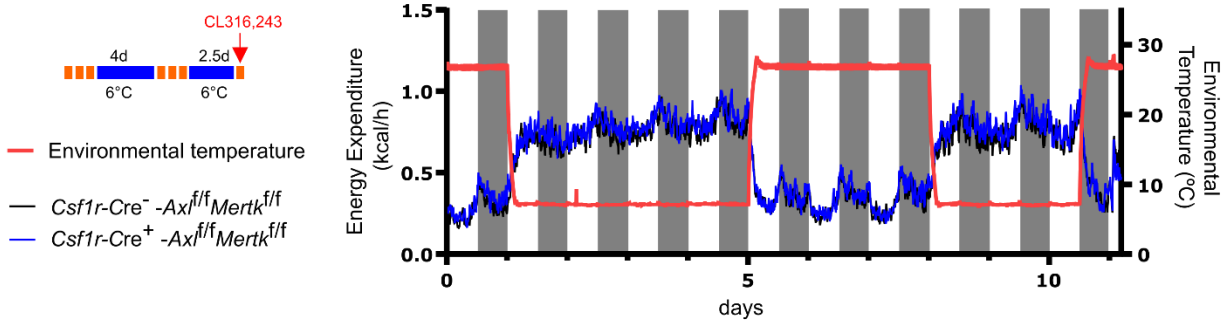

Figure 19: Unchanged energy expenditure between *Csf1r-Cre^{-}-Axl$^{f/f}$Mertk$^{f/f}$* and *Csf1r-Cre^{+}-Axl$^{f/f}$Mertk$^{f/f}$* mice after repeated cold exposure and injection of CL316,243. Mean energy expenditure of male *Csf1r-Cre^{-}-Axl$^{f/f}$Mertk$^{f/f}$* and *Csf1r-Cre^{+}-Axl$^{f/f}$Mertk$^{f/f}$* mice during repeated cold exposure and upon injection of CL316,243 as assessed by indirect calorimetry. n=6/7.

Energy expenditure was not different between *Csf1r*-Cre^{-}-*Axl$^{f/f}$Mertk$^{f/f}$* and *Csf1r*-Cre^{+}-*Axl$^{f/f}$Mertk$^{f/f}$* mice at thermoneutral temperature, during cold exposure (around 6°C) or after injection of CL316,243 (**Figure 19**). Similarly, respiratory exchange ratio, food intake, and locomotor activity remained unchanged (**data not shown**). In addition to the energy expenditure measurement, macrophages were isolated from iBAT and ingWAT at the end of the experiment and analyzed via flow cytometry by **Dr. Imke Liebold**. Results from this analysis are shown in **Figure 20**.

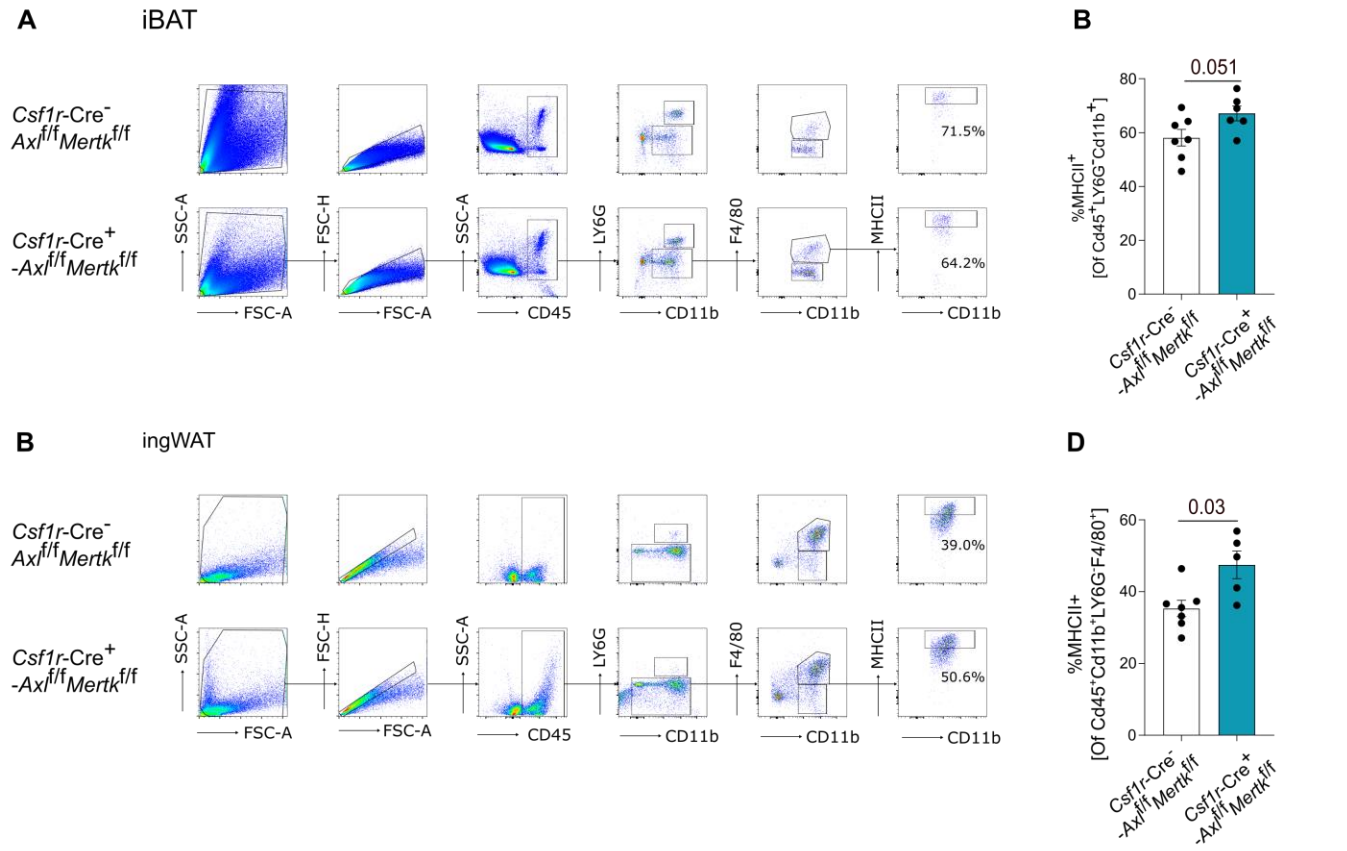

Figure 20: Increased frequency of MHCII⁺ macrophages in iBAT and ingWAT of *Csf1r-Cre⁺-Axl$^{f/f}$Mertk$^{f/f}$* mice after repeated cold exposure and injection of CL316,243. Gating strategy and representative dotplots (**A**) as well the frequency of MHCII⁺ cells among Cd45⁺LY6G⁻CD11b⁺F4/80⁺ macrophages (**B**) in iBAT of male *Csf1r-Cre⁻-Axl$^{f/f}$ Mertk$^{f/f}$* and *Csf1r-Cre⁺-Axl$^{f/f}$ Mertk$^{f/f}$* mice after repeated cold exposure. n=6/7. Mean±SEMs. Mann-Whitney test; Gating strategy and representative dotplots (**C**) as well the frequency of MHCII⁺ cells among Cd45⁺LY6G⁻CD11b⁺F4/80⁺ macrophages (**D**) in ingWAT of male *Csf1r-Cre⁻-Axl$^{f/f}$ Mertk$^{f/f}$* and *Csf1r-Cre⁺-Axl$^{f/f}$* Mertk$^{f/f}$ mice after repeated cold exposure. n=6/7. Mean±SEMs. Mann-Whitney test; Experimental Layout is depicted in **Figure 19**.

A higher frequency of MHCII⁺ cells among Cd45⁺LY6G⁻CD11b⁺F4/80⁺ macrophages was observed in iBAT (**Figure 20, A and B**) and ingWAT (**Figure 20, C and D**), within *Csf1r-Cre⁺-Axl$^{f/f}$Mertk$^{f/f}$* mice following two consecutive cold challenges and CL316,243 injection. MHCII is a key antigen-presenting molecule typically associated with a more pro-inflammatory macrophage phenotype [234]. This suggests that macrophages within iBAT and ingWAT of *Csf1r-Cre⁺-Axl$^{f/f}$Mertk$^{f/f}$* mice exhibit a more pro-inflammatory phenotype. However, no significant differences were detected in the frequencies of macrophages expressing other analyzed markers, indicating that any phenotypical alteration in macrophages due to the absence of *Axl* and *Mertk* is likely mild (**Figure 20**).

Finally, also mRNA expression was measured in iBAT, ingWAT and gWAT of *Csf1r-Cre*$^{-}$*-Axl*$^{f/f}$*Mertk*$^{f/f}$ and *Csf1r-Cre*$^{+}$*-Axl*$^{f/f}$*Mertk*$^{f/f}$ mice as well as protein levels of UCP1 in iBAT.

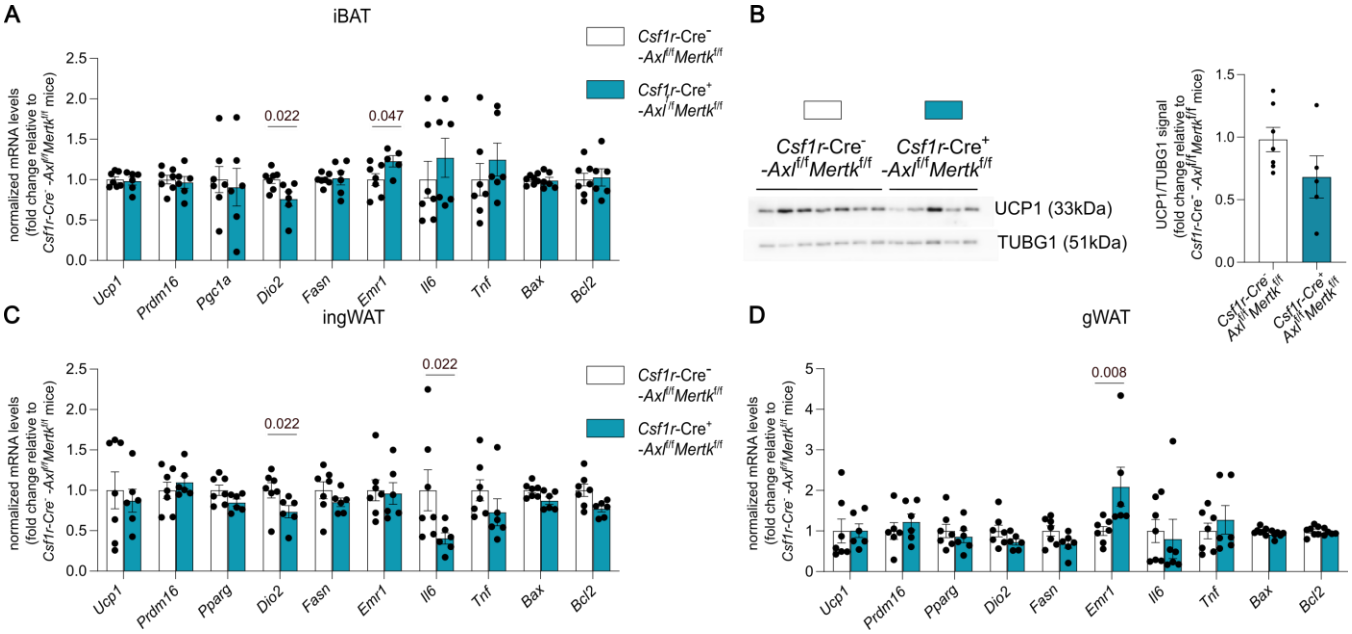

Figure 21: Signs of slight macrophage infiltration on RNA level in iBAT and gWAT of *Csf1r-Cre*$^{+}$*-Axl*$^{f/f}$*Mertk*$^{f/f}$ mice after repeated cold exposure and injection of CL316,243. RNA expression of selected genes related to non-shivering thermogenesis, inflammation or apoptosis assessed by RT-qPCR in iBAT (**A**), ingWAT (**C**) and gWAT (**D**) of male *Csf1r-Cre*$^{-}$*-Axl*$^{f/f}$*Mertk*$^{f/f}$ and *Csf1r-Cre*$^{+}$*-Axl*$^{f/f}$*Mertk*$^{f/f}$mice after repeated cold exposure and injection of CL316,243 as depicted in **Figure 19**. Each datapoint corresponds to one mouse. n=7/6. Mean±SEMs. Mann-Whitney tests; **B**) UCP1 to total TUBG1 protein ratio in iBAT of *Csf1r-Cre*$^{-}$*-Axl*$^{f/f}$ *Mertk*$^{f/f}$ and *Csf1r-Cre*$^{+}$*-Axl*$^{f/f}$ *Mertk*$^{f/f}$ mice after repeated cold exposure assessed by western blotting. n=7/5. Mean±SEMs. Mann-Whitney tests

Thermogenic gene expression was not altered across the adipose tissue depots analyzed (**Figure 21, A, C, and D**) and UCP1 protein levels in iBAT *Csf1r-Cre*$^{+}$*-Axl*$^{f/f}$*Mertk*$^{f/f}$ mice trended lower, (**Figure 21, B**). These findings are consistent with the lack of significant changes in energy expenditure (**Figure 19**). The only notable gene expression changes were the downregulation of *Dio2* in iBAT and ingWAT, and elevated *Emr1* expression in iBAT and especially gWAT *of Csf1r-Cre*$^{+}$*-Axl*$^{f/f}$*Mertk*$^{f/f}$ mice (**Figure 21, A and C**). While the mechanism underlying the *Dio2* downregulation remains unclear, the increase in *Emr1* - which encodes the macrophage marker F4/80 - suggests a higher macrophage presence in iBAT and gWAT of Cre+ mice. This interpretation is supported by the elevated frequencies of MHCII^{+} macrophages in iBAT and ingWAT, indicating accumulation of more inflammatory macrophages in adipose tissue following repeated cold exposure.

Overall, these results suggest that macrophages expressing *Axl* and *Mertk* are not essential for non-shivering thermogenesis (NST) under the experimental conditions tested here in **3.3.1**. Only mild effects on macrophages were observed in the setups that included prior adaptation to thermoneutral housing and repeated cold exposure (**Figure 20 and Figure 21**). These findings align with the limited need for tissue remodeling in young, lean mice with functionally healthy brown and white adipose tissue under cold stress - a point further supported by the relatively low number of macrophages in the BAT of chow-fed young mice (**Figure 19, D** and [244])

3.3.2 Macrophage-specific Axl and Mertk deficiency reduces thermogenic gene expression in humanized adipose tissue after repeated cold exposure

To investigate the role of AXL- and MERTK-mediated efferocytosis on adipose tissue in a setting of more severe adipose tissue remodelling and macrophage infiltration, we started by feeding *Csf1r-Cre*$^{-}$*-Axl*$^{f/f}$Mertk$^{f/f}$ and *Csf1r-Cre*$^{+}$*-Axl*$^{f/f}$Mertk$^{f/f}$ mice a HFD, containing 35% lard for 10-14 weeks at thermoneutral housing conditions (30°C). This approach was chosen to "humanize" adipose tissue physiology and enhance macrophage recruitment. Based on findings from **3.3.1**, mice were then subjected to a repeated cold challenge to study the role of AXL- and MERTK-dependent efferocytosis in a setting of intense adipose tissue stress and remodeling and under conditions where their expression is induced by NE.

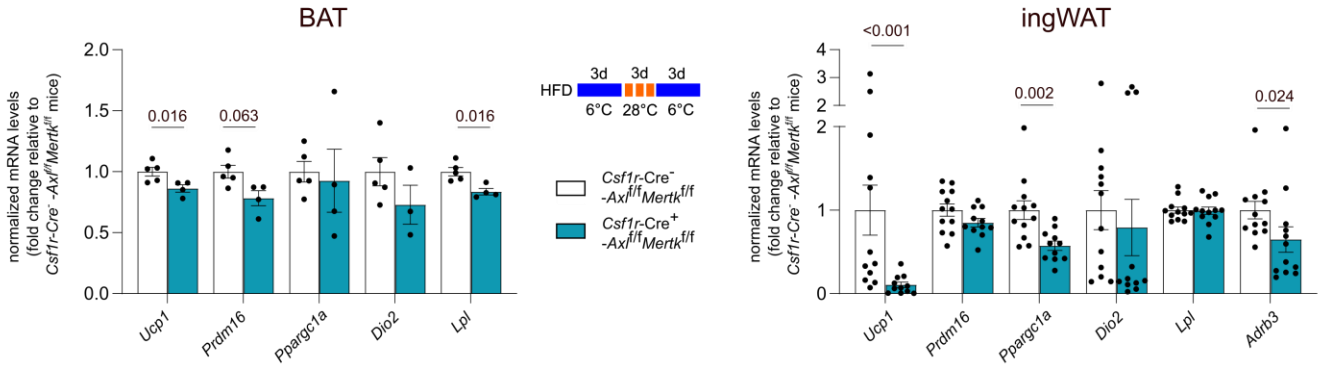

Figure 22: Reduced expression thermogenic genes genes in iBAT and ingWAT of *Csf1r-Cre*$^{+}$*-Axl*$^{f/f}$*Mertk*$^{f/f}$ mice after HFD feeding and repeated cold exposure. RNA expression of genes related to non-shivering thermogenesis genes assessed by RT-qPCR in iBAT and ingWAT of male *Csf1r-Cre*$^{-}$*-Axl*$^{f/f}$*Mertk*$^{f/f}$ and *Csf1r-Cre*$^{+}$*-Axl*$^{f/f}$*Mertk*$^{f/f}$ mice after HFD feeding at thermoneutral housing conditions and repeated cold exposure. Each datapoint corresponds to one mouse. n=5/4 and n=12/11 respectively. Mean±SEMs. Mann-Whitney tests

In this experimental setup, transcription of the key genes controlling non-shivering adipose tissue thermogenesis *Ucp1 and Lpl* (encoding *Pgc-1α*) was significantly lower in iBAT from *Csf1r-Cre*$^{+}$-*Axl*$^{f/f}$*Mertk*$^{f/f}$ mice compared to their littermate controls (**Figure 22, Left**). This indicates an impairment in BAT activation in a setting in which efferocytosis is limited by the lack of *Axl* and *Mertk* in macrophages. Notably, an even more pronounced reduction in mRNA levels of *Ucp1* was observed in ingWAT along with a reduction in *Prdm16*, *Ppargc1a* (encoding PGC-1α) and *Adrb3* (encoding the β3-adrenergic receptor) (**Figure 22, Right**). These findings suggest a marked impairment in thermogenic recruitment in both iBAT and ingWAT of *Csf1r-Cre*$^{+}$-*Axl*$^{f/f}$*Mertk*$^{f/f}$ mice.

To test whether the reduction in thermogenic gene expression impacts the ability of *Csf1r-Cre*$^{+}$-*Axl*$^{f/f}$*Mertk*$^{f/f}$ to perform NST during cold exposure, we performed an indirect calorimetry measurement with the same experimental conditions. Results are shown in **Figure 23**.

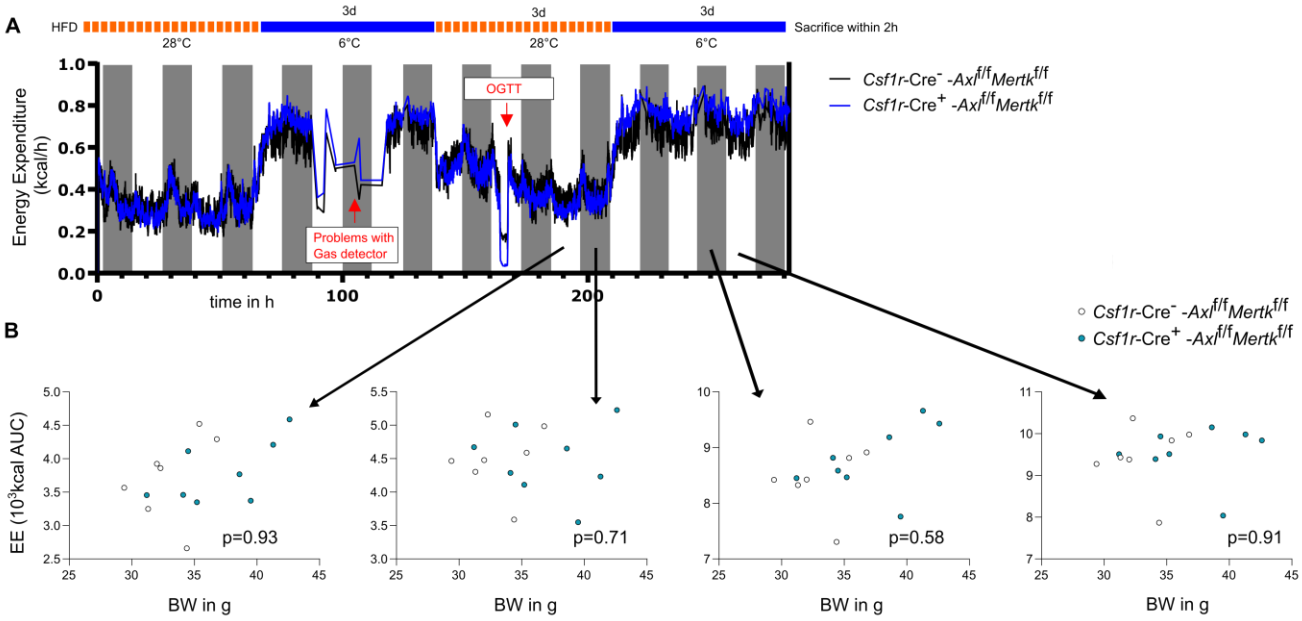

Figure 23: *Csf1r-Cre*$^{+}$*-Axl*$^{f/f}$ *Mertk*$^{f/f}$ show unchanged energy expenditure during repeated cold exposure after prolonged high-fat diet feeding at thermoneutrality. Experimental layout and indirect calorimetry results of male *Csf1r-Cre*$^{-}$*-Axl*$^{f/f}$*Mertk*$^{f/f}$ and *Csf1r-Cre*$^{+}$*-Axl*$^{f/f}$*Mertk*$^{f/f}$ mice that were fed a HFD under thermoneutral housing conditions and were exposed to repeated cold cycles. Mean Energy expenditure results for the two mouse strain over the experiment (**A**) and analysis comparing area-under-the-curve (AUC) values for selected day and night cycles under consideration of bodyweight (**B**). Each datapoint corresponds to one mouse. n=7/8. p-values in (B) were determined using analysis of covariates (ANCOVA).

Despite reduced thermogenic gene expression in iBAT and ingWAT of *Csf1r-Cre*$^{+}$*-Axl*$^{f/f}$*Mertk*$^{f/f}$ mice, no difference in energy expenditure could be found between *Csf1r-Cre*$^{-}$*-Axl*$^{f/f}$*Mertk*$^{f/f}$ and *Csf1r-Cre*$^{+}$*-Axl*$^{f/f}$*Mertk*$^{f/f}$ mice, either in absolute terms (**Figure 23, A**) or when accounting for bodyweight as a covariate (**Figure 23, B**). Similarly, no significant differences were detected in other metabolic parameters, such as the respiratory exchange ratio (RER) (**data not shown**).

These findings are consistent with unchanged UCP1 protein levels in iBAT of *Csf1r-Cre*$^{+}$*-Axl*$^{f/f}$*Mertk*$^{f/f}$ mice relative to controls, as shown by western blot (**Figure 24, A**) and histological analysis (**Figure 24, B and C**). UCP1 protein levels in ingWAT were too low in either genotype to be reliably quantified by western blot or histological staining (**western blot data not shown, Figure 24, B**).

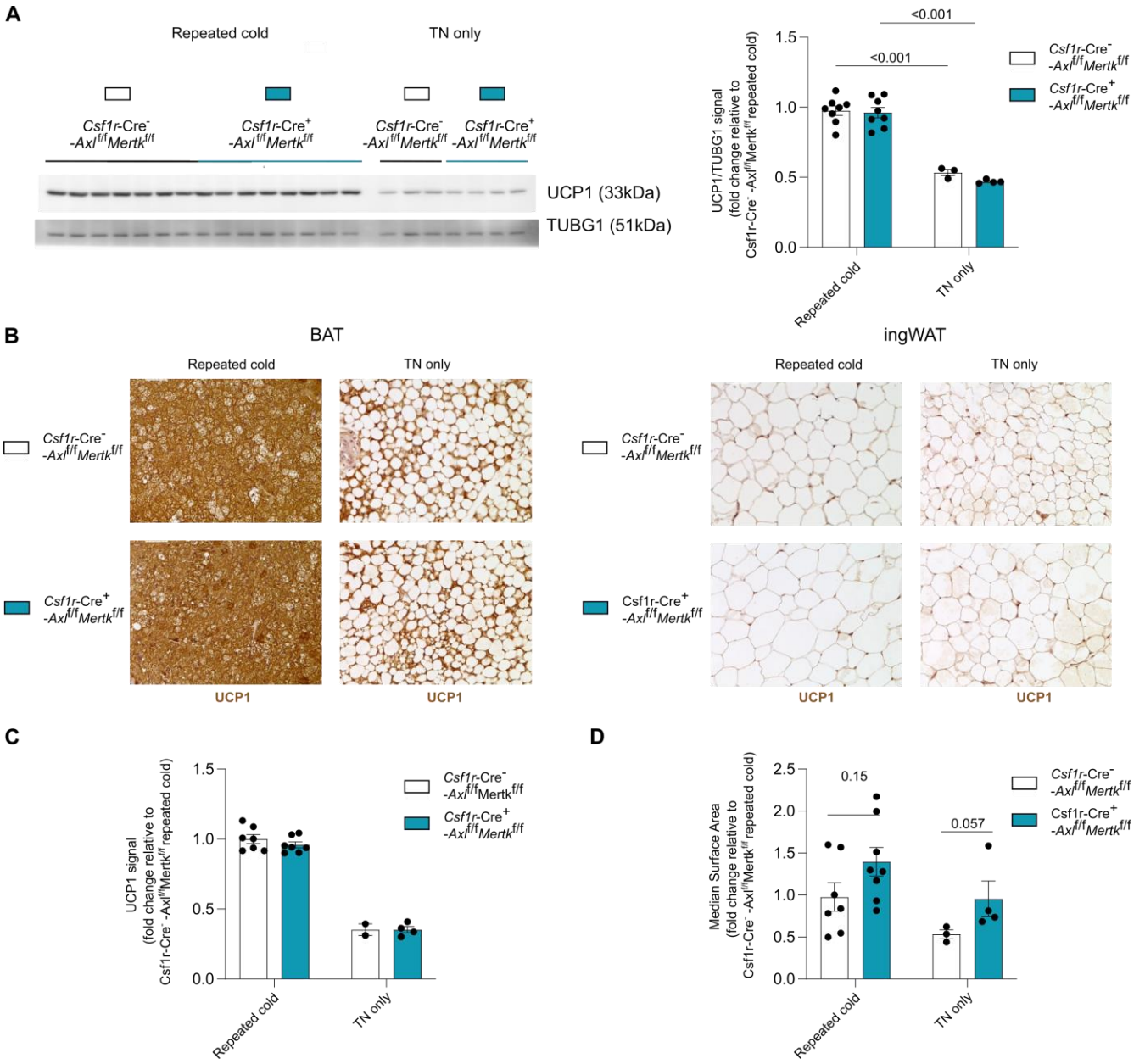

Figure 24: No difference in UCP1 protein levels in iBAT and ingWAT between *Csf1r-Cre⁻-Axl$^{f/f}$Mertk$^{f/f}$* f and *Csf1r-Cre⁺-Axl$^{f/f}$Mertk$^{f/f}$* mice after HFD feeding and repeated cold exposure. (**A**) UCP1 to total TUBG1 ratio in iBAT as assessed by western blotting iBAT of male *Csf1r-Cre⁻-Axl$^{f/f}$Mertk$^{f/f}$* and *Csf1r-Cre⁺-Axl$^{f/f}$Mertk$^{f/f}$* mice after HFD feeding with and without additional repeated cold exposure. Each datapoint corresponds to one mouse. n=7/8/3/4. Mean±SEMs. 2-Way ANOVA; (**B**) Representative results of histological staining for UCP1 protein in iBAT and ingWAT of male *Csf1r-Cre⁻-Axl$^{f/f}$Mertk$^{f/f}$* and *Csf1r-Cre⁺-Axl$^{f/f}$Mertk$^{f/f}$* mice after HFD feeding with and without additional repeated cold exposure. Hematoxylin staining was used as counterstaining; (**C**) Quantification of UCP1 levels in histological sections of iBAT as well as quantification of median adipocyte surface Area (**D**) in ingWAT for sections shown in (A). Each datapoint corresponds to one mouse. n=7/8/2/4 and n=7/8/3/4 respectively. Mean±SEMs. 2-Way ANOVA. The exact experimental layout is shown in **Figure 22** and **Figure 23.**

Only a trend towards larger adipocyte size could be detected in ingWAT of *Csf1r-Cre*$^{+}$*-Axl*$^{f/f}$*Mertk*$^{f/f}$ mice (**Figure 24, D**). Larger adipocyte size is not only correlated with increased fat mass but also with insulin resistance and reduced glucose tolerance in mice and humans [245]. For this reason, we assessed the oral glucose tolerance of *Csf1r-Cre*$^{-}$*-Axl*$^{f/f}$*Mertk*$^{f/f}$ and *Csf1r-Cre*$^{+}$*-Axl*$^{f/f}$*Mertk*$^{f/f}$ mice, before and after one cycle of cold exposure.

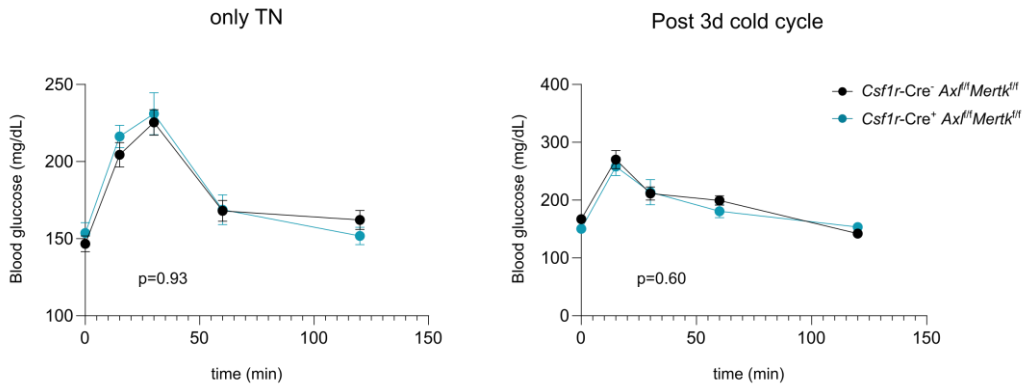

Figure 25: No difference in oral glucose tolerance between *Csf1r-Cre*$^{-}$*-Axl*$^{f/f}$*Mertk*$^{f/f}$ and *Csf1r-Cre*$^{+}$*-Axl*$^{f/f}$*Mertk*$^{f/f}$ mice after HFD feeding pre and post cold exposure. For oral glucose tolerance tests (OGTTs) a 2mg/g BW glucose-NaCl solution was gavaged into male *Csf1r-Cre*$^{-}$*-Axl*$^{f/f}$ *Mertk*$^{f/f}$ and *Csf1r-Cre*$^{+}$*-Axl*$^{f/f}$ *Mertk*$^{f/f}$ mice after HFD feeding at thermoneutral housing and after additional cold exposure for 3d. The exact timing of the OGTT after cold exposure is indicated in Fig Y. For OGTT mice were fasted for 4h before the gavage and blood glucose levels were determined at RT conditions at the timepoint indicated on the graphs. Each datapoint corresponds to one mouse. n=7/8. Mean±SEMs. AUCs were compared using Mann-Whitney tests.

No difference in blood glucose levels after oral gavage could be detected between *Csf1r-Cre*$^{-}$*-Axl*$^{f/f}$*Mertk*$^{f/f}$ and *Csf1r-Cre*$^{+}$*-Axl*$^{f/f}$*Mertk*$^{f/f}$ mice pre and post cold exposure (**Figure 25**). These results indicate that glucose clearance is not affected by *Axl* and *Mertk* deficiency in macrophages in this particular experimental setup.

Overall, results highlighted here in **3.3.2** show that mice lacking *Axl* and *Mertk* expression in macrophages and fed a HFD at thermoneutral housing conditions have no strong alterations in energy expenditure, UCP1 protein expression or oral glucose tolerance at baseline or when challenged with repeated cold exposure (**Figure 23, Figure 24** and **Figure 25**). Nevertheless, results shown in **Figure 22** strongly indicate that thermogenic recruitment on RNA level is impaired in iBAT and ingWAT of *Csf1r*-Cre^{+}*-Axl*$^{f/f}$*Mertk*$^{f/f}$ mice, possibly due to an impairment in adrenergic signaling within adipocytes.

3.3.3 Macrophage-specific *Axl* and *Mertk* deficiency reduces lipolysis in humanized adipose tissue after repeated cold exposure

Next, we analyzed major blood nutrient levels in *Csf1r-Cre*$^{-}$*-Axl*$^{f/f}$*Mertk*$^{f/f}$ and *Csf1r-Cre*$^{+}$*-Axl*$^{f/f}$*Mertk*$^{f/f}$ mice following HFD feeding under thermoneutral conditions and repeated cold exposure. Blood glucose, triglycerides, cholesterol, and NEFAs were measured after a 4-hour fasting period. Pooled results are shown in **Figure 26**.

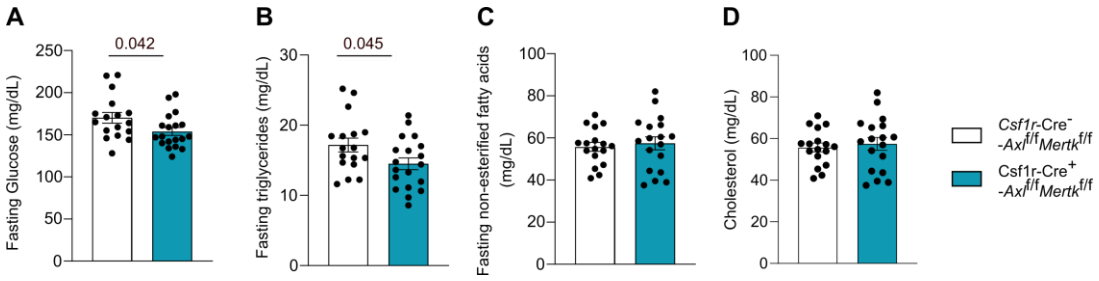

Figure 26: Reduced Fasting glucose and triglyceride levels in mice *Csf1r-Cre*$^{+}$*-Axl*$^{f/f}$ *Mertk*$^{f/f}$ mice after high-fat diet feeding and repeated cold exposure. Fasting glucose levels in blood (**A**) and fasting triglycerides (**B**), NEFA (**C**) and cholesterol (**D**) levels in plasma of male *Csf1r-Cre*$^{-}$*-Axl*$^{f/f}$*Mertk*$^{f/f}$ and *Csf1r-Cre*$^{+}$*-Axl*$^{f/f}$*Mertk*$^{f/f}$ mice that underwent HFD feeding at thermoneutral housing conditions and repeated cold exposure as depicted in **Figure 22** and **Figure 23**. Each datapoint corresponds to one mouse. n=17/19. unpaired t-tests.

After repeated cold challenge, *Csf1r-Cre*$^{+}$*-Axl*$^{f/f}$*Mertk*$^{f/f}$ mice exhibited lower fasting blood glucose levels as well as lower levels of triglycerides in systemic blood plasma (**Figure 26, A** and **B**). Fasted plasma cholesterol and NEFA levels were not different between *Csf1r-Cre*$^{-}$*-Axl*$^{f/f}$*Mertk*$^{f/f}$ and *Csf1r-Cre*$^{+}$*-Axl*$^{f/f}$*Mertk*$^{f/f}$ mice (**Figure 26, B** and **C**).

During cold exposure, BAT and WAT liberate high levels of free fatty acids from TAGs stored in lipid droplets in order to provide energy for NST [94], [185]. Similar to non-shivering thermogenesis, lipolysis is induced in adipocytes upon sensing of NE via the β3- adrenergic receptors. Downstream signaling then involves phosphorylation of PKA targets such as HSL, which in turn catalyses the hydrolysis of fatty acids from diacylglycerides [159] (See also **1.1.2**).

To test whether the altered availability of triglycerides and glucose from the blood depicted in **Figure 26** is accompanied by different rates of lipolysis between *Csf1r-Cre*$^{-}$*-Axl*$^{f/f}$*Mertk*$^{f/f}$ and *Csf1r-Cre*$^{+}$*-Axl*$^{f/f}$*Mertk*$^{f/f}$ mice, we analyzed the ratio of phosphorylated and active HSL (p563HSL) and non-phosphorylated (total) HSL in BAT and ingWAT of *Csf1r-Cre*$^{-}$*-Axl*$^{f/f}$*Mertk*$^{f/f}$ and *Csf1r-Cre*$^{+}$*-Axl*$^{f/f}$*Mertk*$^{f/f}$ mice following HFD feeding at thermoneutrality and repeated cold exposure.

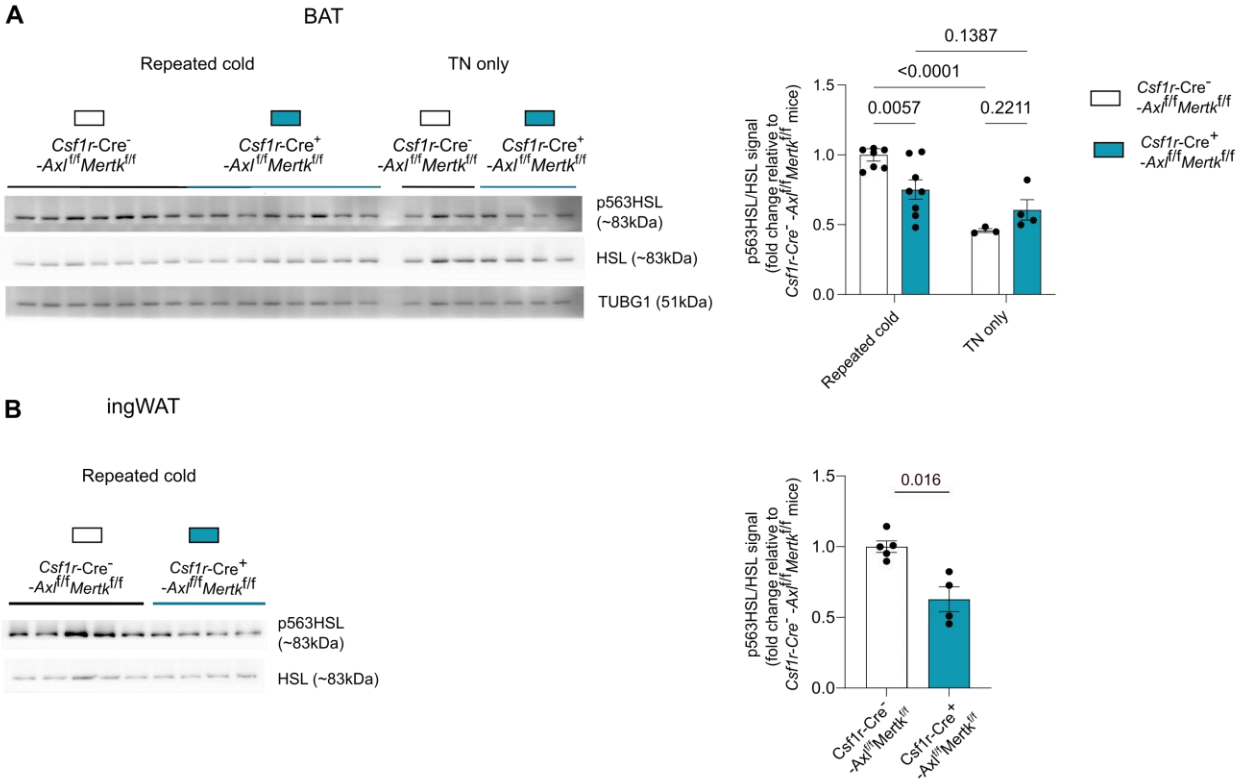

Figure 27: Reduced HSL phosphorylation in iBAT and ingWAT of *Csf1r-Cre⁺-Axl$^{f/f}$Mertk$^{f/f}$* mice after high-fat diet feeding and repeated cold exposure. p563HSL to total HSL ratio assessed by western blotting in iBAT (**A**) and ingWAT (**B**) of male *Csf1r-Cre⁻-Axl$^{f/f}$Mertk$^{f/f}$* and *Csf1r-Cre⁺-Axl$^{f/f}$Mertk$^{f/f}$* mice that underwent HFD feeding at thermoneutral housing conditions and/or repeated cold exposure as shown in in **Figure 22** and **Figure 23**. Each datapoint corresponds to one mouse. n=7/8 for iBAT and n=5/4 for ingWAT. Mean±SEMs. 2-Way ANOVA for iBAT and Mann-Whitney test for ingWAT.

Indeed, *Csf1r-Cre⁺-Axl$^{f/f}$Mertk$^{f/f}$* mice exhibited lower p563HSL to HSL ratio in iBAT as well as in ingWAT after HFD feeding and repeated cold exposure. This was not the case for *Csf1r-Cre⁻-Axl$^{f/f}$Mertk$^{f/f}$* and *Csf1r-Cre⁺-Axl$^{f/f}$Mertk$^{f/f}$* mice kept at thermoneutral housing conditions only (**Figure 27, A**). These results suggest that the adipose tissues of *Csf1r-Cre⁺-Axl$^{f/f}$Mertk$^{f/f}$* mice are unable to fully upregulate lipolysis specifically in response to adrenergic stimulus. To further address this hypothesis, we performed an experiment where we induced lipolysis *ex vivo* in iBAT explants of *Csf1r-Cre⁻-Axl$^{f/f}$Mertk$^{f/f}$* and Csf1r-Cre⁺-*Axl$^{f/f}$Mertk$^{f/f}$* mice using NE. Before harvesting the adipose tissues, the mice again underwent HFD feeding at thermoneutrality as well as repeated cold challenge. As a readout for lipolysis, NEFA levels were determined in cell culture supernatants after incubating BAT explants in them for 1h and 4h with and without additional NE stimulation.

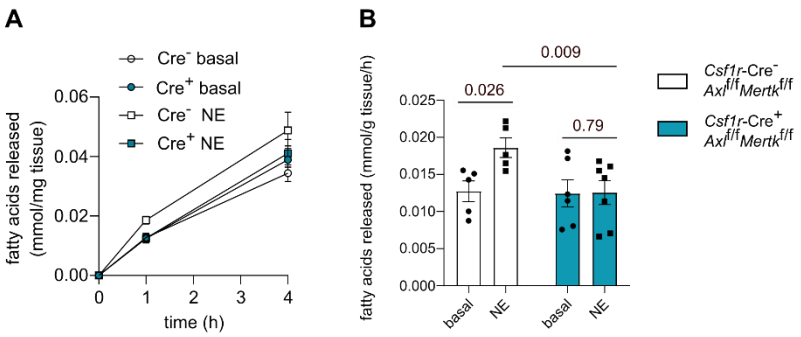

Figure 28: BAT explants of Csf1r-Cre⁺-Axl$^{f/f}$Mertk$^{f/f}$ mice do not release fatty acids after stimulation with NE after mice have been challenged with high-fat diet feeding and repeated cold exposure. Secretion of NEFAs by BAT explants of male *Csf1r-Cre⁻-Axl$^{f/f}$ Mertk$^{f/f}$* and *Csf1r-Cre⁺-Axl$^{f/f}$ Mertk$^{f/f}$* mice into cell culture medium after 1h and 4h (**A**) and 1h only (**B**) with and without stimulation with 1μM NE. BAT explants were prepared from *Csf1r-Cre⁻-Axl$^{f/f}$ Mertk$^{f/f}$* and *Csf1r-Cre⁺-Axl$^{f/f}$ Mertk$^{f/f}$* mice that underwent HFD feeding at thermoneutral housing conditions and repeated cold exposure as shown in in **Figure 22** and **Figure 23**. Each datapoint corresponds to one mouse. n=5/6. Mean±SEMs. 2-way ANOVA.

Matching the results shown in **Figure 27**, BAT explants of *Csf1r-Cre⁺-Axl$^{f/f}$Mertk$^{f/f}$* mice were unable to significantly induce lipolysis in response to NE stimulation. This was different to BAT explants from *Csf1r-Cre⁻-Axl$^{f/f}$Mertk$^{f/f}$* mice (**Figure 28, A** and **B**). Thus, these results directly link *Axl* and *Mertk* deletion in macrophages to an inability of adipocytes to perform lipolysis in response to adrenergic stimulation.

Finally, we performed an experiment in which we maximally activated adipose tissue lipolysis and thermogenesis, via injection of the β3 adrenergic agonist CL316,243 [246], [247]. In this experiment *Csf1r-Cre⁻-Axl$^{f/f}$Mertk$^{f/f}$* and *Csf1r-Cre⁺-Axl$^{f/f}$Mertk$^{f/f}$* mice underwent HFD feeding at thermoneutral housing conditions as well as three cycles of repeated cold exposure, before they were subcutaneously injected with CL316,243 at 1mg/kg BW at thermoneutral temperature. The whole experiment was carried out in the indirect calorimetry system (Sable System®), allowing tight control of environmental conditions as well as observation of mouse energy expenditure and other physiological parameters. The experimental design is detailed in **Figure 29**, alongside western blot results on the lipolytic activation of iBAT and ingWAT.

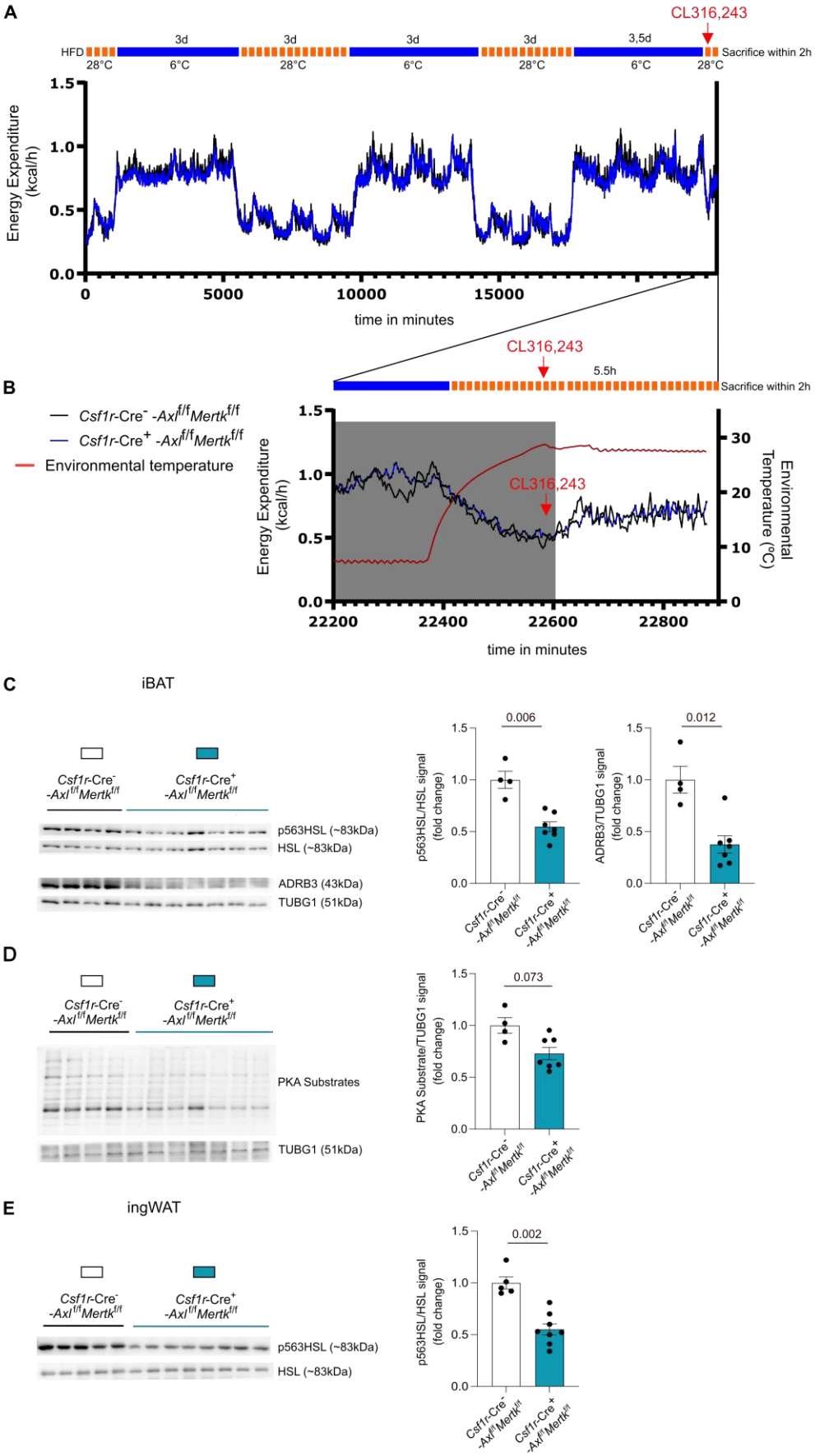

Figure 29: Csf1r-Cre^{+}-Axl$^{f/f}$Mertk$^{f/f}$ show unchanged energy expenditure but reduced HSL phosphorylation after high-fat diet feeding, repeated cold exposure and injection of CL316,243. Experimental Layout and indirect calorimetry results of male *Csf1r-Cre^{-}-Axl$^{f/f}$Mertk$^{f/f}$* and *Csf1r-Cre^{+}-Axl$^{f/f}$Mertk$^{f/f}$* mice that were fed a HFD under thermoneutral housing conditions (**A**) during repeated cold exposure cycles and (**B**) directly after subcutaneous injection of CL316,243 at 1mg/kg BW; n=5/8. (**C**) pHSL, HSL, ADRB3, TUBG1 (**C**) and PKA substrate phosphorylation levels (**D**) in iBAT + pHSL and HSL protein levels in ingWAT (**E**) of male *Csf1r-Cre^{-}-Axl$^{f/f}$Mertk$^{f/f}$* and *Csf1r-Cre^{+}-Axl$^{f/f}$Mertk$^{f/f}$* mice that were fed a HFD under thermoneutral housing conditions after repeated cold exposure cycles and a final injection of after subcutaneous injection of CL316,243 at 1mg/kg BW. Each datapoint corresponds to one mouse. n=5/8 for indirect calorimetry and ingWAT western blot. n=4/8 for iBAT western blot. Mean±SEMs. Mann-Whitney tests.

Energy expenditure did not differ between *Csf1r-Cre*$^{-}$*-Axl*$^{f/f}$*Mertk*$^{f/f}$ and *Csf1r-Cre*$^{+}$*-Axl*$^{f/f}$*Mertk*$^{f/f}$ mice, either throughout the cold cycles (**Figure 29, A**) or following CL316,243 injection (**Figure 29, B**). These findings, consistent with previous data (**Figure 19** and **Figure 23**), suggest that energy expenditure is not the primary process affected by the loss of *Axl* and *Mertk* in macrophages. Notably, we observed reduced HSL phosphorylation (p563 HSL) in both iBAT and ingWAT of *Csf1r-Cre*$^{+}$*-Axl*$^{f/f}$*Mertk*$^{f/f}$ mice compared to *Csf1r-Cre*$^{-}$*-Axl*$^{f/f}$*Mertk*$^{f/f}$ controls (**Figure 29, C and E**). This reduction was even more pronounced than in earlier experiments, supporting the idea that CL316,243 maximally induces HSL phosphorylation at least in *Csf1r-Cre*$^{-}$*-Axl*$^{f/f}$*Mertk*$^{f/f}$ control mice. Interestingly, ADRB3 protein levels were significantly lower in iBAT of *Csf1r-Cre*$^{+}$*-Axl*$^{f/f}$*Mertk*$^{f/f}$ mice (**Figure 29, C**), and phosphorylation of PKA substrates also trended lower (**Figure 29, D**).

In summary, results presented in **3.3.4** demonstrate that AXL and MERTK-dependent efferocytosis in macrophages can influence adipocyte physiology, impairing their response to adrenergic stimulation and subsequent lipolysis.

3.3.4 *Axl* and *Mertk* expression in macrophages controls macrophage infiltration and polarization into humanized ingWAT upon repeated cold challenge

To dive deeper into the potential causes for the reduced adipose tissue adrenergic activation in *Csf1r-Cre*$^{+}$*-Axl*$^{f/f}$*Mertk*$^{f/f}$ mice, we assessed levels of tyrosine hydroxylase (TH) protein in iBAT and ingWAT of *Csf1r-Cre*$^{-}$*-Axl*$^{f/f}$*Mertk*$^{f/f}$ and *Csf1r-Cre*$^{+}$*-Axl*$^{f/f}$*Mertk*$^{f/f}$ mice that had undergone HFD at thermoneutral conditions and were subjected to repeated cold challenge. TH is the rate limiting enzyme in the synthesis of NE within sympathetic neurons in adipose tissue. Commonly, total TH protein levels assessed by western blotting are used to assess the overall degree of innervation within a tissue [248]. At the same time, also total protein levels of the macrophage protein MAC2 were determined as a proxy for macrophage infiltration into the tissue.

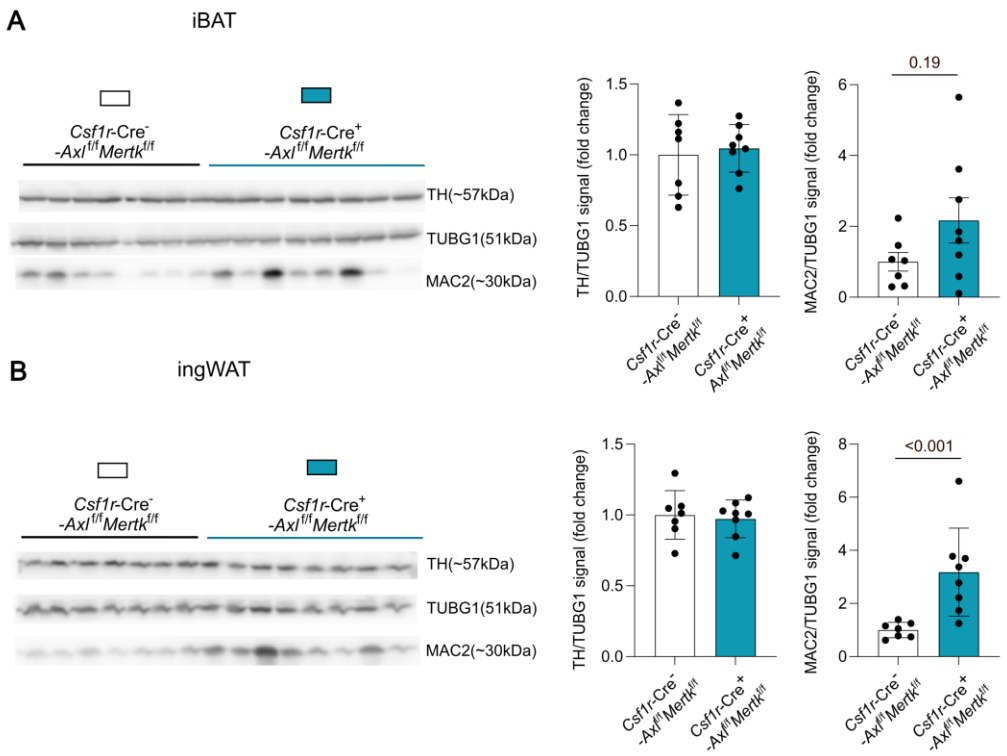

Figure 30: Unchanged TH and increased MAC2 protein levels in iBAT and ingWAT of *Csf1r-Cre*$^{+}$-*Axl*$^{f/f}$*Mertk*$^{f/f}$ mice after HFD feeding and repeated cold exposure. Western blotting results for TH, MAC2 and gamma Tubulin (gT) in iBAT (**A**) and ingWAT (**B**) of male *Csf1r-Cre*$^{-}$-*Axl*$^{f/f}$*Mertk*$^{f/f}$ and *Csf1r-Cre*$^{+}$-*Axl*$^{f/f}$*Mertk*$^{f/f}$ mice after HFD feeding at thermoneutral housing conditions and repeated cold exposure as shown in **Figure 22** and **Figure 23**. Each datapoint corresponds to one mouse. n=7/8. Mean±SEMs. Mann-Whitney tests.

Similar levels of TH were detected in iBAT and ingWAT between *Csf1r-Cre*$^{-}$-*Axl*$^{f/f}$*Mertk*$^{f/f}$ and *Csf1r-Cre*$^{+}$-*Axl*$^{f/f}$*Mertk*$^{f/f}$ mice, suggesting that the reduced adrenergic activation observed in adipose tissue of *Csf1r-Cre*$^{+}$-*Axl*$^{f/f}$*Mertk*$^{f/f}$ mice is not due to alterations in the innervation between the two mouse strains (**Figure 30, A** and **B**). On the other hand, significantly higher levels of MAC2 protein were detected in ingWAT of *Csf1r-Cre*$^{+}$-Axl$^{f/f}$*Mertk*$^{f/f}$ mice indicating substantial macrophage infiltration into the tissue. In the same line, a weak trend towards more MAC2 protein could also be observed in iBAT of *Csf1r-Cre*$^{+}$-*Axl*$^{f/f}$*Mertk*$^{f/f}$ mice (**Figure 30, A** and **B**).

Macrophage infiltration into tissues is often accompanied by a shift towards a pro-inflammatory phenotype [10], [66]. To determine whether this occurs in the adipose tissues of *Csf1r-Cre*$^{+}$-*Axl*$^{f/f}$*Mertk*$^{f/f}$ mice, we performed flow cytometric analysis of iBAT and ingWAT macrophages from both *Csf1r-Cre*$^{-}$-*Axl*$^{f/f}$*Mertk*$^{f/f}$ and *Csf1r-Cre*$^{+}$-*Axl*$^{f/f}$*Mertk*$^{f/f}$ mice following HFD feeding under thermoneutral conditions and repeated cold exposure. Flow cytometry was conducted by **Dr. Imke Liebold**, and the gating strategy, along with the results, is presented in **Figure 31**.

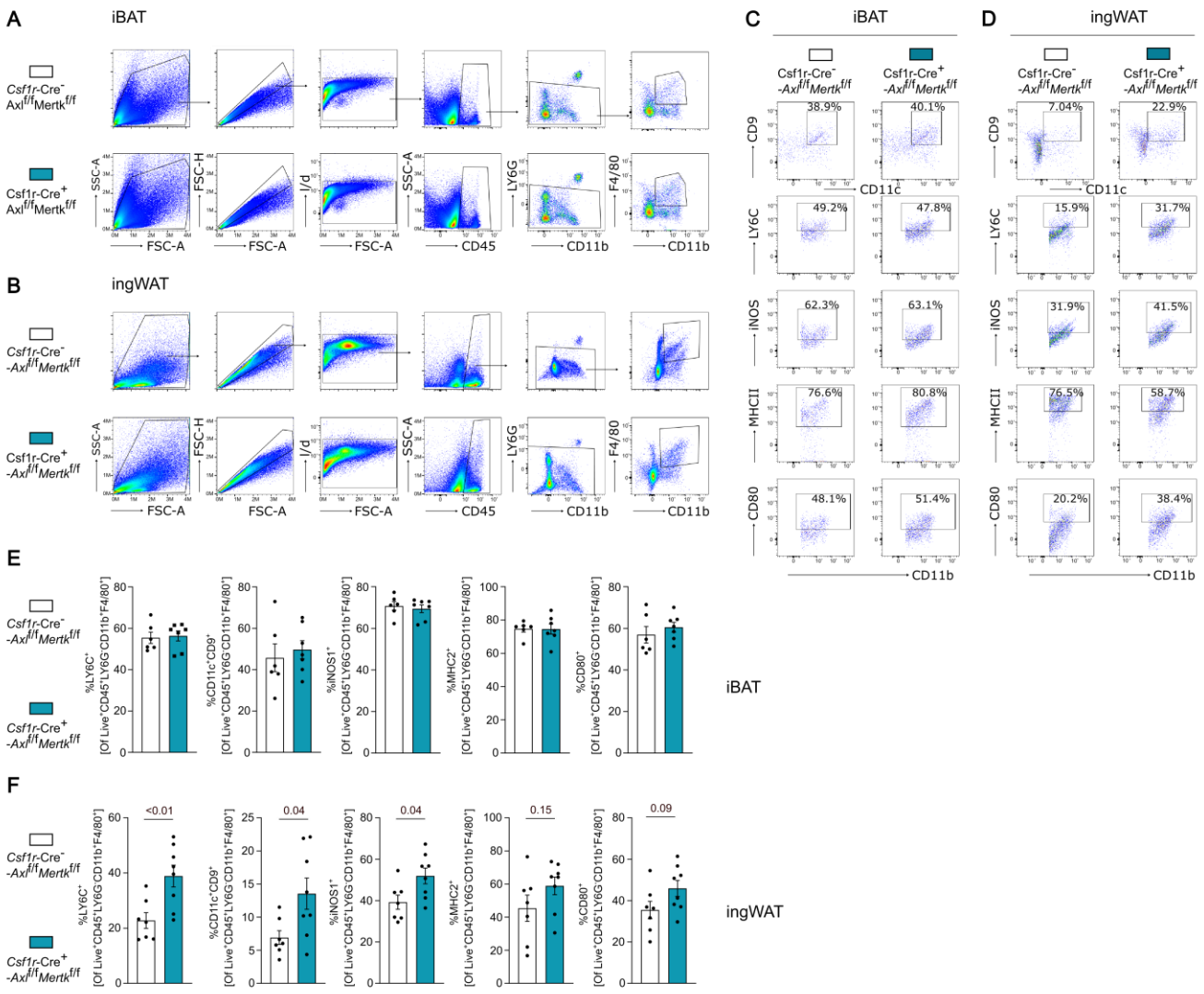

Figure 31: Increased frequency of pro-inflammatory macrophages in ingWAT of Csf1r-Cre+-Axlf/f Mertkf/f mice after HFD feeding and repeated cold exposure. Gating strategy (**A+B**) and representative dotplots (**C**) of flow cytometric analysis comparing iBAT (**D**) ingWAT (**E**) macrophages between male *Csf1r-Cre⁻-Axl*$^{f/f}$*Mertk*$^{f/f}$ and *Csf1r-Cre⁺-Axl*$^{f/f}$*Mertk*$^{f/f}$ mice after HFD feeding at thermoneutral housing conditions and repeated cold exposure as depicted in **Figure 22** and **Figure 23**. Each datapoint corresponds to one mouse. n=6/7 for iBAT and n=7/8 for ingWAT. Mean±SEMs. Mann-Whitney tests.

No major phenotypic differences were observed in BAT macrophages from *Csf1r-Cre⁺-Axl*$^{f/f}$*Mertk*$^{f/f}$ mice compared to their littermate controls (*Csf1r-Cre⁻-Axl*$^{f/f}$*Mertk*$^{f/f}$, **Figure 31, E**). However, changes in thermogenic and lipolytic activity were accompanied by a higher frequency of monocyte-derived LY6C$^+$ cells and lipid-associated (CD11c$^+$CD9$^+$ [211] ,[241], [242]) macrophages, among all CD45$^+$LY6G$^-$CD11b$^+$F4/80$^+$ macrophages in ingWAT of *Csf1r-Cre⁺-Axl*$^{f/f}$*Mertk*$^{f/f}$ mice (**Figure 31, F**). Moreover, ingWAT macrophages in *Csf1r-Cre⁺-Axl*$^{f/f}$*Mertk*$^{f/f}$ mice displayed a more

pro-inflammatory phenotype, evidenced by a significantly higher frequency of iNOS1^{+} macrophages and a trend towards higher expression of the antigen presentation molecule MHCII as well as of the co-stimulatory molecule CD80 (**Figure 31, F**) [234], [249], [250].

This pro-inflammatory profile in ingWAT was further supported by significantly higher mRNA levels of the pro-inflammatory cytokines *Tnf* and *Il6* at the whole-tissue level (**Figure 32, Right**). Moreover, ingWAT of *Csf1r-Cre*$^{+}$*-Axl*$^{f/f}$*Mertk*$^{f/f}$ mice showed higher expression of *Emr1* and *Trem2*, supporting the idea of macrophage infiltration and partial induction of LAM identity suggested by **Figure 30** and **Figure 31** (**Figure 32, E**). No significantly higher expression of inflammation associated genes could be detected in iBAT of *Csf1r-Cre*$^{+}$*-Axl*$^{f/f}$*Mertk*$^{f/f}$ mice, however sample sizes were also much smaller due to technical limitations (**Figure 32, Left**). Nonetheless, consistent with other results presented in **3.3.2**, **3.3.3** and **3.3.4**, the effects of *Axl* and *Mertk* deficiency in macrophages on adipose tissue inflammation seemed more pronounced in ingWAT as compared to iBAT.

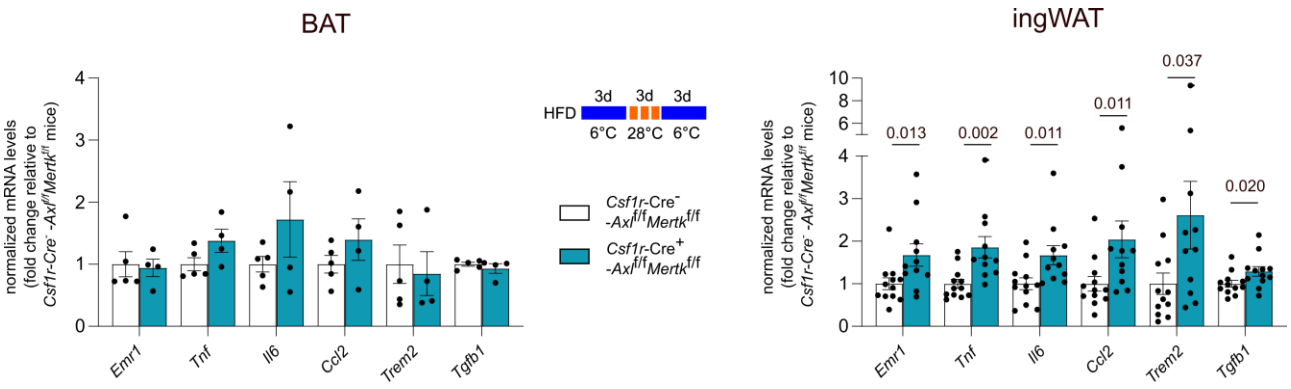

Figure 32: Increased expression of inflammatory genes in ingWAT of *Csf1r-Cre*$^{+}$*-Axl*$^{f/f}$*Mertk*$^{f/f}$ *mice* after HFD feeding and repeated cold exposure. Expression of inflammatory genes assessed by RT-qPCR in iBAT and ingWAT of male *Csf1r-Cre*$^{-}$*-Axl*$^{f/f}$*Mertk*$^{f/f}$ and *Csf1r-Cre*$^{+}$*-Axl*$^{f/f}$*Mertk*$^{f/f}$ mice after HFD feeding at thermoneutral housing conditions and repeated cold exposure as depicted in **Figure 22** and **Figure 23**. Each datapoint corresponds to one mouse. n=5/4 and n=12/11 respectively. Mean±SEMs. Mann-Whitney tests.

Taken together, these results suggest that reduced adipose tissue adrenergic activation in *Csf1r-Cre*$^{+}$*-Axl*$^{f/f}$*Mertk*$^{f/f}$ mice is associated with significant infiltration of inflammatory macrophages into ingWAT. Given that TNF-α has been shown to directly suppress β3-adrenergic receptor expression in adipocytes [251], inflammation may represent a key link between *Axl* and *Mertk* expression in macrophages and adipose tissue sensitivity to adrenergic activation. However, whether an altered inflammatory state in adipose tissue can fully explain the effects observed on thermogenic gene expression and lipolysis remains to be determined.

4. Discussion

4.1 Regulation of efferocytosis in macrophages by norepinephrine

In this work, we observed that F4/80$^+$Cd11b$^+$ iBAT and ingWAT macrophages isolated from cold housed mice, had a significantly higher capacity to perform efferocytosis of apoptotic thymocytes compared to mice that were housed at thermoneutral conditions (**Figure 6**). This increase in efferocytosis capacity upon cold housing was associated with a higher frequency of ATMs expressing efferocytosis receptors such as MERTK as well as with an anti-inflammatory and proliferative ATM phenotype (**Figure 12** and **Figure 13**). Overall, the most pronounced and stable effects of cold exposure on macrophage efferocytosis and *Mertk* expression were observed in iBAT, which also showed the highest absolute levels of efferocytosis (**Figure 6**). The strong response of BAT macrophages to cold thereby fits its dense innervation and the idea that high local NE levels drive this effect. Furthermore, it supports the idea that the high remodeling potential and increased resistance to inflammation observed in BAT [252], [253], [254] may stem from enhanced local efferocytosis.

Cold housing also significantly increased efferocytosis in ingWAT macrophages but not gWAT macrophages (**Figure 6**) and increased mRNA levels of *Mertk* in ingWAT Cd11b$^+$ cells (**Figure 12**). Cold housing had no effect on *Mertk* mRNA levels in gWAT Cd11b$^+$ cells (**Figure *13***) and surface MERTK protein was not increased in ingWAT macrophages following cold challenge (**Figure 12**). Notably, the baseline rate of efferocytosis in ingWAT macrophages was low, not exceeding 5% even for cold housed mice (**Figure 6**). If this indeed reflects an inherent property of ingWAT macrophages is thereby unclear. Instead, this might be connected to technical limitations, since as compared to gWAT and iBAT macrophages, ingWAT macrophages were less viable (**Figure 6**). Lower cell viability *ex vivo* is thereby unlikely to explain the discrepancy between higher efferocytic function and *Mertk* mRNA levels in ingWAT macrophages after cold challenge (**Figure 6**, **Figure 13** and **Figure 12**) and the lack of change in MERTK surface protein (**Figure 12**). Another explanation for this discrepancy may be that MERTK can undergo proteolytic cleavage following apoptotic cell engagement, potentially masking protein-level changes *in vivo* [255], [256]. Furthermore, transcriptional, translational, and functional kinetics are not always literally correlated, and we have not deeply studied the kinetics of the cold induced efferocytic phenotype in ATMs. Results may also simply be limited by sample size. Unfortunately, MERTK protein expression was not measured for gWAT macrophages, but the lack of significant induction of efferocytosis or *Mertk* mRNA levels by cold challenge in these cells is consistent with the idea that gWAT is less reactive to cold challenge compared to iBAT and ingWAT, due to a lower degree of innervation [177]. Instead gWAT is more susceptible to p53-dependend LAM recruitment following repeated catabolic stimulus [213], which could be related to a weaker NE-dependent induction of efferocytosis in gWAT macrophages. Future studies should therefore explore the efferocytosis potential of different ATM populations

under varying conditions of tissue stress and local norepinephrine secretion, possibly also by providing labeled apoptotic cells *in vivo*. While the Ki67 staining presented in **Figure 12** already provides some indirect evidence of enhanced ATM efferocytosis upon cold challenge [65], also other downstream effects could be investigated such as alterations in macrophage OXPHOS capacity [40]. The next challenge would then be to disentangle any changes from other metabolic cues encountered by ATMs such as potential cold-induced changes in the lipid microenvironment.

Importantly. the effect of cold housing on efferocytosis of iBAT and ingWAT macrophages could be recapitulated *in vitro* by treating bone marrow derived macrophages (BMDMs) with NE conditioned brown adipocyte supernatant or NE directly (**Figure 7** and **Figure 8**). This induction was clearly dependent on the adrenergic β2 receptor which is the most highly expressed in nearly all macrophages including BMDMs [225], [257], [258] and could be further replicated with other β2 agonists such as formoterol or isoproterenol (**Figure 10** and **Figure 8**).

The fact that efferocytosis induction in macrophages depends on β2-signaling, as opposed to NE specifically, thereby has upsides for the translation into clinical settings as NE might not always have the desired pharmacological properties [259]. Moreover, NE does not have the strongest affinity to β2 receptors [260] so other compounds could potentially be used at much lower dosages. For this, more detailed dose response curves would have to be determined. Results also suggest that simultaneous engagement of other adrenergic receptors, which is expected with NE but not with formoterol, has no additional stimulating or inhibitory effects on efferocytosis (**Figure *8***). The comparatively lower effect size of NE stimulation on efferocytosis *in vitro,* relative to the effect of cold exposure *in vivo,* might thereby be explained by the fact that BMDMs, differentiated under the conditions used in this thesis, are already highly efferocytic. On the other hand, the presented results only show that NE can induce efferocytosis in macrophages *in principle* and they do not provide evidence that the enhanced efferocytic capacity of ATMs observed during cold housing is solely mediated by NE signaling. The most definitive approach to address this would be to study the efferocytic capacity of ATMs isolated from animals carrying a macrophage-specific deletion of the β2-adrenergic receptor after cold challenge. Another simpler option would be to perform co-cultures between adipocytes and β2 deficient macrophages *in vitro*. If NE is still able to induce efferocytosis in BMDMs in this setting, there are likely additional factors released by NE-activated adipocytes that can drive macrophage efferocytosis. Potential factors could then be investigated, for example, through proteomic analysis of the resulting adipocyte supernatant. While β2-adrenergic signaling alone can induce efferocytosis (**Figure *8***), it indeed seems likely that multiple signals are integrated *in vivo*, including IL4 and other factors secreted by activated BAT, which together ultimately determine ATM efferocytic function. Interactions like this add further complexity to the regulation of efferocytosis by NE and may modulate the response to meet the specific situational requirements in adipose tissue or beyond.

Adrenergic stimulation of BMDMs was able to directly induce mRNA expression of *Axl* and *Mertk* as well as of several LXR downstream targets including *Abca1* (**Figure 9**). Importantly, NE stimulation was not able to induce efferocytosis in *Axl* and *Mertk* deficient BMDMs, suggesting a direct involvement of *Axl* and *Mertk* in the induction of efferocytosis by NE (**Figure 11).** The involvement of LXR signaling is also supported by *in vivo* data, since *Abca1* mRNA expression was significantly induced in iBAT Cd11b^{+} cells following cold challenge. However, cold exposure was also able to induce the expression of efferocytosis receptors CD36 and TIM4 in both iBAT and ingWAT (**Figure 12**). Both receptors have no reported ties with LXR signaling and have been shown to influence the efficiency by which macrophages take up apoptotic T cells [261], [262]. Therefore, further studies will be necessary to test whether AXL and MERTK regulation is really causing the increased efferocytosis capacity of macrophages after NE treatment or whether these receptors play more of a permissive role. For this, the contribution of other efferocytosis receptors to the induction of efferocytosis by NE could be investigated using gene silencing or knockout BMDMs. Also controlled overexpression of both *Axl* and *Mertk* could be performed, to test whether increased *Axl* and *Mertk* expression can lead to higher efferocytosis rates for apoptotic T cells. A first step could also be to simply repeat experiments presented in **Figure 6** and to assess the overlap between macrophages that perform efferocytosis *ex vivo* and macrophages that express AXL or MERTK.

In addition, the exact pathways by which NE signaling is linked to *Axl* and *Mertk* expression need further verification. Several LXR downstream targets were regulated by NE *in vitro* and by cold *in vivo,* but so were non-LXR targets (**Figure 9**, **Figure 12** and **Figure 13**). NE has been shown to induce many signaling pathways in macrophages, including also Erk1/2 signaling, which mediates downstream effects of MERTK after apoptotic cell engagement [65], [263]. Furthermore, adrenergic signaling promotes macrophage anti-inflammatory signaling, which intersects with efferocytosis receptor expression at many points [257], [264]. To prove an involvement of LXR, LXR deficient BMDMs could be used and treated with NE, to test for dependency of the NE-induced efferocytic response on this gene. In addition, various gene silencing approaches could be used to rule out the involvement of other pathways piece by piece. Finally, NE stimulation of β2 knockout BMDMs *in vitro* might be helpful to eliminate potential sources of noise from engagement of other adrenergic receptors, which do not lead to efferocytosis induction.

If LXR signaling is indeed involved in the NE-induced increase in macrophage efferocytosis, the next question is how β2-adrenergic signaling connects to LXR activity. NE has been shown to modulate lipid metabolism in macrophages [265] and LXR may respond to changes in intracellular cholesterol dynamics [266]. To investigate this, macrophage lipid composition could be analyzed following β2-agonist treatment using lipidomic approaches. Additionally, intracellular cholesterol trafficking could be examined through high-resolution imaging techniques. Furthermore, we have not accounted for efferocytosis occurring *between* BMDMs during treatments. NE may influence the extent of cell death in BMDM cultures or modulate efferocytosis via alternative pathways, both of

which could indirectly activate LXR [53]. To address this, *in vitro* treatments could be repeated in the presence of Annexin V which competitively binds to phosphatidylserine on apoptotic cells, preventing macrophage recognition [267]. If LXR targets are still upregulated in response to NE, this would suggest a cell intrinsic effect. Elucidating the exact pathways by which β2-signaling increases efferocytosis will be crucial for any attempts to translate findings into therapeutic approaches. The same goes for translating findings into the human settings.

In agreement with the data collected *in vitro,* injection of NE into wild-type mice resulted in increased efferocytosis in a subset of $F4/80^{+}Cd11b^{+}LY6C^{-}CX3CR1^{+}$ BAT macrophages, likely tissue resident cells (**Figure 14**) [237], [268]. Efferocytosis of apoptotic thymocytes was not significantly higher after NE injection in WAT macrophages (**Figure 14**), although this does not necessarily have to reflect an inherent difference in their response to NE. More likely, NE is readily degraded *in vivo* [259] and was only able to penetrate deep enough into BAT, which is highly vascularized [124]. It therefore remains to be determined whether BAT macrophages are intrinsically more responsive to NE or if the depot dependency observed was due to technical limitations. The same holds true for $CX3CR1^{+}LY6C^{-}$ ATMs vs $LY6C^{+}$ cells. One approach to test this would be to use other β2 agonists in the next experiment, which are more stable *in vivo*. To disentangle effects between $CX3CR1^{+}LY6C^{-}$ ATMs vs $LY6C^{+}$ cells, also larger sample sizes and cell numbers will be necessary. However, the fact that the response favors $CX3CR1^{+}$ cells fits the reported connection between CX3CR1 and macrophage chemotaxis towards apoptotic lymphocytes [16].

Based on the findings described above, we propose that NE-induced efferocytosis enables macrophages to manage increased cell death during cold-induced adipose tissue remodeling. This is supported by elevated expression of apoptosis-related genes in iBAT under cold conditions (**Figure 15**). Furthermore, we suggest that NE-driven engagement of apoptotic cells may synergize with IL4 to promote the tissue remodeling phenotype observed in ATMs (**Figure 12**). Supporting this, cold exposure increases IL4 levels in iBAT (**Figure 16**), (as has been shown in the past by Nguyen et al. (2011) [229] and Qiu Y et al. (2014) [219] and NE directly induces expression of the IL4 receptor (IL4ra) in BMDMs (**Figure 9**).

However, the exact response of macrophages to IL4 depends on the specific type of apoptotic cells that are recognized [60]. Yet, this thesis does not directly address which cells exactly undergo apoptosis upon cold exposure. This should therefore be assessed by histological approaches using for example TUNEL staining, or by screening apoptotic cells using AnnexinV/PI staining and flow cytometry. Moreover, single cell sequencing datasets could potentially help, if analyzed accordingly. Understanding which kind of cells undergo apoptosis upon cold challenge could help

to advance our understanding of adipose tissue biology and could help to provide a more detailed understanding of the requirements posed to ATMs upon cold challenge.

It remains unclear whether the enhanced efferocytic capacity for apoptotic thymocytes following NE treatment extends to other apoptotic cell types. This would be of critical importance to understand the scope of these findings and to assess other settings in which the described induction of efferocytosis by NE might play a role. If the upregulation of *Axl* and *Mertk* is indeed responsible for the increased efferocytosis of thymocytes, one might expect NE to also enhance the uptake of other cells recognized via these receptors. MERTK in particular has long been implicated in the recognition of apoptotic lymphocytes [269], but nowadays this receptor is also strongly associated with the clearance of apoptotic neutrophils [34].

Notably, at least some of the cells undergoing apoptosis during cold exposure appear to be mature adipocytes, based on the fact that *Bax* mRNA expression is also significantly elevated in the mature mAdipocyte fraction in cold housed mice (**Figure 15**). Further studies would need to explore the role of AXL and MERTK in the recognition and clearance of apoptotic adipocytes. Large hypertrophic adipocytes are often cleared via alternative pathways distinct from classical efferocytosis. For instance, macrophages can degrade apoptotic adipocytes through exophagy - a process in which lysosomes fuse with the plasma membrane to release acidic hydrolases and enzymes, breaking down adipocytes extracellularly into smaller lipid and cellular fragments [270], [271]. Given this, the upregulation of *Axl* and *Mertk* in response to NE may primarily modulate inflammatory signaling during the extracellular breakdown of apoptotic adipocytes, rather than directly facilitating their uptake. Nonetheless, it is also possible that these receptors participate in the uptake of adipocyte-derived fragments or EVs, which might occur similarly to the uptake of small immune cells [272], [273].

As highlighted in **1.2.4** direct interactions between ATMs and NE have been previously demonstrated with consequences for adipose tissue biology and thermogenic activation [224], [225], [274]. Beyond adipose tissue, NE has also been shown to profoundly influence macrophage biology and function, including the regulation of hematopoiesis [275], promotion of anti-inflammatory polarization [276], modulation of lipid metabolism [265], as well as antimicrobial and antiviral activity [257].

To our knowledge, we are the first to provide conclusive evidence regarding a positive role for NE in regulating macrophage efferocytosis *in vitro* and *in vivo*. These findings contribute to the growing field of neuroimmune control of efferocytosis [277], [278] and potentially help to explain some of the positive effects of β2-signaling in the resolution of inflammation [279]. An axis linking NE signaling to efferocytosis and tissue remodeling may hold evolutionary significance, considering the role of SNS signaling in stress responses that demand adaptive physiological changes. Notably, a recent study reported β2-dependent downregulation of MERTK and impaired efferocytosis in PD-

L2$^+$ skin macrophages in mice following prolonged stress, which may also explain the absence of beneficial effects under more chronic stress conditions [280], [281].

Finally, evidence is slowly accumulating that adipose tissue thermogenic adaptation requires macrophages to adapt an anti-inflammatory phenotype [220], [282], [200]. Linking NE signaling in macrophages to efferocytosis, which supports anti-inflammatory polarisation, might therefore support adipose tissue function also through this route.

4.2 Impact of AXL/MERTK dependent efferocytosis on adipose tissue

Both cold housing and NE stimulation were able to induce *Axl* and *Mertk* expression in macrophages and to enhance macrophage efferocytosis in mice (**3.1**). Moreover, signs of apoptosis and increased IL4 release suggest that conditions for AXL/MERTK dependent efferocytosis and macrophage polarisation are present in murine BAT upon cold housing (**3.2**). However, no comprehensive studies have yet been performed to investigate the impact of AXL/MERTK dependent efferocytosis on adipose tissue in settings characterized by high NE levels such as cold housing.

We first demonstrated that *Axl* and *Mertk* expression in macrophages does not play a major role in BAT thermogenesis in young, lean mice exposed to cold. No genotype-dependent differences were observed in rectal temperature or BAT *Ucp1* mRNA levels when *Csf1r-Cre*$^+$*-Axl*$^{f/f}$*Mertk*$^{f/f}$ and control mice were adapted to cold temperatures (**Figure 17**). Similarly, no genotype-dependent differences in thermogenic gene expression were detected when *Csf1r-Cre*$^-$*-Axl*$^{f/f}$*Mertk*$^{f/f}$ or *Csf1r-C*re$^+$*-Axl*$^{f/f}$*Mertk*$^{f/f}$ mice were exposed to cold conditions for 4 days after prior adaptation to thermoneutral housing (**Figure 18**). Transitioning from thermoneutrality to cold however led to significantly higher levels of *Trem2* mRNA and a higher frequency of Cd11c$^+$Cd11b$^+$F4/80$^+$ macrophages in BAT of both genotypes, indicating moderate recruitment of lipid-associated macrophages (LAMs), potentially in response to increased cell death or changes in the lipid environment (**Figure 18**). Energy expenditure remained unchanged between genotypes even under repeated thermoneutral-to-cold switching or injection of CL316,243 (**Figure 19**). In the same experiment, expression of thermogenic marker genes in iBAT, ingWAT, and gWAT was unaffected by genotype, except for *Dio2*, which was significantly reduced in iBAT and ingWAT of *Csf1r-Cre* $^+$*-Axl*$^{f/f}$*Mertk*$^{f/f}$ mice (**Figure 21**). The reason for the apparent regulation of *Dio2* remains to be determined and so are the potential impacts of this regulation on adipose tissue or systemic thyroid hormone signaling. Accordingly, levels of active thyroid hormone (T3) should be measured in the blood and the thyroid gland should be investigated for abnormalities. If nothing is found, this could indeed represent an adipose tissue specific effect caused by the lack of *Axl* and *Mertk* in ATMs. However, it remains to be said that the thyroid gland is known to be susceptible to autoimmunity [283] and so are mice lacking *Mertk* expression [284].

Finally, repeated thermal switching with a final injection of CL316,243 appeared to modestly alter the macrophage landscape in *Csf1r-Cre*$^{+}$ mice, as indicated by higher *Emr1* mRNA in iBAT and gWAT and elevated frequencies of MHCII^{+} macrophages in iBAT and ingWAT (**Figure 20** and **Figure 21**). The frequencies of MHCII^{+} macrophages in gWAT were not assessed. As mentioned in **3.3.1**, MHCII is a key antigen-presenting molecule, typically associated with a more pro-inflammatory macrophage phenotype, and has been shown to be specifically and robustly induced by IFNγ through the activation of the CIITA transcriptional machinery [235], [234]. Critically, we did not assess macrophage phenotype as deeply as possible in this particular setting, as for example we did not carry out *ex vivo* stimulation of macrophages and/or subsequent cytokine staining. Single cell sequencing approaches would also have been possible here for a highly sensitive assessment of both immune cells and stromal cells at the same time. MHCII might just have been the most responsive molecule to the particular stimulus present at the time whose expression was assessed. Nonetheless, collectively, these data suggest that *Axl* and *Mertk* deficiency may lead to minor changes in the adipose inflammatory environment, especially under repeated thermal stress, but this had no consequences for thermogenic capacity.

Effects of *Axl*/*Mertk* deficiency on WAT and BAT function were most pronounced when mice were subjected to repeated cold exposure after HFD feeding at thermoneutral conditions. This aligns with the highly increased number of immune cells in ingWAT and especially iBAT in this setting [244], as well as with an increased need for tissue remodeling. In this context *Csf1r-Cre*$^{+}$*-Axl*$^{f/f}$*Mertk*$^{f/f}$ mice displayed significantly lower mRNA expression of thermogenic markers in iBAT and particularly ingWAT (**Figure 22**). These results clearly indicate lower adrenergic and thermogenic activation in *Csf1r-Cre*$^{+}$*-Axl*$^{f/f}$*Mertk*$^{f/f}$ mice. However, no significant difference in energy expenditure or iBAT UCP1 protein levels could be observed between *Csf1r-Cre*$^{-}$*-Axl*$^{f/f}$*Mertk*$^{f/f}$ and *Csf1r-Cre*$^{+}$*-Axl*$^{f/f}$*Mertk*$^{f/f}$ mice (**Figure 23, Figure 24** and **Figure 29**). Again, mRNA levels and protein levels are not always linearly correlated and the reduction in UCP1 mRNA expression in iBAT of *Csf1r-Cre*$^{+}$*-Axl*$^{f/f}$*Mertk*$^{f/f}$ mice was comparatively low (around 20%) (**Figure 22**). Unfortunately, in ingWAT, where the reduction in mRNA levels of thermogenic marker genes was much more pronounced (**Figure 22**), UCP1 protein levels were below the detection limit of the implemented western blot analysis for both *Csf1r-Cre*$^{-}$*-Axl*$^{f/f}$*Mertk*$^{f/f}$ and *Csf1r-Cre*$^{+}$*-Axl*$^{f/f}$*Mertk*$^{f/f}$ mice. Therefore, in order to be able to assess the impact of *Axl* and *Mertk* deficiency in macrophages on UCP1 protein levels in ingWAT, more sensitive approaches would have to be implemented or, even better, the experimental layout would have to be adapted so that more meaningful amounts of UCP1 protein is produced. Perhaps if the feeding period is shortened or the adrenergic stimulus is sustained for a longer time, differences in thermogenic recruitment, visible on mRNA level particularly in ingWAT, would manifest into altered thermogenic function.

Despite unaffected UCP1 protein levels, adipocyte size was higher in ingWAT of *Csf1r-Cre*$^{+}$*-Axl*$^{f/f}$*Mertk*$^{f/f}$ mice by trend (**Figure 24**). Interestingly, this was associated with significantly lower

ratios of p563HSL to HSL in both iBAT and especially ingWAT of *Csf1r-Cre*$^{+}$*-Axl*$^{f/f}$*Mertk*$^{f/f}$ mice after HFD feeding and repeated challenge (**Figure 27**) indicative of lower sympathetic responsiveness. In line, impaired lipolysis was also confirmed by lower release of non-esterified fatty acids by BAT explants (**Figure 28**) and was even more pronounced following pharmacological activation with CL316,243 (**Figure 29**). Whether the impaired lipolysis is causative for the trend towards higher adipocyte size is unclear, although such associations have been previously reported in the context of HSL-deficient mice [285]. Together, these results suggest a profound impairment of iBAT and ingWAT of *Csf1r-Cre*$^{+}$*-Axl*$^{f/f}$*Mertk*$^{f/f}$ to react to adrenergic stimuli to perform lipolysis. Similar to the effects on thermogenic gene expression, the detrimental effects of *Axl* and *Mertk* deficiency in macrophages on p563HSL to HSL ratios appeared to be larger in iBAT than in ingWAT (**Figure 22** and **Figure 29**). Theses similarities suggest a unified origin for the two effects, possibly in NE sensing or cAMP signaling. Unfortunately, NE-induced release of non-esterified fatty acids from ingWAT explants could not be assessed *ex vivo* due to technical limitations.

Csf1r-Cre^{+}*-Axl*$^{f/f}$*Mertk*$^{f/f}$ mice fed with a HFD at thermoneutrality also exhibited significantly lower fasting glucose and TG levels after repeated exposure (**Figure 26**). It thereby remains unclear whether these reductions are directly linked to impaired lipolysis, particularly since plasma levels of NEFAs - the immediate product of lipolysis - were not changed. However, NEFAs are rapidly metabolized and re-esterified into triglycerides by the liver, so a reduction in NEFA release may be masked [286]. It seems also plausible that limited free fatty acids or glycerol availability due to impaired lipolysis led to decreased hepatic triglyceride secretion and therefore a reduction in fasting plasma triglyceride levels in *Csf1r-Cre*$^{+}$*-Axl*$^{f/f}$*Mertk*$^{f/f}$ mice. Furthermore, impaired lipolysis could have led to a compensatory uptake of glucose to meet increased energy demand during cold housing [287], therefore explaining the reduced fasting glucose levels observed in *Csf1r-Cre*$^{+}$*-Axl*$^{f/f}$*Mertk*$^{f/f}$ mice. If this was the case however, this was not reflected in changes in the respiratory exchange index that aims to discriminate between the utilization of different energy sources (**data not shown**). Nonetheless, effects might have simply fallen below the detection limit. Glucose clearance during oral glucose tolerance tests was also unaffected by *Axl* and *Mertk* deficiency in macrophages, although all experiments were conducted at thermoneutrality (**Figure 25**). To investigate differential uptake of lipids or glucose into adipose tissues, more sophisticated uptake or even turnover studies should be carried out, using for example radiolabeled lipids or glucose in mice that are being actively cold challenged. With this techniques, uptake of glucose into iBAT and ingWAT could be compared between *Csf1r-Cre*$^{-}$*-Axl*$^{f/f}$*Mertk*$^{f/f}$ and *Csf1r-Cre*$^{+}$*-Axl*$^{f/f}$*Mertk*$^{f/f}$ mice and the fate of particular lipids could be determined in detail.

Finally, *Csf1r-Cre*$^{+}$*-Axl*$^{f/f}$*Mertk*$^{f/f}$ mice subjected to high-fat diet feeding at thermoneutral temperatures as well as repeated cold challenge exhibited a more pro-inflammatory environment in ingWAT, but not in iBAT. This was evidenced by higher mRNA expression of pro-inflammatory cytokines such as *Tnfα* and *Il6* in ingWAT (**Figure 32**), along with a higher frequency of Ly6C^{+} and

iNOS$^+$ infiltrating and pro-inflammatory macrophages respectively (**Figure *31***). Western blot analysis of MAC2 and higher mRNA expression of *Emr1* further support higher amounts of macrophages in ingWAT of *Csf1r-Cre*$^+$*-Axl*$^{f/f}$*Mertk*$^{f/f}$ mice (**Figure 30, Figure 32**). This exaggerated inflammatory response in ingWAT potentially results from impaired clearance of apoptotic cells or a reduction in the anti-inflammatory effects normally mediated by AXL and MERTK. Despite local inflammation, no signs of altered glucose tolerance (**Figure 25**) could be detected as well as no signs for altered insulin signaling as assessed by western blotting and measurement of insulin levels in plasma (**data not shown**).

Given the impact of *Axl* and *Mertk* deficiency in macrophages on the inflammatory environment in ingWAT, following HFD feeding and repeated cold exposure, we propose that the impaired thermogenic and lipolytic activation in *Csf1r-Cre*$^+$*-Axl*$^{f/f}$*Mertk*$^{f/f}$ mice is driven by local low-grade inflammation rather than altered SNS activity. This notion is supported by unchanged protein levels of TH protein in both iBAT and ingWAT (**Figure 30**). TNFα in particular is known to suppress lipolysis in adipose tissue by downregulating ADRB3 expression in adipocytes [251] and *Tnf*α mRNA was significantly elevated in ingWAT of *Csf1r-Cre*$^+$*-Axl*$^{f/f}$*Mertk*$^{f/f}$ mice. Furthermore, this aligns with our findings of decreased β3 mRNA and protein expression in iBAT and ingWAT of *Csf1r-Cre*$^+$*-Axl*$^{f/f}$*Mertk*$^{f/f}$ mice respectively, following high-fat diet feeding and repeated adrenergic stimulus (**Figure 22** and **Figure 29**). Genetic deletion of Tnf receptors in obese mice led to induced transcriptional activation of *Ucp1* in BAT and genetic ablation of the inflammation amplifying IκB kinase ε led to enhanced *Ucp1* expression in subcutaneous WAT of mice [288], [289]. These findings link inflammatory signaling also directly to the thermogenic activation of both iBAT and ingWAT. Importantly, TNFα is normally repressed by AXL and MERTK via their effects on NF-κB signaling [38], [39].

Still, more data needs to be collected to verify an effect of *Axl* and *Mertk* deficiency in macrophages on adipocyte β3 expression in *Csf1r-Cre*$^+$*-Axl*$^{f/f}$*Mertk*$^{f/f}$ mice after HFD feeding and repeated cold challenge. In our study, we only observed trends towards higher TNFα and IL6 release from iBAT and ingWAT of *Csf1r-Cre*$^+$*-Axl*$^{f/f}$*Mertk*$^{f/f}$ explants under these conditions (**data not shown**). This emphasizes the need for further investigation into whether TNFα or secretion of other inflammatory cytokines from *Csf1r-Cre*$^+$*-Axl*$^{f/f}$*Mertk*$^{f/f}$ represents the link between macrophage *Axl/Mertk* expression and adipocyte function. For this, TNFα expression should be directly assessed in ATMs from *Csf1r-Cre*$^+$*-Axl*$^{f/f}$*Mertk*$^{f/f}$ and *Csf1r-Cre*$^+$*-Axl*$^{f/f}$*Mertk*$^{f/f}$ mice and studies could be conducted utilizing TNFα neutralizing antibodies.

However, despite changes in mRNA expression and lipolysis rates, we did not observe elevated inflammatory signaling in iBAT of *Csf1r-Cre*$^+$*-Axl*$^{f/f}$*Mertk*$^{f/f}$ mice after HFD feeding and repeated cold challenge. This underscores the need for more sensitive methods to assess macrophage inflammatory status, such as targeted cytokine staining of BAT-resident macrophages. Should these approaches fail to reveal differences in inflammation between *Csf1r-Cre*$^+$*-Axl*$^{f/f}$*Mertk*$^{f/f}$ and

Csf1r-Cre^{-}*-Axl*$^{f/f}$*Mertk*$^{f/f}$ littermate controls, alternative mechanisms should be explored to explain the observed effects of *Axl* and *Mertk* deficiency on adipose tissue function. Especially given the known influence of macrophages on adipose SNS activity [200], more detailed histological analyses would be important to assess potential changes in adipose tissue innervation. If possible, these studies should also asses effects on vascularization, given the reported role of macrophages on angiogenesis inside and outside of adipose tissue [62], [290]. Moreover, adipose tissue macrophages secrete other factors than inflammatory cytokines that could potentially influence adipocyte differentiation and lipolysis directly [214]. How *Axl* and *Mertk* in turn could impact the secretion of these factors independent of macrophage inflammatory polarization, would also warrant further research. Here, single cell sequencing approaches might prove valuable which are able to provide information on a whole spectrum of macrophage functions and can simultaneously assess interaction with other cell types. Moreover, biased or unbiased chromatography based proteomic studies could help to capture protein level interaction between *Axl*/*Mertk* deficient macrophages and brown adipocytes and could help to provide a valuable overview on the differences between the BAT of *Csf1r-Cre*$^{-}$*-Axl*$^{f/f}$*Mertk*$^{f/f}$ and *Csf1r-Cre*$^{+}$*-Axl*$^{f/f}$*Mertk*$^{f/f}$ mice. Despite noticeable changes in *Dio2* expression, altered systemic thyroid signaling does not seem likely to explain the differences in lipolysis between *Csf1r-Cre*$^{-}$*-Axl*$^{f/f}$*Mertk*$^{f/f}$ and *Csf1r-Cre*$^{+}$*-Axl*$^{f/f}$*Mertk*$^{f/f}$ mice. If anything, *Dio2* was reduced in our experiments (**Figure 21** and **Figure 22**). *Dio2* expression is known to be negatively regulated by T3 levels [291], so decreased levels of *Dio2* expression would suggest higher levels of circulating T3, which in turn should be stimulative for lipolysis [292]. Although thyroid signaling in *Csf1r-Cre*$^{+}$*-Axl*$^{f/f}$*Mertk*$^{f/f}$ mice should be further investigated, the presented results are therefore more consistent with an adipose tissue intrinsic effect. Still, the fact that inflammatory signaling in ingWAT was more affected by *Axl* and *Mertk* deficiency is consistent with the larger effect size on adipocyte function in this depot as well as the increased susceptibility of WAT to local inflammation as compared to BAT [293].

In 2021, Petkevicius et al. reported that macrophage β2-adrenergic receptor signaling is dispensable for adipose tissue inflammation and function [258]. This appears to contradict the idea that NE-induced *Axl* and *Mertk* expression contributes to adipose tissue remodeling. However, we propose that prior adaptation to thermoneutral housing as well as HFD feeding and repeated or prolonged cold exposure are necessary to create conditions where *Axl*- and *Mertk*-dependent efferocytosis becomes essential for maintaining adipose tissue homeostasis. Only then, the regulation of AXL/MERTK dependent efferocytosis by NE in ATMs might impact adipose tissue metabolism and systemic metabolic outcomes. Therefore, to fully assess the role of the NE-AXL/MERTK axis, future studies should expose genetic models of *Adrb2* deficiency in macrophages to the same or similar experimental conditions used in this thesis. These studies could also help distinguish between effects driven by NE-induced *Axl* and *Mertk* expression versus baseline loss of these receptors. Furthermore, the experimental conditions in this thesis may better reflect the

human physiological context, as this regiment has been shown to produce more human-like adipose tissue in mice [131]. Nonetheless, β2-adrenergic signaling in macrophages may influence adipose tissue remodeling through additional mechanisms beyond efferocytosis, for example by modulating inflammatory polarization [294]. For this reason, mice lacking *Axl* and *Mertk* expression in macrophages might represent the most suitable model to study the impact of NE induced macrophage efferocytosis on adipose tissue biology until details in the pathway are elucidated. This data might prove especially valuable, since it remains challenging to assess the role of *Axl* and *Mertk* expression by macrophages in metabolic regulations in humans, as both *Axl* and *Mertk* are also expressed by non-macrophage cells that have been shown to affect metabolic outcomes [295], [296], [297].

4.3 Other implications and possible next steps

Adrenergic signaling in macrophages plays a crucial role in regulating immune responses and maintaining physiological balance through various mechanisms [257]. Activation of α-adrenergic receptors is generally linked to pro-inflammatory effects in macrophages, whereas β-adrenergic signaling more dominantly promotes an anti-inflammatory, resolving phenotype. However, the specific effects of NE on macrophage efferocytosis remain poorly understood [257].

Here, we demonstrated that β2-adrenergic receptor activation enhances macrophage efferocytic capacity by upregulating efferocytic receptors such as *Axl* and *Mertk* (**3.1.2**, **3.1.3** and **3.1.5**). Notably, we suggest this mechanism has important implications for adipose tissue remodeling and homeostasis, as impaired *Axl*- and *Mertk*-dependent efferocytosis is associated with reduced thermogenic and lipolytic activity in adipose tissue under conditions described here in this thesis (**3.3.2** and **3.3.3**).

Interestingly, effects of NE stimulation on macrophage efferocytosis were not only observed in ATMs but also in BMDMs (**Figure *8***). Given the hematopoietic origin of BMDMs, it seems likely that the effect of NE can in principle be extended to other macrophage populations, especially since some tissue resident macrophage populations are also constantly replenished from the circulation [298]. This is especially true for settings of tissue injury or stress [299]. Nonetheless, the effect of NE on efferocytosis shown in **Figure 14** was most pronounced in $CX3CR1^{+}Ly6C^{-}$ macrophages, not suggesting a history of recent infiltration. However, as discussed in **4.1**, the presented data is not sufficient to claim that NE signaling specifically affects $CX3CR1^{+}Ly6C^{-}$ and instead higher *Ax*l and *Mertk* levels might just show the strongest impact on efferocytosis if chemotaxis of macrophages towards apoptotic thymocytes is strongest [268]. That said, the differential effects on different tissue macrophages and macrophage subpopulations should therefore definitely be studied in more detail.

If indeed the effect of NE can be extended beyond BMDMs and ATMs towards all macrophages, the next important question would be in which other settings and locations NE concentrations can rise high enough to meaningfully affect macrophage efferocytosis. Reliable data on extracellular NE levels in tissues are limited, but blood catecholamine levels can rise up to 2000pg/mL (11.8nM) without being considered abnormal [300] and physiological stress such as cold exposure can increase plasma concentrations of NE by 150% [301]. Although this is still substantially lower than the 1μM used for stimulation of BMDMs, we did not deeply characterize dose response relationships in the induction of efferocytosis by NE. Epinephrine levels in the blood are also highly variable and can reach around 7.5nM or 200nM in acute stress or maximal stress situations respectively [302]. Of note, epinephrine has a 10- to 100 fold higher affinity for the β2-adrenergic receptor as compared to NE and therefore could potentially more easily reach concentrations in the systemic circulation to induce meaningful amounts of efferocytosis [260].

Convincingly, loss of β2 adrenergic receptor expression in macrophages has been shown to affect outcomes in various disease models. β2-signaling in muscularis macrophages has been shown to limit neuronal damage following enteric helminth infection through an arginase 1-polyamine axis [303]. Conditional knockout of β2AR in macrophages also leads to increased severity of renal ischemia-reperfusion injury, while adoptive transfer of β2AR-activated macrophages was protective [304]. Moreover leukocyte-expressing β2-adrenergic receptors are essential for survival after acute myocardial injury, a setting in which local extracellular noradrenaline concentrations can reach 100– to 1,000 times the normal concentration [305], [306]. Interestingly, MERTK-dependent efferocytosis by monocytic myeloid-derived suppressor cells has also been shown to be important for resolving ischemia/reperfusion injury after lung transplantation [307], making ischemia a setting where both leukocyte expression of the β2 receptor as well as *Mertk* expression are associated with better outcomes.

β2-adrenergic receptor signaling in macrophages has also been shown to have detrimental effects. For instance, biliary injuries caused by helminth infection were promoted by β2 signaling concomitant with IL4 signaling to enhance alternative activation in macrophages [263]. Anti-inflammatory polarization by β2 activation has also been shown to promote breast cancer progression through macrophages [308]. *Mertk* expression by macrophages is also closely associated with cancer progression and immunotherapy resistance, offering another setting with reported roles for β2 signaling and *Mertk* expression [309]. Some overlap between settings in which β2 or Mertk signaling play an important role can thereby be expected as both pathways converge on macrophage anti-inflammatory polarization. Nonetheless, potential interactions or even synergies between the two pathways have not yet been reported in any context.

Adrenergic agonists are routinely used in clinical settings, primarily for their potent effects on the cardiovascular system [310]. β2 specific agents are routinely used for their effects on

bronchodilation [311] and have also been shown to block insulin-stimulated peripheral glucose disposal in rodents and healthy men [312]. Effects on efferocytosis might thereby be an unknown outcome of these drugs or might even in some circumstances contribute to their mechanism of action. NE is also considered the first-line vasopressor for managing septic shock due to its effectiveness in increasing vascular tone and improving organ perfusion [313]. Although effects on macrophages may be of secondary concern in these settings, potential side effects of NE on efferocytosis and especially on bacterial phagocytosis may warrant investigation.

The broad use of β2-agonistic substances also provides a valuable opportunity to obtain patient samples to validate some of our findings or to repurpose existing medications to treat conditions that could benefit from an increased rate of efferocytosis (**see 1.1.3**). However, at this time the risk of cardiovascular side effects - even with β2-specific agonists - remains a major barrier to their use beyond bronchodilation. Still, β2 agonist side effects are often mild and manageable, suggesting that in appropriate contexts, the benefits of increased *Axl* and *Mertk* expression in macrophages could outweigh the risks [314], [315]. A deeper understanding of how adrenergic signaling regulates efferocytosis may also reveal new therapeutic targets and strategies to reduce side effects. For example, if β2 stimulation indeed activates LXR signaling in macrophages, targeting adrenergic signaling could provide an alternative to existing LXR agonists, offering a different pharmacological profile.

The discovery that macrophage-expressed *Axl* and *Mertk* influence adipose tissue function and inflammation establishes efferocytosis also as a novel potential therapeutic target for diseases like type 2 diabetes, which have been shown to be driven by local inflammation and impaired removal of dead cells [204]. Consequently, medications targeting *Axl* and *Mertk* expression through β2-signaling pathways or through other means could be evaluated for their potential effectiveness in treating metabolic disease. In the future, *Axl* and *Mertk* expression in ATM could also be targeted through other approaches, such as ligand based strategies or by genetic manipulation of ATMs either *in vivo* or *ex vivo*.

Beiging of white adipose has also long been investigated for its potential to support weight loss [316]. If the detrimental effects in Csf1r-*Cre*$^{-}$-Axl$^{f/f}$Mertk$^{f/f}$ on ingWAT thermogenic activation hold true, AXL/MERTK dependent efferocytosis might indeed represent a critical junction in ingWAT browning. Understanding the exact mechanism by which *Axl* and *Mertk* expressing macrophages impact this process could aid in the development of therapeutic strategies and prevent adverse outcomes.

Finally, in light of the recent surge in the use of modern weight loss medications, understanding and targeting macrophage efferocytosis in adipose tissue has also become increasingly important. Rapid weight loss and lipolysis promote a dynamic immune response in adipose tissue [317] and these treatments dramatically alter adipose tissue composition and inflammatory signaling [318]

[319]. Efficient clearance of dead cells and debris might be especially important in these settings to prevent chronic inflammation and to maintain metabolic homeostasis. The findings presented in this thesis may deepen our understanding of these processes and inform new therapeutic strategies to mitigate adverse effects and promote healthier, more sustainable fat loss.

5. Materials and Methods

5.1 Experimental animal models

5.1.1 Mouse models and housing

All mouse experiments were approved by the Animal Welfare Officers of University Medical Centre Hamburg-Eppendorf (UKE) and Behörde für Gesundheit und Verbraucherschutz Hamburg. During the experiments, mice were housed individually with wood bedding in a light- and temperature-controlled facility with a 12h/12h dark regime. Unless stated otherwise, mice were housed at 22°C (RT) and were fed a standard laboratory chow diet ad libitum (19.10% protein, 4% fat, 6% fiber, from Altromin Spezialfutter GmbH & Co. KG, Germany). All experiments were started when mice were between 8 and 12 weeks of age. At the end of the experiments mice were sacrificed by a lethal dose (15µL/g mouse bodyweight) of a mixture containing Ketamin (23mg/mL)/Xylazin (0.2%) in 0.9% NaCl and after a 4h fasting period. Systemic blood was withdrawn by cardiac puncture with syringes containing 5µL 0.5M EDTA (Sigma-Aldrich). Subsequently, animals were perfused with PBS (Thermo Fisher Scientific) and their harvested tissues were immediately either conserved in 3.7% formaldehyde solution, processed to isolate ATMs, or were stored at −80°C for further use.

Wild type mice were of the C57BL/6 genetic background and were housed and bred in the animal facility of the UKE at 22°C under a day-night cycle of 12h and ad libitum access to food and drinking water.

Mice with a total deletion of the Adrenergic beta 2 receptor as well as their control littermates (Adrβ2$^{+/+}$ and Adrβ2$^{-/-}$ mice, Adrb2tm1Bkk/J; the Jackson Laboratory, no. 031496) exhibited FVB/129 genetic background and were kindly gifted from the lab of AG Keller (UKE) [320]. Genotyping for these mice was carried out externally by AG Keller and mice were received briefly before BMDMs were isolated.

Mice with a macrophage specific deletion of *Axl* and *Mertk* (*Csf1r-Cre*$^{-}$*Axl*$^{f/f}$*Mertk*$^{f/f}$ or *Csf1r-Cre*$^{+}$*Axl*$^{f/f}$*Mertk*$^{f/f}$ mice) were of the C57BL/6 genetic background and housed and bred in the animal facility of the UKE at 22°C under a day-night cycle of 12h and ad libitum access to food and drinking water. In brief, the knock-out strategy for the *Mertk* gene targets exon 18 of the WT mouse allele, which encodes residues W779-L824 of the tyrosine kinase domain. Deletion of this exon leads to a

functional and protein null [240]. The knock-out strategy for the *Axl* gene involved LoxP site insertions upstream and downstream of exon 9, allowing Cre-mediated excision [239], [321]. Before each experiment, mice were manually genotyped for the presence of LoxP insertions in both the *Axl* and *Mertk* gene, as well as for the presence of a *Csf1r*-Cre allele.

5.1.1 Cold challenge

For cold challenges animals were housed at 6°C for a period of 1-7 days while keeping their respective diets and housing conditions as outlined in **5.1.1**. Depending on the experimental design, corresponding control groups were kept under identical housing conditions, except for the environmental temperature.

5.1.2 High fat diet (HFD) feeding

For studies involving HFD feeding, mice were kept under the housing conditions outlined in **5.1.1** except for the diet, which was changed to a high fat diet (HFD) containing 35% lard (Bio-Serv, F3282, 20.5% Protein; 36,0% Fat; 35,7% Carbohydrates; 0% Fiber Fat). HFD feeding was started when mice were 8-12 weeks of age and was carried out under thermoneutral temperature housing conditions (30°C). The diet was kept over the whole course of the experiment, including during cold challenges. During the feeding period food intake was monitored and mice were weighed once a week. At the end of the experiments blood glucose was determined using an Accu-Chek Aviva (Roche) after the regular 4h fasting period.

5.1.3 Norepinephrine/CL316,243 injections

To induce efferocytosis in macrophages, 5µl/g bodyweight of a 200 µg/ml norepinephrine (Cayman Chemicals) 0.9% NaCl solution were injected subcutaneously into the interscapular region of mice, for a total dose of 1mg/kg bodyweight. Injections were carried out twice, 12h and 30 minutes before sacrificing the mice. During the experiments mice were housed at RT under the conditions specified in **5.1.1**.

To induce adipocyte specific thermogenesis, 10 µl/g bodyweight of a 100 µg/ml CL316,243 (Tocris Bioscience) 0.9% NaCl solution were injected subcutaneously into the interscapular region of mice for a total dose of 1mg/kg bodyweight. The injection was carried out at the indicated timepoints, while mice were kept in metabolic cages at thermoneutral temperature conditions (28°C).

5.2 Genotyping

5.2.1 DNA isolation

To isolate DNA from tail biopsies, they were first digested overnight at 37°C using 700 µL STE buffer to which 10 µL proteinase K (Thermo Fisher Scientific) was added. After addition of 70µL 10% SDS and 270 µL 5M NaCl to the lysate, the precipitated proteins were pelleted by centrifugation at RT for 10 min at 13.000xg. 450µL of the DNA-containing supernatant was washed in 900 µL 70% EtOH, and the DNA was then pelleted by centrifugation at 4°C for 30 min at 13.000xg. The excess EtOH was removed, and the DNA pellet was dried for 2 hours at 42°C and 300 rpm. DNA was taken up in 50 µL ddH2O.

5.2.2 PCR Reaction

Mice were genotyped for the presence of a *Csf1r*-Cre allele as well as for the presence of LoxP insertions in both the *Axl* and *Mertk* locus. For this the following reactions were mixed.

Table 1: PCR reaction for *Csf1r*-Cre status

Material	Amount (µL)
ddH20	16.40
10XPCR-Buffer GREEN	2.50
10 mM dNTPs	1.00
10 µM Primer 26326	1.00
10 µM Primer 31704	1.00
10 µM Primer 31705	1.00
10 µM Primer 43161	1.00
Taq-Polymerase (5 U/µl)	0.1
DNA	1.0
Total Reaction	25.0

Table 2: PCR reaction for *Axl*- and *Mertk*-flox alleles

Material	Amount (µL)
ddH20	18.40
10XPCR-Buffer GREEN	2.50
10 mM dNTPs	1.00
Mer-SC1/Axl-PINK 3	1.00
Mer-PRPL 4/Axl-SDL2	1.00
Taq-Polymerase (5 U/µl)	0.1
DNA	1.0
Total Reaction	25.0

Table 3: PCR primer sequences from 5' to 3'

Primer	Sequence
26326	GCA GGT TGG AGA CTT TCC TCT
31704	AGT GGC CTC TTC CAG AAA TG
31705	TGC GAC TGT GTC TGA TTT CC
43161	CTT CCA AAG CAT GGT CCA GT
Mer-SC1	ATG TGA CCT TCA GAG ATT CCC AGG
Mer-PRPL 4	TGA CGA AGC ACA CAG AGC TGG
Axl-PINK 3	CTG TTG TAC CAT GTC CAC TGT GG
Axl-SDL2	CCC TTG TCT CTA CAT TTG TCT CCA

The PCR reactions were briefly centrifuged down and the PCRs were carried out according to the following programs:

Table 4: PCR program for *Csf1r*-Cre reactions

Step	Temperature	Time
1	95°C	3min
2	95°C	30sec
3	57°C	30sec
4	72°C	60sec
	Repeat steps 2-4 for 40 cycles	
5	72°C	5min
6	4°C	oo

Table 5: PCR program for *Axl*- and *Mertk*-flox reactions

Step	Temperature	Time
1	94°C	3min
2	94°C	30sec
3	60°C	30sec
4	72°C	60sec
	Repeat steps 2-4 for 35 cycles	
5	72°C	10min
6	4°C	oo

5.2.3 Visualization

The PCR products were separated on 1.5% agarose gels (1.5g agarose, 100ml TBE buffer, 5µl Roti®-GelStain) by means of gel electrophoresis at a current of 120 mA for 60 min. 5µl of GeneRuler™ DNA Ladder Mix were applied as a marker. The bands were made visible under UV light and photographed.

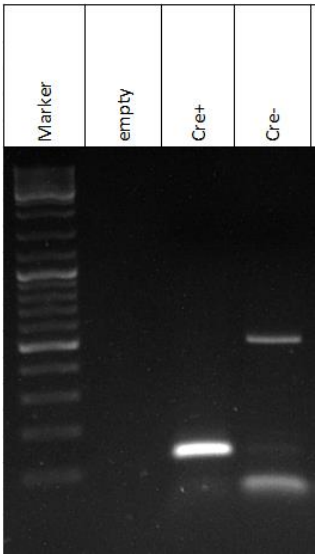

Figure 33: Exemplary results of a genotyping PCR assessing *Csf1r*-Cre status. *PCR products are expected at 150bp (Csf1r-Cre) and 521bp (internal loading control).*

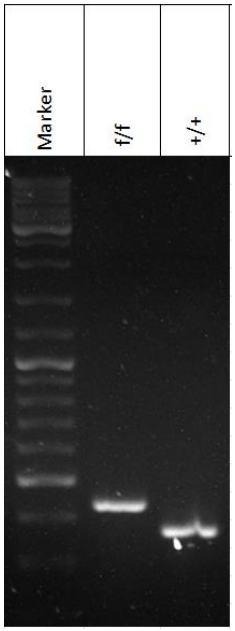

Figure 34: Exemplary results of a genotyping PCR assessing Mertk-flox status. PCR products are expected at 367 bp*bp (Mertk$^{Wild\text{-}type}$) and 437 bp (Mertk$^{f/f}$).*

5.3 Efferocytosis assays

5.3.1 *Ex vivo* (ATMs)

For ex vivo efferocytosis assays using adipose tissue macrophages (ATMs), 8- to 12-week old male wild-type mice were sacrificed as outlined in **5.1.1**. Adipose tissues were collected and minced with scissors, before they were digested in a solution containing 1,5U/mL Collagenase D (Miltenyi Biotec, Germany), 2,4U/mL Dispase (Thermo Fisher Scientific) and 1mM $CaCl_2$ for 45 minutes. Adipose tissues of 3 mice were pooled per sample and 6mL of digestion solution were used per sample. The resulting solutions were filtered through 100 µM and 40 µM cell strainer and were subjected to centrifugation at 600xg for 5 minutes. Afterwards the flow-through was discarded and the pellet was used to perform magnetic separation of $Cd11b^+$ cells following the manufacturer's instructions (Miltenyi Biotec GmbH, Germany) and as described previously [322]. In brief, the cell pellet was re-suspended in 900 µl MACS buffer and incubated with 100 µl Cd11b MicroBeads (Miltenyi Biotec GmbH, Germany) at 4°C for 15 min. After centrifugation, the cell pellet was re-suspended and the cell suspension, including the magnetically labeled $Cd11b^+$ macrophages, was applied to LS columns (Miltenyi Biotec GmbH, Germany). After washing, $Cd11b^+$ ATMs were collected from the LS columns, counted, and plated in a 48-well plate format at the highest possible density to ensure equal cell numbers across all samples (approximately between 50.000 cells/well in 200.000 cells/well). Cells were seeded in RPMI 1640 GlutaMAX™ (Thermo Fisher Scientific) media containing 10% fetal bovine serum (FBS, Thermo Fisher Scientific), 10-20% L929-supplement (L929 cell supernatant in RPMI 1640 GlutaMAX™ [323], and 1% Penicilin/Steptavidin (Thermo Fisher Scientific) and left to attach for approximately 2 h before CFSE (Thermo Fisher Scientific, C34554) labeled apoptotic thymocytes (aTs) were provided at 750.000 cells/well. ATMs were co-incubated with aTs for 1.5 hours at 37°C (Uptake) or on ice (Binding control) and then detached with cold PBS (Thermo Fisher Scientific no. C34554) after thorough washing. All cells were collected in round bottom 96-well plate and were stained for surface expression of LY6G, CD11b and F4/80 as well as with a viability dye (Invitrogen, L34961) as described in **5.5**. For experiments shown in **Figure 14** also CX3CR1 and LY6C antibodies were added to the antibody mix. Finally, $Cd11b^+F4/80^+$ ATMs were analyzed by flow cytometry for the presence of the aT-dye using FACSymphony™ A3 Cell Analyzer (BDBiosciences). The efferocytic index was defined as the difference between BMDMs positive for the apoptotic cell dye (CFSE) at 37°C and 4°C. Data analysis was carried out using FlowJo software V10 (Tree Star).

5.3.2 *In vitro* (BMDMs)

BMDMs were differentiated from bone marrow precursors, from 6- to 14-week-old female mice. Briefly, femur and tibia were collected and cut open on one epiphysis and the

hematopoietic pluripotent stem cells were isolated by centrifugation of the bones. The hematopoietic pluripotent stem cell homogenate was filtered over a 40 µm strainer and cells were seeded into RPMI 1640 GlutaMAX™ (Thermo Fisher Scientific) containing 10% fetal bovine serum (FBS, Thermo Fisher Scientific), 10-20% L929-supplement (L929 cell supernatant in RPMI 1640 GlutaMAX™ [323], and 1% Penicilin/Steptavidin (Thermo Fisher Scientific). During the propagation and differentiation of BMDMs, half of the media was changed at day 3. At day 5, cells were split and at day 7, the differentiated BMDMs were collected and seeded for the experiment. 0.33×10^6 cells/wells were seeded into 24-well plates in the evening before the start of treatment. Treatments were carried out in the same RPMI media containing FBS, 10-20%, L929-supplement, and Penicilin/Steptavidin. Compounds used for treatment of BMDMs were diluted in either media or DMSO according to their properties and appropriate vehicle treatments were added to the controls. To assess the efferocytosis capacity of BMDMs, CFSE (Thermo Fisher Scientific no. C34554) labeled aTs were provided at a 5:1 ratio. BMDMs were co-incubated with aTs for 45 minutes at 37°C (Uptake) or on ice (Binding control) and then detached with cold PBS (Thermo Fisher Scientific no. C34554) after thorough washing. All cells were collected in round bottom 96-well plates and were stained for surface expression of CD45, CD11b and F4/80 as well as with a cell viability dye (Invitrogen, L34961) as described in **5.5**. Finally, $Cd11b^+F4/80^+$ BMDMs were analyzed by flow cytometry for the presence of the aT-dye using a FACSymphony™ A3 Cell Analyzer (BDBiosciences). The efferocytic index was defined as the difference between BMDMs positive for the apoptotic cell dye (CFSE) at 37°C and 4°C. Data analysis was carried out using FlowJo software V10 (Tree Star).

5.3.3 Generation of NE conditioned brown adipocyte supernatant

To generate NE conditioned brown adipocyte supernatant primary, brown adipocytes were differentiated from stromal-vascular fractions (SVF) from BAT and WAT of wild type mice (C57BL/6J, male, age 4-6 weeks) as described previously [324], [325]. In brief, adipose tissues were digested for 45 minutes using a solution containing 1.5% BSA (Sigma-Aldrich) and 600U/mL collagenase II (**Sigma-Aldrich**) in adipocyte isolation buffer. The obtained stromal vascular cells were subsequently cultured in DMEM GlutaMAX™ media (4.5g/L Glucose, Thermo Fisher Scientific) supplemented with 10% newborn calf serum (Sigma-Aldrich, N4637-500ML), 1% penicillin and streptomycin (Thermo Fisher Scientific), 2.4 nM of insulin (Sigma-Aldrich) and 1µM of rosiglitazone (Cayman Chemicals). After 7 days of differentiation, mature adipocytes were treated with 1µM NE (Cayman Chemicals) and the resulting media was transferred in whole to BMDMs.

5.3.4 Preparation and staining of apoptotic thymocytes

For the isolation of thymocytes, one or more thymuses were harvested and smashed over a 40 µm strainer to obtain a single-cell solution. Cells were then pelleted and re-suspended in RPMI 1640 GlutaMAX™ (Thermo Fisher Scientific) containing 5% fetal bovine serum (FBS, Thermo Fisher Scientific). Induction of apoptosis in thymocytes was done by incubating them overnight in 6mL of this low serum media. Apoptosis levels were verified using the FITC Annexin V Apoptosis Detection Kit (BioLegend no. 640914), following the manufacturer's instructions. Next, aTs were stained with CFSE dye (Thermo Fisher Scientific no. C34554) for 20 minutes at 37°C at a concentration of 0.2 µL/mL and 10^6 cells.

5.4 Gene Expression Analysis (RT-qPCR)

5.4.1 RNA isolation and preparation of cDNA

Tissues or cell pellets were homogenized in 1ml of TRIzol™ reagent (Thermo Fisher Scientific) using a Tissue Lyser type 3 (QIAGEN; 20 Hz for 2 × 3 min). 250 µL chloroform were added and samples were mixed and centrifuged at 13,000xg at 4°C for 15 min. The resulting supernatant was mixed with 600 µL of 70% ethanol. Further purification was performed by using NucleoSpin RNAII Kit (Machery&Nagel) according to the manufacturer's instructions. Double-stranded DNA was digested using rDNase (Machery&Nagel). RNA content was measured using NanoPhotometer® N60 (IMPLEN, Germany) and subsequently 400ng of RNA was transcribed to cDNA using High-Capacity cDNA Reverse Transcription Kit (Applied Biosystems). Reverse transcription PCR program was as follows: 1. 10 min, 25°C; 2. 120 min, 37°C; 3.5 s, 85°C.

5.4.2 Quantitative real time PCR

Gene expression was assessed in cDNA samples using Taqman® assays supplied as assays-on-demand™ (Applied Biosystems, **Table 6**) together with Taqman™ Universal PCR MasterMix (Applied Biosystems) or by using custom primers from Eurofins (**Table 7**) together with SYBR™ Green Universal Master (Applied Biosystems). PCR reactions were performed by QuantstudioTM 5 Real-Time PCR Systems (Applied Biosystems) and cycling parameters were as followed: 1 cycle of 95°C for 10 min, 40 cycles of 95°C for 15 s then 60°C for 60 s. Gene copy number was calculated with the formula (10((Ct-35)/-3.3219)) and gene expression was always normalized for copy number of TATA-box binding protein (*Tbp*).

Table 6: TaqMan® Assays-on-Demand™ used in this thesis

Gene name	Full name	Assay-on-Demand™
Abca1	ATP-binding cassette, sub-family A (ABC1), member 1	Mm00442646_m1
Adrb3	*adrenergic receptor, beta 3*	Mm00442669_m1
Bax	BCL2-associated X protein	Mm00432050_m1
Bcl2	B-cell leukemia/lymphoma 2	Mm00477631;m1
Ccl2	chemokine (C-C motif) ligand 2	Mm00441242_m1
Cd36	CD36 antigen	Mm00432403_m1
Dio2	deiodinase, iodothyronine, type II	Mm00515664_m1
Emr1	adhesion G protein-coupled receptor E1	Mm00802530_m1
Fasn	fatty acid synthase	Mm00662319_m1
Il10	interleukin 10	Mm00439616_m1
Il6	interleukin 6	Mm00446190_m1
LXRα (Nr1h3)	nuclear receptor subfamily 1, group H, member 3	Mm00443454_m1
Lpl	lipoprotein lipase	Mm00434764_m1
Ppargc1a (Pgc1-α)	peroxisome proliferative activated receptor, gamma, coactivator 1 alpha	Mm00447183_m1
Prdm16	PR domain containing 16	Mm00712556_m1

Tbp	TATA box binding protein	Mm00446973_m1
Tgfb1	transforming growth factor, beta 1	Mm00441724_m1
Timd4	T cell immunoglobulin and mucin domain containing 4	*Timd4*
Tnf	tumor necrosis factor	Mm00443258_m1
Trem2	triggering receptor expressed on myeloid cells 2	Mm00451744_m1
Ucp1	uncoupling protein 1 (mitochondrial, proton carrier)	Mm00494069_m1

Table 7: Custom primers used for gene expression analysis from 5' to 3'

Gene name	Full name
mAxl for	*TGCCAGTCAAGTGGATTGCT*
mAxl Rev	*CACACATCGCTCTTGCTGGT*
mMertk fw	*GTAGATTACGCACCCTCGTCAAC*
Mertk Rv	GCCGAGGATGATGAACATAGAGT

5.4.3 Bulk RNA-sequencing

For Bulk RNA sequencing of mature adipocytes (mAdipocytes) and SVFs, murine brown adipose tissue was collected and digested using a collagenase and dispase solution as described in **5.3.1**. The resulting solution was centrifuged at 600xg for 5 minutes and the upper fatty layer (mAdipocytes) as well as the pellet (SVF) were collected in 1 ml of TRIzol reagent (Thermo Fisher Scientific). For Bulk RNA sequencing of NE treated BMDMs, cells were differentiated and seeded as described **5.3.2** and after treatment with 1µM NE for 24h BMDMs were also collected in 1ml of TRIzol. RNA isolations were carried out as described in **5.4.1**. 200ng of RNA were then sent to BGI (BGI TECH SOLUTIONS, Hongkong) where RNA sequencing was performed. Library preparation and

transcriptome sequencing were performed using 100 bases/paired-end reads on BGI's DNBSEQ Technology Platform. The mRNA sequencing with subsequent filtering (removal of adapters, low-quality reads, N reads and polyX) and quality control was performed on DNBSEQ Technology by BGI. The reads for each sample were aligned to the mouse genome (GRCm39) using STAR aligner (version 2.7.10b). The sequencing data obtained from the mAdipocyte and SVF fractions were kindly analyzed by Dr. Lorenz Adlung (UKE). The obtained sequencing data obtained from BMDMs were analyzed using the Dr. Tom web-based data visualization and analysis platform (Beijing Genomics Institute, BGI, accessed January 2025; (https://www.bgi.com/global/service/dr-tom)).

5.5 Flow cytometric analysis

For flow cytometric analysis of adipose tissue macrophages, adipose tissues were digested as described in **5.3.1** and the stromal vascular fraction (SVF) was collected before the magnetic separation step. Cells directly isolated from mouse adipose tissues or from culture plates were incubated with Fc block (BioLegend, anti-CD16/CD32 no.101301) diluted 1:10000 in PBS + 2% FBS for 15 min at 4°C before the staining. Washing steps with PBS + 2% FBS were repeated three times and performed after each antibody incubation. For each washing step or change of buffer, cells were pelleted at 800xg for 2 min. For the staining of surface epitopes, cells were incubated with the antibody cocktail for 35 min at 4°C in the dark. If a viability staining was included in the analysis, viability dye (Invitrogen, L34961) was added to this mix. If intracellular epitopes were analyzed, cells were fixed using 2% paraformaldehyde (Electron Microscopy Sciences) and permeabilized (BD Biosciences Perm/Wash no. 554723) for 15 min at RT before staining. Intracellular antibodies were diluted in permeabilization buffer. Cells were analyzed either on a FACSymphony™ A3 Cell Analyzer (BDBiosciences) or on a Cytek® Aurora (whenever Dr. Imke Liebold carried out the FACS analysis). All data was analyzed using the FlowJo software V10 (Tree Star). Antibodies used for flow cytometry were purchased from commercial sources (**Table 8**).

Table 8: List of antibodies used

Protein name	Fluorophore	Producer	Reference	Experiment
ARG1	BUV805	invitrogen	368-3697-82	**Figure 12**
CD11b	APC/Cy7	BioLegend	101222	**Figure 12**, **Figure 20**, **Figure 31**

CD11b	AF700	BioLegend	101222	**Figure 6**, **Figure 7**, **Figure 8**, **Figure 10**, **Figure 11**, **Figure 14**, **Figure 18**
CD11c	PE/Cy5	BioLegend	117316	**Figure 18**
CD36	PE-Cy7	BioLegend	102615	**Figure 12**
CD45	BV421	BioLegend	103134	**Figure 7**
CD45	BV510	BioLegend	103137	**Figure 12**, **Figure 20**, **Figure 31**
CD80	SparkNIR 685	BioLegend	104761	**Figure 20**, **Figure 31**
CD9	PE-Dazzle	BioLegend	124821	**Figure 31**
CD163	APC/Fire 810	BioLegend	155321	**Figure 12**
CX3CR1	PE-Cy7	BioLegend	149015	**Figure 14**
F4/80	AF700	BioLegend	123130	**Figure 6**, **Figure 7**, **Figure 8**, **Figure 10**, **Figure 11**, **Figure 14**, **Figure 18**
F4/80	APC/Cy7	BioLegend	123118	**Figure 12**, **Figure 20**, **Figure 31**
iNOS	BUV737	invitrogen	367-5920-82	**Figure 31**
Ki67	BV650	BioLegend	151215	**Figure 12**
LY6C	BV510/480	BioLegend	TIM4	**Figure 14**
LY6C	BV570	BioLegend	128030	**Figure 31**
LY6G	PerCP-Cy5.5	BioLegend	127616	**Figure 6**, **Figure 14**, **Figure 18**
LY6G	BUV395	BioLegend	563978	**Figure 20**, **Figure 31**
MERTK	PE	BioLegend	151505	**Figure 10**
MERTK	RealBlue780	BD	755415	**Figure 12**
MHCII	Spark Blue 550	BioLegend	107661	**Figure 12**, **Figure 20**, **Figure 31**
RELMa	Polyclonal rabbit IgG + BV421, Anti-rabbit IgG,	Peprotech	500-P214-100ug	**Figure 12**, **Figure 20**, **Figure 31**
TIM4	PerCP-eF710	invitrogen	1556928	**Figure 12**, **Figure 20**, **Figure 31**
YM1	Polyclonal Goat IgG+ Anti-goat IgG-FITC	R&D	AF2446	**Figure 12**, **Figure 20**, **Figure 31**

5.6 Western blotting

Protein lysates were prepared by homogenizing adipose tissues using metal beads and a tissue lyzer (Qiagen). During this procedure, adipose tissues were kept in cold RIPA buffer ((10x (v/w), 20 mM Tris-HCl pH 7.4, 5 mM EDTA, 50 mM sodium chloride, 10 mM sodium pyrophosphate, 50 mM sodium fluoride, 1 mM sodium orthovanadate, 1 % NP-40, 0.1% SDS supplemented with Complete Mini Protease Inhibitor Cocktail Tablets (Roche) and phosphatase inhibitors (Sigma-Aldrich)). Lysates were centrifuged at 10.000 xg, for 5 min at 4˚C and the resulting aqueous phase without the fatty layer was taken for protein determination using the Pierce™ BCA Protein Assay (Thermo Fisher Scientific). Protein samples were diluted in RIPA under addition of 4xNuPAGE sample buffer (Invitrogen) and 10x reducing agent (Invitrogen), so that 50 µg protein could be loaded per lane. Resulting samples were denatured for 10 min at 65°C. Samples were separated by SDS-PAGE on a 10% SDS-polyacrylamide Tris-glycine gels and were transferred to a nitrocellulose membrane (Amersham) overnight using a wet blotting system. Ponceau S (Sigma-Aldrich) staining was performed to ensure equal loading and membranes were cut according to the size of the proteins of interest. Membrane fragments that were to be stained for p563HSL were blocked in Roti®Block (Carl Roth, 1:10 diluted with aqua dest) for 1h at RT while all other membrane fragments were blocked in 5% milk (Millipore) in TBST (0.2 M Tris, 1.37 M sodium chloride, 0.1 % (v/v) Tween 20). After washing with TBST, membrane fragments were incubated with primary antibody in 5% Bovine Serum Albumin (BSA, Sigma-Aldrich) +0.02% NaAzid in TBST overnight at 4°C. Primary antibodies used were (BAX (Cell signaling, #2772, 1:1000); rabbit-anti-gTubulin (Abcam, TUBG1, ab179503, 1:2000); mouse-anti-UCP1 (R&D Systems, MAB6158, 1:500); rabbit-anti-p563HSL (Cell signaling, 413S, 1:1000); rabbit-anti-HSL (Cell signaling, 4107S, 1:1000); rabbit-Phospho-PKA Substrate (Cell signaling, 9621, 1:1000); rabbit-anti-ADRB3 (Abcam, ab94506, 1:1000) rabbit-anti-Tyrosine Hydroxylase (TH, Abcam, ab137869, 1:1000); rat-anti-MAC2 (Santa Cruz, sc23938, 1:1000). After another round of thorough washing with TBST, membrane fragments were incubated with secondary antibody in 5% milk in TBST for 1h at RT. Secondary antibodies used were HRP-conjugated goat anti-rabbit (Cell Signaling, #7074, 1:5000); HRP-conjugated rabbit anti-mouse (CiteAb Ltd, P0161, 1:5000) or HRP-conjugated donkey anti-rat (Jackson ImmunoResearch, AM_23040641, 1:5000).

After more rounds of washing in TBST, membrane fragments were developed on Amersham Imager600 (GE Healthcare) using either luminol (Sigma-Aldrich) or SuperSignal™ West Femto Maximum Sensitivity Substrat (Thermo Scientific™ 34096X4). Quantification of the bands was done in Image Studio Lite (version 5.2.5) and protein expression was normalized as indicated in the respective Figures. For each analysis, the average of the normalized values in the control group were set to 1 and relative values were calculated accordingly. Importantly, after quantification some membrane fragments were stripped using incubation with 1x Restore™ Fluorescent Western Blot

Stripping Buffer (Thermo Fisher Scientific) and reincubated with another primary antibody to determine the levels of a second protein of interest. This was the case in particular for membranes used to quantify p563HSL, which were subsequently incubated with antibodies for total HSL. Furthermore, this was the case for proteins that ran at the same range as γ-Tubulin (TUBG1). Quantification of results was done using ImageJ Version 1.54g. Protein expression was normalized as indicated in the respective Figures and the mean of the control group was set to 1.

5.7 Explant cytokine secretion assay

To measure cytokine secretion from iBAT and ingWAT, freshly isolated whole adipose tissues were collected and placed in DMEM GlutaMAX™ media (4.5g/L Glucose, Thermo Fisher Scientific) supplemented with 10% fetal bovine serum (FBS, Thermo Fisher Scientific), 1% penicillin and streptomycin (Thermo Fisher Scientific). Afterwards medium was discarded and explants were transferred to fresh medium and incubated for another 4 h at 37°C. Cytokines secreted into the media by iBAT and iWAT explants were assessed by Dr. Stephany Leyk using the LEGENDplex– Th1/Th2 Panel (8-plex) Assay (BioLegend no. 741054) following the manufacturers protocol. Data was collected using the FACS LSR and was analyzed via LEGENDplex software v8.0 (BioLegend).

5.8 Indirect calorimetry

For studies on systemic energy expenditure, mice were put in metabolic cages (Sable Systems Europe GmbH, Germany) and the system was operated according to the manufactures guidelines. Mice were acclimated to the metabolic cages for at least 2 days at 28°C prior to recording. 28°C was used as the standard thermoneutral temperature and change of temperature occurred at 7 am and the light phase was from 7 am – 7 pm. During the experiment consumption of O_2, production of CO_2, respiratory exchange ratio (RER), energy expenditure, food intake, water intake, body core temperature and activity were measured.

5.9 Histology – Immunohistochemistry

For histological analysis of UCP1 expression, tissues were fixed in 3.7% formaldehyde (diluted in PBS) and embedded in paraffin. 4µm paraffin sections were made, deparaffinized and subsequently rehydrated in xylene and descending ethanol series. Next, slides were cooked in 10 mM citrate buffer (pH 6.0) for 30 minutes for antigen retrieval and left in the buffer for an additional 30 min to cool down. After washing, slides were blocked with 3% BSA in PBS for 1h at RT. For UCP1 IHC stainings we used rabbit-anti-UCP1 (Abcam, ab10983) in a dilution of 1:500 in 3% BSA (Sigma) and Horseradish

peroxidase (HRP) coupled goat anti-rabbit (Cell Signaling, #7074) was used as secondary antibody. After addition of DAB-Substrate (Abcam) and Hematoxylin (Sigma-Aldrich) counterstaining slides were sealed using Eukitt (O.Kindler GmbH). Images were taken using a NikonA1 Ti microscope equipped with a DS-Fi-U3 brightfield camera and quantified using Image J Version 1.54g.

5.10 Blood and plasma parameters

After heart blood collection as described in **5.1.1** the whole blood was centrifuged at 4°C for 10 min at 10.000 xg for 5 min. The plasma was then transferred to a new reaction tube and was stored at -80°C if it was not directly analyzed. For plasma TG and cholesterol determination, 5µL of plasma was pipetted in duplicates into 96-wells plates and concentrations were determined using commercial kits following the manufacturer's instructions (DiaSys Diagnostic Systems). For plasma non-esterified FA (NEFA) concentrations 20 µL plasma was pipetted in duplicates into a 96-well plate and concentrations were determined using the commercial kit NEFA-HR(2) Assay by FUJIFILM. For all assays, absorbance was read at the indicated wavelengths. NEFA concentrations were determined via linear regression using a standard curve.

5.11 Ex vivo Lipolysis assay

For ex vivo Lipolysis assays 2-3 small, freshly isolated iBAT pieces of around 20mg were weighed and placed in 200µl of DMEM, high glucose, HEPES, no phenol red (Thermo Fisher Scientific) supplemented with 0.2% fatty acid free BSA (Capricorn Scientific) for 1h at 37 °C. Afterwards, media was discarded and explants were transferred to fresh media containing FA-free BSA and incubated at 37 °C for 4 h. To stimulate lipolysis, explants were transferred to medium supplemented with an additional 1µM NE (Cayman Chemicals). NEFA release into the media was analyzed by using a colorimetric assay (NEFA-HR(2) Assay, FUJIFILM) as described in **5.10**. Results were normalized to the weight of the respective explants and results from one mouse were averaged to equal one biological replicate.

5.12 Statistics

Data are presented as mean ± SEM (Standard Error of the Mean). Graphs as well as statistical analysis were made in Graph Pad Prism (Version 10.0). Outliers were using the ROUT method with a Q cut-off value of 1%. Sample sizes, p values, as well as the statistical tests implemented can be found in the figures or the figure legends. A p-value <0.05 was considered significant. No statistical method was used to predetermine sample sizes.

6. References

[1] E. Boada-Romero, J. Martinez, B. L. Heckmann, and D. R. Green, “The clearance of dead cells by efferocytosis,” *Nat Rev Mol Cell Biol*, vol. 21, no. 7, pp. 398–414, Jul. 2020, doi: 10.1038/S41580-020-0232-1.

[2] A. C. Doran, A. Yurdagul, and I. Tabas, “Efferocytosis in health and disease,” *Nature Reviews Immunology 2019 20:4*, vol. 20, no. 4, pp. 254–267, Dec. 2019, doi: 10.1038/s41577-019-0240-6.

[3] S. Arandjelovic and K. S. Ravichandran, “Phagocytosis of apoptotic cells in homeostasis,” *Nature Immunology 2015 16:9*, vol. 16, no. 9, pp. 907–917, Aug. 2015, doi: 10.1038/ni.3253.

[4] I. Kourtzelis, G. Hajishengallis, and T. Chavakis, “Phagocytosis of Apoptotic Cells in Resolution of Inflammation,” *Front Immunol*, vol. 11, p. 526246, Mar. 2020, doi: 10.3389/FIMMU.2020.00553/XML/NLM.

[5] K. S. Ravichandran, “Beginnings of a good apoptotic meal: the find-me and eat-me signaling pathways,” *Immunity*, vol. 35, no. 4, pp. 445–455, Oct. 2011, doi: 10.1016/J.IMMUNI.2011.09.004.

[6] J. F. R. Kerr, A. H. Wyllie, and A. R. Currie, “Apoptosis: a basic biological phenomenon with wide-ranging implications in tissue kinetics,” *Br J Cancer*, vol. 26, no. 4, pp. 239–257, 1972, doi: 10.1038/BJC.1972.33.

[7] D. L. Bratton, V. A. Fadok, D. A. Richter, J. M. Kailey, L. A. Guthrie, and P. M. Henson, “Appearance of Phosphatidylserine on Apoptotic Cells Requires Calcium-mediated Nonspecific Flip-Flop and Is Enhanced by Loss of the Aminophospholipid Translocase,” *Journal of Biological Chemistry*, vol. 272, no. 42, pp. 26159–26165, Oct. 1997, doi: 10.1074/JBC.272.42.26159.

[8] D. Bertheloot, E. Latz, and B. S. Franklin, “Necroptosis, pyroptosis and apoptosis: an intricate game of cell death,” *Cellular & Molecular Immunology 2021 18:5*, vol. 18, no. 5, pp. 1106–1121, Mar. 2021, doi: 10.1038/s41423-020-00630-3.

[9] M. K. Callahan, P. Williamson, and R. A. Schlegel, “Surface expression of phosphatidylserine on macrophages is required for phagocytosis of apoptotic thymocytes,” *Cell Death Differ*, vol. 7, no. 7, pp. 645–653, 2000, doi: 10.1038/sj.cdd.4400690.

[10] M. R. Elliott and K. S. Ravichandran, “The Dynamics of Apoptotic Cell Clearance,” vol. 38, no. 2, pp. 147–160, Jul. 2016, doi: 10.1016/J.DEVCEL.2016.06.029.

[11] C. B. Medina *et al.*, “Metabolites released from apoptotic cells act as tissue messengers,” *Nature*, vol. 580, no. 7801, pp. 130–135, Apr. 2020, doi: 10.1038/S41586-020-2121-3.

[12] F. B. Chekeni *et al.*, “Pannexin 1 channels mediate ‘find-me’ signal release and membrane permeability during apoptosis,” *Nature 2010 467:7317*, vol. 467, no. 7317, pp. 863–867, Oct. 2010, doi: 10.1038/nature09413.

[13] M. R. Elliott *et al.*, “Nucleotides released by apoptotic cells act as a find-me signal to promote phagocytic clearance,” *Nature 2009 461:7261*, vol. 461, no. 7261, pp. 282–286, Sep. 2009, doi: 10.1038/nature08296.

[14] K. Lauber *et al.*, “Apoptotic cells induce migration of phagocytes via caspase-3-mediated release of a lipid attraction signal,” *Cell*, vol. 113, no. 6, pp. 717–730, Jun. 2003, doi: 10.1016/S0092-8674(03)00422-7.

[15] D. R. Gude *et al.*, “Apoptosis induces expression of sphingosine kinase 1 to release sphingosine-1-phosphate as a ‘come-and-get-me’ signal,” *The FASEB Journal*, vol. 22, no. 8, pp. 2629–2638, Aug. 2008, doi: 10.1096/FJ.08-107169.

[16] L. A. Truman *et al.*, “CX3CL1/fractalkine is released from apoptotic lymphocytes to stimulate macrophage chemotaxis,” *Blood*, vol. 112, no. 13, pp. 5026–5036, Dec. 2008, doi: 10.1182/BLOOD-2008-06-162404.

[17] C. B. Medina *et al.*, “Metabolites released from apoptotic cells act as tissue messengers,” *Nature 2020 580:7801*, vol. 580, no. 7801, pp. 130–135, Mar. 2020, doi: 10.1038/s41586-020-2121-3.

[18] C. B. Medina and K. S. Ravichandran, “Do not let death do us part: ‘find-me’ signals in communication between dying cells and the phagocytes,” *Cell Death & Differentiation 2016 23:6*, vol. 23, no. 6, pp. 979–989, Feb. 2016, doi: 10.1038/cdd.2016.13.

[19] P. Mehrotra and K. S. Ravichandran, “Drugging the efferocytosis process: concepts and opportunities,” *Nature Reviews Drug Discovery 2022 21:8*, vol. 21, no. 8, pp. 601–620, Jun. 2022, doi: 10.1038/s41573-022-00470-y.

[20] S. Y. Park *et al.*, “Stabilin-1 mediates phosphatidylserine-dependent clearance of cell corpses in alternatively activated macrophages,” *J Cell Sci*, vol. 122, no. 18, pp. 3365–3373, Sep. 2009, doi: 10.1242/JCS.049569.

[21] M. Miyanishi, K. Tada, M. Koike, Y. Uchiyama, T. Kitamura, and S. Nagata, “Identification of Tim4 as a phosphatidylserine receptor,” *Nature 2007 450:7168*, vol. 450, no. 7168, pp. 435–439, Oct. 2007, doi: 10.1038/nature06307.

[22] G. Lemke and C. V. Rothlin, “Immunobiology of the TAM receptors,” *Nature Reviews Immunology 2008 8:5*, vol. 8, no. 5, pp. 327–336, May 2008, doi: 10.1038/nri2303.

[23] L. Jiménez-García, C. Mayer, P. G. Burrola, Y. Huang, M. N. Shokhirev, and G. Lemke, “The TAM receptor tyrosine kinases Axl and Mer drive the maintenance of highly phagocytic macrophages,” *Front Immunol*, vol. 13, p. 960401, Jul. 2022, doi: 10.3389/FIMMU.2022.960401/BIBTEX.

[24] R. S. Scott *et al.*, “Phagocytosis and clearance of apoptotic cells is mediated by MER,” *Nature 2001 411:6834*, vol. 411, no. 6834, pp. 207–211, May 2001, doi: 10.1038/35075603.

[25] M. Nakaya, M. Kitano, M. Matsuda, and S. Nagata, “Spatiotemporal activation of Rac1 for engulfment of apoptotic cells,” *Proc Natl Acad Sci U S A*, vol. 105, no. 27, pp. 9198–9203, Jul. 2008, doi: 10.1073/PNAS.0803677105/SUPPL_FILE/SM9.MOV.

[26] C. Yin and B. Heit, “Cellular Responses to the Efferocytosis of Apoptotic Cells,” *Front Immunol*, vol. 12, p. 631714, Apr. 2021, doi: 10.3389/FIMMU.2021.631714.

[27] J. Rink, E. Ghigo, Y. Kalaidzidis, and M. Zerial, “Rab conversion as a mechanism of progression from early to late endosomes,” *Cell*, vol. 122, no. 5, pp. 735–749, Sep. 2005, doi: 10.1016/J.CELL.2005.06.043.

[28] J. M. Kinchen and K. S. Ravichandran, “Identification of two evolutionarily conserved genes regulating processing of engulfed apoptotic cells,” *Nature*, vol. 464, no. 7289, p. 778, Apr. 2010, doi: 10.1038/NATURE08853.

[29] G. Cantalupo, P. Alifano, V. Roberti, C. B. Bruni, and C. Bucci, “Rab-interacting lysosomal protein (RILP): the Rab7 effector required for transport to lysosomes,” *EMBO J*, vol. 20, no. 4, p. 683, Feb. 2001, doi: 10.1093/EMBOJ/20.4.683.

[30] M. Johansson *et al.*, “Activation of endosomal dynein motors by stepwise assembly of Rab7–RILP–p150Glued, ORP1L, and the receptor βIII spectrin,” *J Cell Biol*, vol. 176, no. 4, p. 459, Feb. 2007, doi: 10.1083/JCB.200606077.

[31] R. E. Harrison, C. Bucci, O. V. Vieira, T. A. Schroer, and S. Grinstein, “Phagosomes Fuse with Late Endosomes and/or Lysosomes by Extension of Membrane Protrusions along Microtubules: Role of Rab7 and RILP,” *Mol Cell Biol*, vol. 23, no. 18, p. 6494, Sep. 2003, doi: 10.1128/MCB.23.18.6494-6506.2003.

[32] C. Yin, Y. Kim, D. Argintaru, and B. Heit, “Rab17 mediates differential antigen sorting following efferocytosis and phagocytosis,” *Cell Death Dis*, vol. 7, no. 12, p. e2529, 2016, doi: 10.1038/CDDIS.2016.431.

[33] A. M. Grabiec, A. Goenka, M. E. Fife, T. Fujimori, and T. Hussell, “Axl and MerTK receptor tyrosine kinases maintain human macrophage efferocytic capacity in the presence of viral triggers,” *Eur J Immunol*, vol. 48, no. 5, p. 855, May 2018, doi: 10.1002/EJI.201747283.

[34] G. Zizzo, B. A. Hilliard, M. Monestier, and P. L. Cohen, “Efficient Clearance of Early Apoptotic Cells by Human Macrophages Requires M2c Polarization and MerTK Induction,” *The Journal of Immunology*, vol. 189, no. 7, pp. 3508–3520, Oct. 2012, doi: 10.4049/JIMMUNOL.1200662.

[35] M. N. Sharif *et al.*, “Twist mediates suppression of inflammation by type I IFNs and Axl,” *J Exp Med*, vol. 203, no. 8, p. 1891, Aug. 2006, doi: 10.1084/JEM.20051725.

[36] P. Saas, C. Chagué, M. Maraux, and T. Cherrier, “Toward the Characterization of Human Pro-Resolving Macrophages?,” *Front Immunol*, vol. 11, p. 593300, Nov. 2020, doi: 10.3389/FIMMU.2020.593300.

[37] B. Moon, S. Yang, H. Moon, J. Lee, and D. Park, “After cell death: the molecular machinery of efferocytosis,” *Experimental & Molecular Medicine 2023 55:8*, vol. 55, no. 8, pp. 1644–1651, Aug. 2023, doi: 10.1038/s12276-023-01070-5.

[38] K. V. Myers, S. R. Amend, and K. J. Pienta, “Targeting Tyro3, Axl and MerTK (TAM receptors): implications for macrophages in the tumor microenvironment,” *Mol Cancer*, vol. 18, no. 1, p. 94, May 2019, doi: 10.1186/S12943-019-1022-2.

[39] P. Sen *et al.*, “Apoptotic cells induce Mer tyrosine kinase-dependent blockade of NF-kappaB activation in dendritic cells,” *Blood*, vol. 109, no. 2, pp. 653–660, Jan. 2007, doi: 10.1182/BLOOD-2006-04-017368.

[40] S. Zhang *et al.*, “Efferocytosis Fuels Requirements of Fatty Acid Oxidation and the Electron Transport Chain to Polarize Macrophages for Tissue Repair,” *Cell Metab*, vol. 29, no. 2, p. 443, Feb. 2018, doi: 10.1016/J.CMET.2018.12.004.

[41] A. M. Fond, C. S. Lee, I. G. Schulman, R. S. Kiss, and K. S. Ravichandran, “Apoptotic cells trigger a membrane-initiated pathway to increase ABCA1,” *J Clin Invest*, vol. 125, no. 7, p. 2748, Jul. 2015, doi: 10.1172/JCI80300.

[42] Y. Kojima, I. L. Weissman, and N. J. Leeper, “The Role of Efferocytosis in Atherosclerosis,” *Circulation*, vol. 135, no. 5, p. 476, Jan. 2017, doi: 10.1161/CIRCULATIONAHA.116.025684.

[43] C. Liu, Z. Jiang, Z. Pan, and L. Yang, “The Function, Regulation and Mechanism of Programmed Cell Death of Macrophages in Atherosclerosis,” *Front Cell Dev Biol*, vol. 9, p. 809516, Jan. 2022, doi: 10.3389/FCELL.2021.809516/BIBTEX.

[44] N. Wang and A. R. Tall, “Regulation and mechanisms of ATP-binding cassette transporter A1-mediated cellular cholesterol efflux,” *Arterioscler Thromb Vasc Biol*, vol. 23, no. 7, pp. 1178–1184, Jul. 2003, doi: 10.1161/01.ATV.0000075912.83860.26.

[45] N. A-Gonzalez *et al.*, “Apoptotic cells promote their own clearance and immune tolerance through activation of LXR,” *Immunity*, vol. 31, no. 2, p. 245, Aug. 2009, doi: 10.1016/J.IMMUNI.2009.06.018.

[46] T. Rőszer *et al.*, “Autoimmune Kidney Disease and Impaired Engulfment of Apoptotic Cells in Mice with Macrophage Peroxisome Proliferator-Activated Receptor γ or Retinoid X Receptor α Deficiency,” *J Immunol*, vol. 186, no. 1, p. 621, Jan. 2010, doi: 10.4049/JIMMUNOL.1002230.

[47] L. Mukundan *et al.*, “PPAR-δ senses and orchestrates clearance of apoptotic cells to promote tolerance,” *Nat Med*, vol. 15, no. 11, p. 1266, Nov. 2009, doi: 10.1038/NM.2048.

[48] N. Ipseiz *et al.*, “The Nuclear Receptor Nr4a1 Mediates Anti-Inflammatory Effects of Apoptotic Cells,” *The Journal of Immunology*, vol. 192, no. 10, pp. 4852–4858, May 2014, doi: 10.4049/JIMMUNOL.1303377.

[49] V. Li, M. D. Binder, and T. J. Kilpatrick, “The Tolerogenic Influence of Dexamethasone on Dendritic Cells Is Accompanied by the Induction of Efferocytosis, Promoted by MERTK,” *Int J Mol Sci*, vol. 24, no. 21, p. 15903, Nov. 2023, doi: 10.3390/IJMS242115903/S1.

[50] Y. S. Yoon, S. Y. Kim, M. J. Kim, J. H. Lim, M. S. Cho, and J. L. Kang, “PPARγ activation following apoptotic cell instillation promotes resolution of lung inflammation and fibrosis via regulation of efferocytosis and proresolving cytokines,” *Mucosal Immunology 2015 8:5*, vol. 8, no. 5, pp. 1031–1046, Jan. 2015, doi: 10.1038/mi.2014.130.

[51] M. Viaud *et al.*, “Lysosomal cholesterol hydrolysis couples efferocytosis to anti-inflammatory oxysterol production,” *Circ Res*, vol. 122, no. 10, pp. 1369–1384, May 2018, doi: 10.1161/CIRCRESAHA.117.312333/-/DC1.

[52] T. Rőszer *et al.*, “Autoimmune Kidney Disease and Impaired Engulfment of Apoptotic Cells in Mice with Macrophage Peroxisome Proliferator-Activated Receptor γ or Retinoid X Receptor α Deficiency,” vol. 186, no. 1, doi: 10.4049/JIMMUNOL.1002230.

[53] N. A-Gonzalez *et al.*, “Apoptotic cells promote their own clearance and immune tolerance through activation of LXR,” *Immunity*, vol. 31, no. 2, p. 245, Aug. 2009, doi: 10.1016/J.IMMUNI.2009.06.018.

[54] A. Szanto *et al.*, “STAT6 Transcription Factor Is a Facilitator of the Nuclear Receptor PPARγ-Regulated Gene Expression in Macrophages and Dendritic Cells,” *Immunity*, vol. 33, no. 5, p. 699, Nov. 2010, doi: 10.1016/J.IMMUNI.2010.11.009.

[55] N. A-Gonzalez and A. Hidalgo, “Nuclear receptors and clearance of apoptotic cells: Stimulating the macrophage’s appetite,” *Front Immunol*, vol. 5, no. MAY, p. 87894, May 2014, doi: 10.3389/FIMMU.2014.00211/BIBTEX.

[56] C. Yin and B. Heit, “Cellular Responses to the Efferocytosis of Apoptotic Cells,” *Front Immunol*, vol. 12, p. 631714, Apr. 2021, Accessed: May 01, 2025. [Online]. Available: https://pmc.ncbi.nlm.nih.gov/articles/PMC8093429/

[57] E. Y. Chung *et al.*, “Interleukin-10 Expression in Macrophages during Phagocytosis of Apoptotic Cells Is Mediated by the TALE homeoproteins Pbx-1 and Prep-1,” *Immunity*, vol. 27, no. 6, p. 952, Dec. 2007, doi: 10.1016/J.IMMUNI.2007.11.014.

[58] Y. Q. Xiao, C. G. Freire-de-Lima, W. P. Schiemann, D. L. Bratton, R. W. Vandivier, and P. M. Henson, “Transcriptional and Translational Regulation of Transforming Growth Factor-β Production in Response to Apoptotic Cells,” *J Immunol*, vol. 181, no. 5, p. 3575, Sep. 2008, doi: 10.4049/JIMMUNOL.181.5.3575.

[59] L. Bosurgi *et al.*, “Macrophage function in tissue repair and remodeling requires IL-4 or IL-13 with apoptotic cells,” *Science*, vol. 356, no. 6342, p. 1072, Jun. 2017, doi: 10.1126/SCIENCE.AAI8132.

[60] I. Liebold *et al.*, “Apoptotic cell identity induces distinct functional responses to IL-4 in efferocytic macrophages,” *Science (1979)*, vol. 384, no. 6691, Apr. 2024, doi: 10.1126/SCIENCE.ABO7027/SUPPL_FILE/SCIENCE.ABO7027_DATA_S1.ZIP.

[61] S. Y. Kim and M. G. Nair, “Macrophages in wound healing: activation and plasticity,” *Immunol Cell Biol*, vol. 97, no. 3, p. 258, Mar. 2019, doi: 10.1111/IMCB.12236.

[62] K. Yamaji-Kegan, Q. Su, D. J. Angelini, H. C. Champion, and R. A. Johns, “Hypoxia-induced mitogenic factor has proangiogenic and proinflammatory effects in the lung via VEGF and VEGF receptor-2,” *Am J Physiol Lung Cell Mol Physiol*, vol. 291, no. 6, Dec. 2006, doi: 10.1152/AJPLUNG.00168.2006.

[63] L. Li *et al.*, “M2a Macrophage-Secreted CHI3L1 Promotes Extracellular Matrix Metabolic Imbalances via Activation of IL-13Rα2/MAPK Pathway in Rat Intervertebral Disc Degeneration,” *Front Immunol*, vol. 12, p. 666361, Jun. 2021, doi: 10.3389/FIMMU.2021.666361.

[64] H. S. Kim *et al.*, “Detrimental influence of Arginase-1 in infiltrating macrophages on poststroke functional recovery and inflammatory milieu,” *Proc Natl Acad Sci U*

S A, vol. 122, no. 7, p. e2413484122, Feb. 2025, doi: 10.1073/PNAS.2413484122/SUPPL_FILE/PNAS.2413484122.SM01.MP4.

[65] B. D. Gerlach *et al.*, "Efferocytosis Induces Macrophage Proliferation to Help Resolve Tissue Injury," *Cell Metab*, vol. 33, no. 12, p. 2445, Dec. 2021, doi: 10.1016/J.CMET.2021.10.015.

[66] P. J. Murray and T. A. Wynn, "Protective and pathogenic functions of macrophage subsets," *Nat Rev Immunol*, vol. 11, no. 11, p. 723, Nov. 2011, doi: 10.1038/NRI3073.

[67] M. R. Elliott, K. M. Koster, and P. S. Murphy, "Efferocytosis signaling in the regulation of macrophage inflammatory responses," *J Immunol*, vol. 198, no. 4, p. 1387, Feb. 2017, doi: 10.4049/JIMMUNOL.1601520.

[68] Y. ZHANG, Y. WANG, J. DING, and P. LIU, "Efferocytosis in multisystem diseases," *Mol Med Rep*, vol. 25, no. 1, p. 13, Jan. 2021, doi: 10.3892/MMR.2021.12529.

[69] B. Rong *et al.*, "Unraveling the role of macrophages in diabetes: Impaired phagocytic function and therapeutic prospects," *Medicine (United States)*, vol. 104, no. 8, p. e41613, Feb. 2025, doi: 10.1097/MD.0000000000041613.

[70] Z. Kuzmina, D. Stroncek, and S. Z. Pavletic, "Extracorporeal Photopheresis as a Therapy for Autoimmune Diseases," *J Clin Apher*, vol. 30, no. 4, p. 224, Aug. 2014, doi: 10.1002/JCA.21367.

[71] A. Dangi and X. Luo, "Harnessing Apoptotic Cells for Transplantation Tolerance: Current Status and Future Perspectives," *Curr Transplant Rep*, vol. 4, no. 4, p. 270, Dec. 2017, doi: 10.1007/S40472-017-0167-4.

[72] V. Davra *et al.*, "Axl and Mertk receptors cooperate to promote breast cancer progression by combined oncogenic signaling and evasion of host anti-tumor immunity," *Cancer Res*, vol. 81, no. 3, p. 698, Feb. 2020, doi: 10.1158/0008-5472.CAN-20-2066.

[73] S. Demirsoy *et al.*, "Targeting Tyro3, Axl, and MerTK Receptor Tyrosine Kinases Significantly Sensitizes Triple-Negative Breast Cancer to CDK4/6 Inhibition," *Cancers (Basel)*, vol. 16, no. 12, p. 2253, Jun. 2024, doi: 10.3390/CANCERS16122253/S1.

[74] R. M. A. Linger *et al.*, "Mer or Axl Receptor Tyrosine Kinase Inhibition Promotes Apoptosis, Blocks Growth, and Enhances Chemosensitivity of Human Non-Small Cell Lung Cancer," *Oncogene*, vol. 32, no. 29, p. 3420, Jul. 2012, doi: 10.1038/ONC.2012.355.

[75] S. M. Post *et al.*, "AXL/MERTK inhibitor ONO-7475 potently synergizes with venetoclax and overcomes venetoclax resistance to kill *FLT3*-ITD acute myeloid

leukemia," *Haematologica*, vol. 107, no. 6, pp. 1311–1322, Jun. 2022, doi: 10.3324/HAEMATOL.2021.278369.

[76] J. Wu *et al.*, "MerTK as a therapeutic target in glioblastoma," *Neuro Oncol*, vol. 20, no. 1, p. 92, Jan. 2017, doi: 10.1093/NEUONC/NOX111.

[77] J. M. Huelse, D. M. Fridlyand, S. Earp, D. DeRyckere, and D. K. Graham, "MERTK in Cancer Therapy: Targeting the Receptor Tyrosine Kinase in Tumor Cells and the Immune System," *Pharmacol Ther*, vol. 213, p. 107577, Sep. 2020, doi: 10.1016/J.PHARMTHERA.2020.107577.

[78] C. T. Cummings, D. DeRyckere, H. S. Earp, and D. K. Graham, "Molecular Pathways: MERTK Signaling in Cancer," *Clin Cancer Res*, vol. 19, no. 19, p. 5275, Oct. 2013, doi: 10.1158/1078-0432.CCR-12-1451.

[79] K. V. Myers, S. R. Amend, and K. J. Pienta, "Targeting Tyro3, Axl and MerTK (TAM receptors): implications for macrophages in the tumor microenvironment," *Mol Cancer*, vol. 18, no. 1, p. 94, May 2019, doi: 10.1186/S12943-019-1022-2.

[80] J. Cruz Cruz *et al.*, "Inhibiting efferocytosis reverses macrophage-mediated immunosuppression in the leukemia microenvironment," *Front Immunol*, vol. 14, p. 1146721, 2023, doi: 10.3389/FIMMU.2023.1146721/FULL.

[81] L. Bosurgi *et al.*, "Paradoxical role of the proto-oncogene Axl and Mer receptor tyrosine kinases in colon cancer," *Proc Natl Acad Sci U S A*, vol. 110, no. 32, pp. 13091–13096, Aug. 2013, doi: 10.1073/PNAS.1302507110/SUPPL_FILE/PNAS.201302507SI.PDF.

[82] R. Fernandez-Boyanapalli, S. C. Frasch, D. W. H. Riches, R. W. Vandivier, P. M. Henson, and D. L. Bratton, "PPARγ activation normalizes resolution of acute sterile inflammation in murine chronic granulomatous disease," *Blood*, vol. 116, no. 22, p. 4512, Nov. 2010, doi: 10.1182/BLOOD-2010-02-272005.

[83] C. N. Serhan, "Novel Pro-Resolving Lipid Mediators in Inflammation Are Leads for Resolution Physiology," *Nature*, vol. 510, no. 7503, p. 92, 2014, doi: 10.1038/NATURE13479.

[84] A. C. Tosello-Trampont, K. Nakada-Tsukui, and K. S. Ravichandran, "Engulfment of apoptotic cells is negatively regulated by Rho-mediated signaling," *J Biol Chem*, vol. 278, no. 50, pp. 49911–49919, Dec. 2003, doi: 10.1074/JBC.M306079200.

[85] A. Tajbakhsh *et al.*, "Statin-regulated phagocytosis and efferocytosis in physiological and pathological conditions," *Pharmacol Ther*, vol. 238, Oct. 2022, doi: 10.1016/J.PHARMTHERA.2022.108282.

[86] K. Morimoto *et al.*, "Lovastatin Enhances Clearance of Apoptotic Cells (Efferocytosis) with Implications for Chronic Obstructive Pulmonary Disease," *The*

Journal of Immunology, vol. 176, no. 12, pp. 7657–7665, Jun. 2006, doi: 10.4049/JIMMUNOL.176.12.7657.

[87] D. J. Wu *et al.*, "Effects of fasudil on early atherosclerotic plaque formation and established lesion progression in apolipoprotein E-knockout mice," *Atherosclerosis*, vol. 207, no. 1, pp. 68–73, Nov. 2009, doi: 10.1016/J.ATHEROSCLEROSIS.2009.04.025.

[88] T. M. Yang *et al.*, "Targeting macrophages in atherosclerosis using nanocarriers loaded with liver X receptor agonists: A narrow review," *Front Mol Biosci*, vol. 10, p. 1147699, Mar. 2023, doi: 10.3389/FMOLB.2023.1147699/XML/NLM.

[89] S. B. Joseph *et al.*, "Synthetic LXR ligand inhibits the development of atherosclerosis in mice," *Proc Natl Acad Sci U S A*, vol. 99, no. 11, p. 7604, May 2002, doi: 10.1073/PNAS.112059299.

[90] M. B. Fessler, "The challenges and promise of targeting the Liver X Receptors for treatment of inflammatory disease," *Pharmacol Ther*, vol. 181, pp. 1–12, Jan. 2018, doi: 10.1016/J.PHARMTHERA.2017.07.010.

[91] E. D. Rosen and B. M. Spiegelman, "What we talk about when we talk about fat," *Cell*, vol. 156, no. 1–2, pp. 20–44, Jan. 2014, doi: 10.1016/J.CELL.2013.12.012/ASSET/9971D271-C55A-4A5C-8D2D-CCD765B3C2AC/MAIN.ASSETS/GR4.JPG.

[92] A. Sakers, M. K. De Siqueira, P. Seale, and C. J. Villanueva, "Adipose tissue plasticity in health and disease," *Cell*, vol. 185, no. 3, p. 419, Feb. 2022, doi: 10.1016/J.CELL.2021.12.016.

[93] E. D. Rosen and B. M. Spiegelman, "Adipocytes as regulators of energy balance and glucose homeostasis," *Nature*, vol. 444, no. 7121, p. 847, Dec. 2006, doi: 10.1038/NATURE05483.

[94] B. Cannon and J. Nedergaard, "Brown adipose tissue: function and physiological significance," *Physiol Rev*, vol. 84, no. 1, pp. 277–359, Jan. 2004, doi: 10.1152/PHYSREV.00015.2003.

[95] B. L. Wajchenberg, "Subcutaneous and Visceral Adipose Tissue: Their Relation to the Metabolic Syndrome," *Endocr Rev*, vol. 21, no. 6, pp. 697–738, Dec. 2000, doi: 10.1210/EDRV.21.6.0415.

[96] E. Börgeson, J. Boucher, and C. E. Hagberg, "Of mice and men: Pinpointing species differences in adipose tissue biology," *Front Cell Dev Biol*, vol. 10, p. 1003118, Sep. 2022, doi: 10.3389/FCELL.2022.1003118/BIBTEX.

[97] K. Karastergiou, S. R. Smith, A. S. Greenberg, and S. K. Fried, “Sex differences in human adipose tissues - The biology of pear shape,” *Biol Sex Differ*, vol. 3, no. 1, pp. 1–12, May 2012, doi: 10.1186/2042-6410-3-13/FIGURES/2.

[98] K. E. Davis *et al.*, “The sexually dimorphic role of adipose and adipocyte estrogen receptors in modulating adipose tissue expansion, inflammation, and fibrosis,” *Mol Metab*, vol. 2, no. 3, pp. 227–242, Aug. 2013, doi: 10.1016/J.MOLMET.2013.05.006.

[99] U. S. Pettersson, T. B. Waldén, P. O. Carlsson, L. Jansson, and M. Phillipson, “Female Mice are Protected against High-Fat Diet Induced Metabolic Syndrome and Increase the Regulatory T Cell Population in Adipose Tissue,” *PLoS One*, vol. 7, no. 9, p. e46057, Sep. 2012, doi: 10.1371/JOURNAL.PONE.0046057.

[100] H. Waller-Evans *et al.*, “Nutrigenomics of High Fat Diet Induced Obesity in Mice Suggests Relationships between Susceptibility to Fatty Liver Disease and the Proteasome,” *PLoS One*, vol. 8, no. 12, p. e82825, Dec. 2013, doi: 10.1371/JOURNAL.PONE.0082825.

[101] M. S. Siersbæk *et al.*, “C57BL/6J substrain differences in response to high-fat diet intervention,” *Scientific Reports 2020 10:1*, vol. 10, no. 1, pp. 1–15, Aug. 2020, doi: 10.1038/s41598-020-70765-w.

[102] D. T. Chu, E. Malinowska, M. Jura, and L. P. Kozak, “C57BL/6J mice as a polygenic developmental model of diet-induced obesity,” *Physiol Rep*, vol. 5, no. 7, p. e13093, Apr. 2017, doi: 10.14814/PHY2.13093.

[103] I. Zucker and A. K. Beery, “Males still dominate animal studies,” *Nature 2010 465:7299*, vol. 465, no. 7299, pp. 690–690, Jun. 2010, doi: 10.1038/465690a.

[104] K. E. Wellen and G. S. Hotamisligil, “Inflammation, stress, and diabetes,” *J Clin Invest*, vol. 115, no. 5, pp. 1111–1119, May 2005, doi: 10.1172/JCI25102.

[105] S. A. Porter, J. M. Massaro, U. Hoffmann, R. S. Vasan, C. J. O’Donnel, and C. S. Fox, “Abdominal subcutaneous adipose tissue: a protective fat depot?,” *Diabetes Care*, vol. 32, no. 6, pp. 1068–1075, Jun. 2009, doi: 10.2337/DC08-2280.

[106] H. Li *et al.*, “Fibroblast growth factor 21 increases insulin sensitivity through specific expansion of subcutaneous fat,” *Nature Communications 2018 9:1*, vol. 9, no. 1, pp. 1–16, Jan. 2018, doi: 10.1038/s41467-017-02677-9.

[107] A. Chait and L. J. den Hartigh, “Adipose Tissue Distribution, Inflammation and Its Metabolic Consequences, Including Diabetes and Cardiovascular Disease,” *Front Cardiovasc Med*, vol. 7, p. 522637, Feb. 2020, doi: 10.3389/FCVM.2020.00022/XML/NLM.

[108] A. Fedorenko, P. V. Lishko, and Y. Kirichok, “Mechanism of Fatty-Acid-Dependent UCP1 Uncoupling in Brown Fat Mitochondria,” *Cell*, vol. 151, no. 2, p. 400, Oct. 2012, doi: 10.1016/J.CELL.2012.09.010.

[109] S. B. Levy, “Field and laboratory methods for quantifying brown adipose tissue thermogenesis,” *Am J Hum Biol*, vol. 31, no. 4, Jul. 2019, doi: 10.1002/AJHB.23261.

[110] A. M. Mesa *et al.*, “Identification and characterization of novel abdominal and pelvic brown adipose depots in mice,” *Adipocyte*, vol. 11, no. 1, p. 616, 2022, doi: 10.1080/21623945.2022.2133415.

[111] E. Verduci *et al.*, “Brown Adipose Tissue: New Challenges for Prevention of Childhood Obesity. A Narrative Review,” *Nutrients*, vol. 13, no. 5, p. 1450, May 2021, doi: 10.3390/NU13051450.

[112] A. M. Cypess *et al.*, “Identification and importance of brown adipose tissue in adult humans,” *N Engl J Med*, vol. 360, no. 15, pp. 1509–1517, Apr. 2009, doi: 10.1056/NEJMOA0810780.

[113] K. A. Virtanen *et al.*, “Functional brown adipose tissue in healthy adults,” *N Engl J Med*, vol. 360, no. 15, pp. 1518–1525, Apr. 2009, doi: 10.1056/NEJMOA0808949.

[114] W. D. van Marken Lichtenbelt *et al.*, “Cold-activated brown adipose tissue in healthy men,” *N Engl J Med*, vol. 360, no. 15, pp. 1500–1508, Apr. 2009, doi: 10.1056/NEJMOA0808718.

[115] M. Saito *et al.*, “High incidence of metabolically active brown adipose tissue in healthy adult humans: effects of cold exposure and adiposity,” *Diabetes*, vol. 58, no. 7, pp. 1526–1531, Jul. 2009, doi: 10.2337/DB09-0530.

[116] J. Orava *et al.*, “Different metabolic responses of human brown adipose tissue to activation by cold and insulin,” *Cell Metab*, vol. 14, no. 2, pp. 272–279, Aug. 2011, doi: 10.1016/J.CMET.2011.06.012.

[117] T. Yoneshiro *et al.*, “Brown adipose tissue, whole-body energy expenditure, and thermogenesis in healthy adult men,” *Obesity (Silver Spring)*, vol. 19, no. 1, pp. 13–16, Jan. 2011, doi: 10.1038/OBY.2010.105.

[118] C. Huo *et al.*, “Effect of Acute Cold Exposure on Energy Metabolism and Activity of Brown Adipose Tissue in Humans: A Systematic Review and Meta-Analysis,” *Front Physiol*, vol. 13, p. 917084, Jun. 2022, doi: 10.3389/FPHYS.2022.917084/BIBTEX.

[119] M. Saito, “Brown Adipose Tissue as a Regulator of Energy Expenditure and Body Fat in Humans,” *Diabetes Metab J*, vol. 37, no. 1, p. 22, Feb. 2013, doi: 10.4093/DMJ.2013.37.1.22.

[120] P. Lee, J. R. Greenfield, K. K. Y. Ho, and M. J. Fulham, “A critical appraisal of the prevalence and metabolic significance of brown adipose tissue in adult humans,” *Am J Physiol Endocrinol Metab*, vol. 299, no. 4, Oct. 2010, doi: 10.1152/AJPENDO.00298.2010.

[121] M. Matsushita, T. Yoneshiro, S. Aita, T. Kameya, H. Sugie, and M. Saito, “Impact of brown adipose tissue on body fatness and glucose metabolism in healthy humans,” *Int J Obes (Lond)*, vol. 38, no. 6, pp. 812–817, 2014, doi: 10.1038/IJO.2013.206.

[122] Q. Wang *et al.*, “Brown Adipose Tissue Activation Is Inversely Related to Central Obesity and Metabolic Parameters in Adult Human,” *PLoS One*, vol. 10, no. 4, p. e0123795, Apr. 2015, doi: 10.1371/JOURNAL.PONE.0123795.

[123] T. Becher *et al.*, “Brown adipose tissue is associated with cardiometabolic health,” *Nature Medicine 2021 27:1*, vol. 27, no. 1, pp. 58–65, Jan. 2021, doi: 10.1038/s41591-020-1126-7.

[124] I. Shimizu *et al.*, “Vascular rarefaction mediates whitening of brown fat in obesity,” *J Clin Invest*, vol. 124, no. 5, pp. 2099–2112, May 2014, doi: 10.1172/JCI71643.

[125] X. X. Pan *et al.*, “Senescent T Cell Induces Brown Adipose Tissue ‘Whitening’ Via Secreting IFN-γ,” *Front Cell Dev Biol*, vol. 9, p. 637424, Mar. 2021, doi: 10.3389/FCELL.2021.637424/BIBTEX.

[126] K. Ziqubu *et al.*, “An insight into brown/beige adipose tissue whitening, a metabolic complication of obesity with the multifactorial origin,” *Front Endocrinol (Lausanne)*, vol. 14, p. 1114767, Feb. 2023, doi: 10.3389/FENDO.2023.1114767/XML/NLM.

[127] S. Kajimura, B. M. Spiegelman, and P. Seale, “Brown and beige fat: Physiological roles beyond heat generation,” *Cell Metab*, vol. 22, no. 4, pp. 546–559, Oct. 2015, doi: 10.1016/J.CMET.2015.09.007/ASSET/2B63AD8D-7BE4-421F-9B57-6E90C20F8086/MAIN.ASSETS/GR2.JPG.

[128] J. Wu *et al.*, “Beige adipocytes are a distinct type of thermogenic fat cell in mouse and human,” *Cell*, vol. 150, no. 2, pp. 366–376, Jul. 2012, doi: 10.1016/j.cell.2012.05.016.

[129] B. S. Finlin *et al.*, “Human adipose beiging in response to cold and mirabegron,” *JCI Insight*, vol. 3, no. 15, p. e121510, Aug. 2018, doi: 10.1172/JCI.INSIGHT.121510.

[130] B. S. Magro and D. P. M. Dias, “Brown and beige adipose tissue: New therapeutic targets for metabolic disorders,” *Health Sciences Review*, vol. 10, p. 100148, Mar. 2024, doi: 10.1016/J.HSR.2024.100148.

[131] J. M. A. de Jong *et al.*, “Human brown adipose tissue is phenocopied by classical brown adipose tissue in physiologically humanized mice,” *Nat Metab*, vol. 1, no. 8, pp. 830–843, Aug. 2019, doi: 10.1038/S42255-019-0101-4.

[132] A. W. Fischer, B. Cannon, and J. Nedergaard, “Optimal housing temperatures for mice to mimic the thermal environment of humans: An experimental study,” *Mol Metab*, vol. 7, pp. 161–170, Jan. 2018, doi: 10.1016/J.MOLMET.2017.10.009.

[133] R. J. Havel, “Postprandial lipid metabolism: an overview,” *Proceedings of the Nutrition Society*, vol. 56, no. 2, pp. 659–666, Jul. 1997, doi: 10.1079/PNS19970065.

[134] G. Ranganathan *et al.*, “The lipogenic enzymes DGAT1, FAS, and LPL in adipose tissue: effects of obesity, insulin resistance, and TZD treatment,” *J Lipid Res*, vol. 47, no. 11, p. 2444, Nov. 2006, doi: 10.1194/JLR.M600248-JLR200.

[135] A. R. Saltiel and C. R. Kahn, “Insulin signalling and the regulation of glucose and lipid metabolism,” *Nature*, vol. 414, no. 6865, pp. 799–806, Dec. 2001, doi: 10.1038/414799A.

[136] D. E. James, M. Strube, and M. Muecdler, “Molecular cloning and characterization of an insulin-regulatable glucose transporter,” *Nature 1989 338:6210*, vol. 338, no. 6210, pp. 83–87, 1989, doi: 10.1038/338083a0.

[137] Z. Song, A. M. Xiaoli, and F. Yang, “Regulation and Metabolic Significance of De Novo Lipogenesis in Adipose Tissues,” *Nutrients*, vol. 10, no. 10, p. 1383, Oct. 2018, doi: 10.3390/NU10101383.

[138] M. A. Herman *et al.*, “A novel ChREBP isoform in adipose tissue regulates systemic glucose metabolism,” *Nature 2012 484:7394*, vol. 484, no. 7394, pp. 333–338, Apr. 2012, doi: 10.1038/nature10986.

[139] C. Schlein *et al.*, “Endogenous Fatty Acid Synthesis Drives Brown Adipose Tissue Involution,” *Cell Rep*, vol. 34, no. 2, Jan. 2021, doi: 10.1016/J.CELREP.2020.108624.

[140] J. Sanchez-Gurmaches *et al.*, “Brown fat AKT2 is a cold-induced kinase that stimulates ChREBP-mediated de novo lipogenesis to optimize fuel storage and thermogenesis,” *Cell Metab*, vol. 27, no. 1, p. 195, Jan. 2017, doi: 10.1016/J.CMET.2017.10.008.

[141] L. Scheja, J. Behrens, J. Heeren, and M. Heine, “Compensatory metabolic responses in ChREBP-deficient brown adipose tissue,” *Atherosclerosis*, vol. 395, p. 118512, Aug. 2024, doi: 10.1016/j.atherosclerosis.2024.118512.

[142] M. Adlanmerini *et al.*, “Circadian lipid synthesis in brown fat maintains murine body temperature during chronic cold,” *Proc Natl Acad Sci U S A*, vol. 116, no. 37,

pp. 18691–18699, Sep. 2019, doi: 10.1073/PNAS.1909883116/SUPPL_FILE/PNAS.1909883116.SAPP.PDF.

[143] J. R. Mead, S. A. Irvine, and D. P. Ramji, “Lipoprotein lipase: Structure, function, regulation, and role in disease,” *J Mol Med*, vol. 80, no. 12, pp. 753–769, 2002, doi: 10.1007/S00109-002-0384-9/METRICS.

[144] A. Bartelt *et al.*, “Brown adipose tissue activity controls triglyceride clearance,” *Nat Med*, vol. 17, no. 2, pp. 200–206, Feb. 2011, doi: 10.1038/NM.2297.

[145] V. P. Knutson, “The release of lipoprotein lipase from 3T3-L1 adipocytes is regulated by microvessel endothelial cells in an insulin-dependent manner,” *Endocrinology*, vol. 141, no. 2, pp. 693–701, 2000, doi: 10.1210/ENDO.141.2.7315.

[146] B. S. J. Davies *et al.*, “GPIHBP1 Is Responsible for the Entry of Lipoprotein Lipase into Capillaries,” *Cell Metab*, vol. 12, no. 1, p. 42, Jul. 2010, doi: 10.1016/J.CMET.2010.04.016.

[147] M. Heine *et al.*, “Lipolysis Triggers a Systemic Insulin Response Essential for Efficient Energy Replenishment of Activated Brown Adipose Tissue in Mice,” *Cell Metab*, vol. 28, no. 4, pp. 644-655.e4, Oct. 2018, doi: 10.1016/j.cmet.2018.06.020.

[148] A. W. Fischer *et al.*, “Lysosomal lipoprotein processing in endothelial cells stimulates adipose tissue thermogenic adaptation,” *Cell Metab*, vol. 33, no. 3, pp. 547-564.e7, Mar. 2021, doi: 10.1016/J.CMET.2020.12.001/ATTACHMENT/245DFB6A-637B-43FD-B4F6-E961DC0849C0/MMC2.PDF.

[149] J. J. F. P. Luiken *et al.*, “Insulin induces the translocation of the fatty acid transporter FAT/CD36 to the plasma membrane,” *Am J Physiol Endocrinol Metab*, vol. 282, no. 2 45-2, 2002, doi: 10.1152/AJPENDO.00419.2001/ASSET/IMAGES/LARGE/H10220708004.JPEG.

[150] L. Maréchal *et al.*, “The CD36-PPARγ Pathway in Metabolic Disorders.,” *Int J Mol Sci*, vol. 19, no. 5, pp. E1529–E1529, May 2018, doi: 10.3390/IJMS19051529.

[151] P. Tontonoz, L. Nagy, J. G. A. Alvarez, V. A. Thomazy, and R. M. Evans, “PPARγ promotes monocyte/macrophage differentiation and uptake of oxidized LDL,” *Cell*, vol. 93, no. 2, pp. 241–252, Apr. 1998, doi: 10.1016/S0092-8674(00)81575-5/ASSET/18820DC3-6DAD-45E6-81BC-A126DA0A9BED/MAIN.ASSETS/GR9.JPG.

[152] B. W. Parks *et al.*, “CD36, but not G2A, modulates efferocytosis, inflammation, and fibrosis following bleomycin-induced lung injury,” *J Lipid Res*, vol. 54, no. 4, p. 1114, Apr. 2013, doi: 10.1194/JLR.M035352.

[153] Y. Li, Z. Li, D. A. Ngandiri, M. Llerins Perez, A. Wolf, and Y. Wang, “The Molecular Brakes of Adipose Tissue Lipolysis,” *Front Physiol*, vol. 13, p. 826314, Feb. 2022, doi: 10.3389/FPHYS.2022.826314/XML/NLM.

[154] J. Zhao, L. Unelius, T. Bengtsson, B. Cannon, and J. Nedergaard, “Coexisting beta-adrenoceptor subtypes: significance for thermogenic process in brown fat cells,” *Am J Physiol*, vol. 267, no. 4 Pt 1, 1994, doi: 10.1152/AJPCELL.1994.267.4.C969.

[155] M. J. Riis-Vestergaard, B. Richelsen, J. M. Bruun, W. Li, J. B. Hansen, and S. B. Pedersen, “Beta-1 and Not Beta-3 Adrenergic Receptors May Be the Primary Regulator of Human Brown Adipocyte Metabolism,” *J Clin Endocrinol Metab*, vol. 105, no. 4, pp. E994–E1005, Apr. 2020, doi: 10.1210/CLINEM/DGZ298.

[156] D. P. Blondin *et al.*, “Human Brown Adipocyte Thermogenesis Is Driven by β2-AR Stimulation,” *Cell Metab*, vol. 32, no. 2, pp. 287-300.e7, Aug. 2020, doi: 10.1016/J.CMET.2020.07.005.

[157] C. Cero, H. J. Lea, K. Y. Zhu, F. Shamsi, Y. H. Tseng, and A. M. Cypess, “β3-Adrenergic receptors regulate human brown/beige adipocyte lipolysis and thermogenesis,” *JCI Insight*, vol. 6, no. 11, Jun. 2021, doi: 10.1172/JCI.INSIGHT.139160.

[158] S. P. Pydi *et al.*, “Adipocyte β-arrestin-2 is essential for maintaining whole body glucose and energy homeostasis,” *Nature Communications 2019 10:1*, vol. 10, no. 1, pp. 1–14, Jul. 2019, doi: 10.1038/s41467-019-11003-4.

[159] M. VAUGHAN, J. E. BERGER, and D. STEINBERG, “Hormone-sensitive Lipase and Monoglyceride Lipase Activities in Adipose Tissue,” *Journal of Biological Chemistry*, vol. 239, no. 2, pp. 401–409, Feb. 1964, doi: 10.1016/S0021-9258(18)51692-6.

[160] H. Miyoshi *et al.*, “Perilipin Promotes Hormone-sensitive Lipase-mediated Adipocyte Lipolysis via Phosphorylation-dependent and -independent Mechanisms,” *Journal of Biological Chemistry*, vol. 281, no. 23, pp. 15837–15844, Jun. 2006, doi: 10.1074/JBC.M601097200.

[161] C. Desgrouas, T. Thalheim, M. Cerino, C. Badens, and N. Bonello-Palot, “Perilipin 1: a systematic review on its functions on lipid metabolism and atherosclerosis in mice and humans,” *Cardiovasc Res*, vol. 120, no. 3, pp. 237–248, Mar. 2024, doi: 10.1093/CVR/CVAE005.

[162] A. Lass *et al.*, “Adipose triglyceride lipase-mediated lipolysis of cellular fat stores is activated by CGI-58 and defective in Chanarin-Dorfman Syndrome,” *Cell Metab*, vol. 3, no. 5, pp. 309–319, May 2006, doi: 10.1016/J.CMET.2006.03.005.

[163] M. W. Anthonsen, L. Rönnstrand, C. Wernstedt, E. Degerman, and C. Holm, “Identification of novel phosphorylation sites in hormone-sensitive lipase that are phosphorylated in response to isoproterenol and govern activation properties in vitro,” *J Biol Chem*, vol. 273, no. 1, pp. 215–221, Jan. 1998, doi: 10.1074/JBC.273.1.215.

[164] A. J. GARTON, D. G. CAMPBELL, D. CARLING, D. G. HARDIE, R. J. COLBRAN, and S. J. YEAMAN, “Phosphorylation of bovine hormone-sensitive lipase by the AMP-activated protein kinase. A possible antilipolytic mechanism,” *Eur J Biochem*, vol. 179, no. 1, pp. 249–254, 1989, doi: 10.1111/J.1432-1033.1989.TB14548.X.

[165] S. Martin, S. Okano, C. Kistler, M. A. Fernandez-Rojo, M. M. Hill, and R. G. Parton, “Spatiotemporal Regulation of Early Lipolytic Signaling in Adipocytes,” *J Biol Chem*, vol. 284, no. 46, p. 32097, 2009, doi: 10.1074/JBC.M109.002675.

[166] R. E. Duncan, M. Ahmadian, K. Jaworski, E. Sarkadi-Nagy, and H. S. Sul, “Regulation of Lipolysis in Adipocytes,” *Annu Rev Nutr*, vol. 27, p. 79, 2007, doi: 10.1146/ANNUREV.NUTR.27.061406.093734.

[167] P. M. McDonough *et al.*, “Quantification of Hormone Sensitive Lipase Phosphorylation and Colocalization with Lipid Droplets in Murine 3T3L1 and Human Subcutaneous Adipocytes via Automated Digital Microscopy and High-Content Analysis,” *Assay Drug Dev Technol*, vol. 9, no. 3, p. 262, Jun. 2011, doi: 10.1089/ADT.2010.0302.

[168] M. A. Linden *et al.*, “Pharmacological inhibition of lipolysis prevents adverse metabolic outcomes during glucocorticoid administration,” *Mol Metab*, vol. 74, p. 101751, Aug. 2023, doi: 10.1016/J.MOLMET.2023.101751.

[169] M. Wang and C. Fotsch, “Small-Molecule Compounds that Modulate Lipolysis in Adipose Tissue: Targeting Strategies and Molecular Classes,” *Chem Biol*, vol. 13, no. 10, pp. 1019–1027, Oct. 2006, doi: 10.1016/J.CHEMBIOL.2006.09.010.

[170] W. Sui *et al.*, “Bladder drug mirabegron exacerbates atherosclerosis through activation of brown fat-mediated lipolysis,” *Proc Natl Acad Sci U S A*, vol. 166, no. 22, pp. 10937–10942, May 2019, doi: 10.1073/PNAS.1901655116/SUPPL_FILE/PNAS.1901655116.SAPP.PDF.

[171] A. M. Cypess *et al.*, “Activation of Human Brown Adipose Tissue by a β3-Adrenergic Receptor Agonist,” *Cell Metab*, vol. 21, no. 1, p. 33, Jan. 2015, doi: 10.1016/J.CMET.2014.12.009.

[172] K. Braun, J. Oeckl, J. Westermeier, Y. Li, and M. Klingenspor, “Non-adrenergic control of lipolysis and thermogenesis in adipose tissues,” *Journal of Experimental Biology*, vol. 121, no. Suppl_1, Mar. 2018, doi: 10.1242/JEB.165381/33995.

[173] L. Luo and M. Liu, “Adipose tissue in control of metabolism,” *J Endocrinol*, vol. 231, no. 3, p. R77, 2016, doi: 10.1530/JOE-16-0211.

[174] Y. Yang *et al.*, “O-GlcNAc transferase inhibits visceral fat lipolysis and promotes diet-induced obesity,” *Nature Communications 2020 11:1*, vol. 11, no. 1, pp. 1–15, Jan. 2020, doi: 10.1038/s41467-019-13914-8.

[175] X. Yang *et al.*, “Switching harmful visceral fat to beneficial energy combustion improves metabolic dysfunctions,” *JCI Insight*, vol. 2, no. 4, p. e89044, Feb. 2017, doi: 10.1172/JCI.INSIGHT.89044.

[176] M. A. Zuriaga, J. J. Fuster, N. Gokce, and K. Walsh, “Humans and Mice Display Opposing Patterns of ‘Browning’ Gene Expression in Visceral and Subcutaneous White Adipose Tissue Depots,” *Front Cardiovasc Med*, vol. 4, p. 27, May 2017, doi: 10.3389/FCVM.2017.00027.

[177] J. Chi *et al.*, “Three-Dimensional Adipose Tissue Imaging Reveals Regional Variation in Beige Fat Biogenesis and PRDM16-Dependent Sympathetic Neurite Density,” *Cell Metab*, vol. 27, no. 1, pp. 226-236.e3, Jan. 2018, doi: 10.1016/J.CMET.2017.12.011.

[178] X. Yang *et al.*, “Switching harmful visceral fat to beneficial energy combustion improves metabolic dysfunctions,” *JCI Insight*, vol. 2, no. 4, Feb. 2017, doi: 10.1172/JCI.INSIGHT.89044.

[179] S. Kajimura, B. M. Spiegelman, and P. Seale, “Brown and beige fat: Physiological roles beyond heat-generation,” *Cell Metab*, vol. 22, no. 4, p. 546, Oct. 2015, doi: 10.1016/J.CMET.2015.09.007.

[180] L. Y. Cheong and A. Xu, “Intercellular and inter-organ crosstalk in browning of white adipose tissue: molecular mechanism and therapeutic complications,” *J Mol Cell Biol*, vol. 13, no. 7, pp. 466–479, Oct. 2021, doi: 10.1093/JMCB/MJAB038.

[181] J. S. Rim and L. P. Kozak, “Regulatory motifs for CREB-binding protein and Nfe2l2 transcription factors in the upstream enhancer of the mitochondrial uncoupling protein 1 gene,” *J Biol Chem*, vol. 277, no. 37, pp. 34589–34600, Sep. 2002, doi: 10.1074/JBC.M108866200.

[182] S. Herzig *et al.*, “CREB regulates hepatic gluconeogenesis through the coactivator PGC-1,” *Nature*, vol. 413, no. 6852, pp. 179–183, Sep. 2001, doi: 10.1038/35093131.

[183] P. J. Fernandez-Marcos and J. Auwerx, “Regulation of PGC-1α, a nodal regulator of mitochondrial biogenesis1,” *Am J Clin Nutr*, vol. 93, no. 4, p. 884S, Apr. 2011, doi: 10.3945/AJCN.110.001917.

[184] P. Seale *et al.*, “Transcriptional Control of Brown Fat Determination by PRDM16,” *Cell Metab*, vol. 6, no. 1, p. 38, Jul. 2007, doi: 10.1016/J.CMET.2007.06.001.

[185] A. Desai, Z. Y. Loureiro, T. DeSouza, Q. Yang, J. Solivan-Rivera, and S. Corvera, “cAMP driven UCP1 induction in human adipocytes requires ATGL-catalyzed lipolysis,” *Mol Metab*, vol. 90, p. 102051, Dec. 2024, doi: 10.1016/J.MOLMET.2024.102051.

[186] L. A. de Jesus *et al.*, “The type 2 iodothyronine deiodinase is essential for adaptive thermogenesis in brown adipose tissue,” *J Clin Invest*, vol. 108, no. 9, pp. 1379–1385, Nov. 2001, doi: 10.1172/JCI13803.

[187] J. E. Silva and P. R. Larsen, “Adrenergic activation of triiodothyronine production in brown adipose tissue,” *Nature*, vol. 305, no. 5936, pp. 712–713, 1983, doi: 10.1038/305712A0.

[188] K. Ikeda, P. Maretich, and S. Kajimura, “The common and distinct features of brown and beige adipocytes,” *Trends Endocrinol Metab*, vol. 29, no. 3, p. 191, Mar. 2018, doi: 10.1016/J.TEM.2018.01.001.

[189] K. Ikeda and T. Yamada, “UCP1 Dependent and Independent Thermogenesis in Brown and Beige Adipocytes,” *Front Endocrinol (Lausanne)*, vol. 11, p. 544307, Jul. 2020, doi: 10.3389/FENDO.2020.00498/BIBTEX.

[190] B. Prapaharan, M. Lea, and J. L. Beaudry, “Weighing in on the role of brown adipose tissue for treatment of obesity,” *Journal of Pharmacy and Pharmaceutical Sciences*, vol. 27, p. 13157, Jul. 2024, doi: 10.3389/JPPS.2024.13157/XML/NLM.

[191] M. S. Rahman and H. Jun, “The Adipose Tissue Macrophages Central to Adaptive Thermoregulation,” *Front Immunol*, vol. 13, p. 884126, Apr. 2022, doi: 10.3389/FIMMU.2022.884126.

[192] J. C. Chang *et al.*, “Adaptive adipose tissue stromal plasticity in response to cold stress and antibody-based metabolic therapy.,” *Sci Rep*, vol. 9, no. 1, pp. 8833–8833, Jun. 2019, doi: 10.1038/S41598-019-45354-1.

[193] F. Shamsi *et al.*, “Vascular smooth muscle-derived TRPV1-positive progenitors are a source of cold-induced thermogenic adipocytes,” *Nat Metab*, vol. 3, no. 4, p. 485, Apr. 2021, doi: 10.1038/S42255-021-00373-Z.

[194] R. B. Burl, E. A. Rondini, H. Wei, R. Pique-Regi, and J. G. Granneman, “Deconstructing cold-induced brown adipocyte neogenesis in mice,” *Elife*, vol. 11, Jul. 2022, doi: 10.7554/ELIFE.80167.

[195] A. Asano, M. Morimatsu, H. Nikami, T. Yoshida, and M. Saito, “Adrenergic activation of vascular endothelial growth factor mRNA expression in rat brown

adipose tissue: implication in cold-induced angiogenesis," *Biochem J*, vol. 328 (Pt 1), no. Pt 1, pp. 179–183, Nov. 1997, doi: 10.1042/BJ3280179.

[196] I. Murano, G. Barbatelli, A. Giordano, and S. Cinti, "Noradrenergic parenchymal nerve fiber branching after cold acclimatisation correlates with brown adipocyte density in mouse adipose organ," *J Anat*, vol. 214, no. 1, pp. 171–178, 2009, doi: 10.1111/J.1469-7580.2008.01001.X.

[197] C. Tabuchi and H. S. Sul, "Signaling Pathways Regulating Thermogenesis," *Front Endocrinol (Lausanne)*, vol. 12, p. 595020, Mar. 2021, doi: 10.3389/FENDO.2021.595020.

[198] F. Gao, B. Litchfield, and H. Wu, "Adipose tissue lymphocytes and obesity," *The journal of cardiovascular aging*, vol. 4, no. 1, p. 5, Jan. 2023, doi: 10.20517/JCA.2023.38.

[199] D. Thomas and C. Apovian, "Macrophage functions in lean and obese adipose tissue," *Metabolism*, vol. 72, p. 120, Jul. 2017, doi: 10.1016/J.METABOL.2017.04.005.

[200] M. S. Rahman and H. Jun, "The Adipose Tissue Macrophages Central to Adaptive Thermoregulation," *Front Immunol*, vol. 13, p. 884126, Apr. 2022, doi: 10.3389/FIMMU.2022.884126.

[201] W. Liang *et al.*, "The Roles of Adipose Tissue Macrophages in Human Disease," *Front Immunol*, vol. 13, p. 908749, Jun. 2022, doi: 10.3389/FIMMU.2022.908749.

[202] A. D. Ruggiero, C. C. C. Key, and K. Kavanagh, "Adipose Tissue Macrophage Polarization in Healthy and Unhealthy Obesity," *Front Nutr*, vol. 8, p. 625331, Feb. 2021, doi: 10.3389/FNUT.2021.625331.

[203] C. N. Lumeng, J. L. Bodzin, and A. R. Saltiel, "Obesity induces a phenotypic switch in adipose tissue macrophage polarization," *Journal of Clinical Investigation*, vol. 117, no. 1, p. 175, Jan. 2007, doi: 10.1172/JCI29881.

[204] S. Cinti *et al.*, "Adipocyte death defines macrophage localization and function in adipose tissue of obese mice and humans," *J Lipid Res*, vol. 46, no. 11, pp. 2347–2355, Nov. 2005, doi: 10.1194/JLR.M500294-JLR200/ASSET/8D378E46-99C4-4338-ADC9-6B0E93836180/MAIN.ASSETS/GR4.JPG.

[205] S. P. Weisberg, D. McCann, M. Desai, M. Rosenbaum, R. L. Leibel, and J. Anthony W Ferrante, "Obesity is associated with macrophage accumulation in adipose tissue," *Journal of Clinical Investigation*, vol. 112, no. 12, p. 1796, Dec. 2003, doi: 10.1172/JCI19246.

[206] M. S. Burhans, D. K. Hagman, J. N. Kuzma, K. A. Schmidt, and M. Kratz, "Contribution of adipose tissue inflammation to the development of type 2

diabetes mellitus," *Compr Physiol*, vol. 9, no. 1, p. 1, Jan. 2018, doi: 10.1002/CPHY.C170040.

[207] G. S. Hotamisligil, "Inflammation and metabolic disorders," *Nature 2006 444:7121*, vol. 444, no. 7121, pp. 860–867, Dec. 2006, doi: 10.1038/nature05485.

[208] X. Li *et al.*, "Adipose tissue macrophages as potential targets for obesity and metabolic diseases," *Front Immunol*, vol. 14, p. 1153915, Apr. 2023, doi: 10.3389/FIMMU.2023.1153915/XML/NLM.

[209] D. Korns, S. C. Frasch, R. Fernandez-Boyanapalli, P. M. Henson, and D. L. Bratton, "Modulation of macrophage efferocytosis in inflammation," *Front Immunol*, vol. 2, no. NOV, p. 12942, Nov. 2011, doi: 10.3389/FIMMU.2011.00057/BIBTEX.

[210] S. Michlewska, I. Dransfield, I. L. Megson, and A. G. Rossi, "Macrophage phagocytosis of apoptotic neutrophils is critically regulated by the opposing actions of pro-inflammatory and anti-inflammatory agents: key role for TNF-alpha," *FASEB J*, vol. 23, no. 3, pp. 844–854, Mar. 2009, doi: 10.1096/FJ.08-121228.

[211] D. A. Jaitin *et al.*, "Lipid-Associated Macrophages Control Metabolic Homeostasis in a Trem2-Dependent Manner," *Cell*, vol. 178, no. 3, pp. 686-698.e14, Jul. 2019, doi: 10.1016/J.CELL.2019.05.054.

[212] B. R. Coats *et al.*, "Metabolically activated adipose tissue macrophages perform detrimental and beneficial functions during diet-induced obesity," *Cell Rep.*, vol. 20, no. 13, pp. 3149–3161, Sep. 2017, doi: 10.1016/j.celrep.2017.08.096.

[213] I. Reinisch *et al.*, "Adipocyte p53 coordinates the response to intermittent fasting by regulating adipose tissue immune cell landscape," *Nature Communications 2024 15:1*, vol. 15, no. 1, pp. 1–21, Feb. 2024, doi: 10.1038/s41467-024-45724-y.

[214] F. Sciarretta *et al.*, "Lipid-associated macrophages reshape BAT cell identity in obesity," *Cell Rep*, vol. 43, no. 7, p. 114447, Jul. 2024, doi: 10.1016/J.CELREP.2024.114447.

[215] M. Rosina *et al.*, "Ejection of damaged mitochondria and their removal by macrophages ensure efficient thermogenesis in brown adipose tissue," *Cell Metab*, vol. 34, no. 4, pp. 533-548.e12, Apr. 2022, doi: 10.1016/J.CMET.2022.02.016.

[216] R. Cereijo *et al.*, "CXCL14, a Brown Adipokine that Mediates Brown-Fat-to-Macrophage Communication in Thermogenic Adaptation," *Cell Metab*, vol. 28, no. 5, pp. 750-763.e6, Nov. 2018, doi: 10.1016/j.cmet.2018.07.015.

[217] R. R. Rao *et al.*, “Meteorin-like is a hormone that regulates immune-adipose interactions to increase beige fat thermogenesis,” *Cell*, vol. 157, no. 6, p. 1279, Jun. 2014, doi: 10.1016/J.CELL.2014.03.065.

[218] M. W. Lee *et al.*, “Activated Type 2 Innate Lymphoid Cells regulate Beige Fat Biogenesis,” *Cell*, vol. 160, no. 0, p. 74, Jan. 2014, doi: 10.1016/J.CELL.2014.12.011.

[219] Y. Qiu *et al.*, “Eosinophils and type 2 cytokine signaling in macrophages orchestrate development of functional beige fat,” *Cell*, vol. 157, no. 6, p. 1292, Jun. 2014, doi: 10.1016/J.CELL.2014.03.066.

[220] Y. N. Wang *et al.*, “Slit3 secreted from M2-like macrophages increases sympathetic activity and thermogenesis in adipose tissue,” *Nat Metab*, vol. 3, no. 11, pp. 1536–1551, Nov. 2021, doi: 10.1038/S42255-021-00482-9.

[221] L. Li *et al.*, “IL-25–induced shifts in macrophage polarization promote development of beige fat and improve metabolic homeostasis in mice,” *PLoS Biol*, vol. 19, no. 8, p. e3001348, Aug. 2021, doi: 10.1371/JOURNAL.PBIO.3001348.

[222] Y. Wolf *et al.*, “Brown adipose tissue macrophages control tissue innervation and homeostatic energy expenditure,” *Nat Immunol*, vol. 18, no. 6, p. 665, May 2017, doi: 10.1038/NI.3746.

[223] M. K. Yadav *et al.*, “MAFB in macrophages regulates cold-induced neuronal density in brown adipose tissue,” *Cell Rep*, vol. 43, no. 4, Apr. 2024, doi: 10.1016/J.CELREP.2024.113978.

[224] H. Jun *et al.*, “An immune-beige adipocyte communication via nicotinic acetylcholine receptor signaling,” *Nat Med*, vol. 24, no. 6, p. 814, Jun. 2018, doi: 10.1038/S41591-018-0032-8.

[225] A. J. Knights *et al.*, “Acetylcholine-synthesizing macrophages in subcutaneous fat are regulated by β2-adrenergic signaling,” *EMBO J*, vol. 40, no. 24, p. e106061, Dec. 2021, doi: 10.15252/EMBJ.2020106061.

[226] K. D. Nguyen *et al.*, “Alternatively activated macrophages produce catecholamines to sustain adaptive thermogenesis,” *Nature*, vol. 480, no. 7375, p. 104, Dec. 2011, doi: 10.1038/NATURE10653.

[227] K. Fischer *et al.*, “Alternatively activated macrophages do not synthesize catecholamines or contribute to adipose tissue adaptive thermogenesis,” *Nat Med*, vol. 23, no. 5, p. 623, May 2017, doi: 10.1038/NM.4316.

[228] R. M. Pirzgalska *et al.*, “Sympathetic neuron-associated macrophages contribute to obesity by importing and metabolizing norepinephrine,” *Nat Med*, vol. 23, no. 11, p. 1309, Nov. 2017, doi: 10.1038/NM.4422.

[229] K. D. Nguyen *et al.*, “Alternatively activated macrophages produce catecholamines to sustain adaptive thermogenesis,” *Nature*, vol. 480, no. 7375, Dec. 2011, doi: 10.1038/nature10653.

[230] Y. Qiu *et al.*, “Eosinophils and type 2 cytokine signaling in macrophages orchestrate development of functional beige fat,” *Cell*, vol. 157, no. 6, p. 1292, Jun. 2014, doi: 10.1016/j.cell.2014.03.066.

[231] Y. Xue *et al.*, “Hypoxia-Independent Angiogenesis in Adipose Tissues during Cold Acclimation,” *Cell Metab*, vol. 9, no. 1, pp. 99–109, Jan. 2009, doi: 10.1016/J.CMET.2008.11.009/ATTACHMENT/5C4CFAB6-FC45-4081-A76B-17A5F2A6A220/MMC2.AVI.

[232] Y. Zhang, B. Zhang, and X. Sun, “The molecular mechanism of macrophage-adipocyte crosstalk in maintaining energy homeostasis,” *Front Immunol*, vol. 15, p. 1378202, Apr. 2024, doi: 10.3389/FIMMU.2024.1378202/XML/NLM.

[233] J. Gerdes, U. Schwab, H. Lemke, and H. Stein, “Production of a mouse monoclonal antibody reactive with a human nuclear antigen associated with cell proliferation,” *Int J Cancer*, vol. 31, no. 1, pp. 13–20, Jan. 1983, doi: 10.1002/IJC.2910310104.

[234] M. Buxadé *et al.*, “Macrophage-specific MHCII expression is regulated by a remote Ciita enhancer controlled by NFAT5,” *J Exp Med*, vol. 215, no. 11, p. 2901, Nov. 2018, doi: 10.1084/JEM.20180314.

[235] M. C. Kiritsy *et al.*, “A genetic screen in macrophages identifies new regulators of ifnγ-inducible mhcii that contribute to t cell activation,” *Elife*, vol. 10, Nov. 2021, doi: 10.7554/ELIFE.65110.

[236] A. Weinstock, H. Moura Silva, K. J. Moore, A. M. Schmidt, and E. A. Fisher, “Leukocyte Heterogeneity in Adipose Tissue, Including in Obesity,” *Circ Res*, vol. 126, no. 11, pp. 1590–1612, May 2020, doi: 10.1161/CIRCRESAHA.120.316203/ASSET/D3BF1D15-5809-43B5-8A55-B3B35525FCB4/ASSETS/IMAGES/LARGE/CIRCRESAHA.120.316203.FIG02.JPG.

[237] J. Yang, L. Zhang, C. Yu, X. F. Yang, and H. Wang, “Monocyte and macrophage differentiation: Circulation inflammatory monocyte as biomarker for inflammatory diseases,” *Biomark Res*, vol. 2, no. 1, pp. 1–9, Jan. 2014, doi: 10.1186/2050-7771-2-1/TABLES/4.

[238] D. Zhai, C. Jin, Z. Huang, A. C. Satterthwait, and J. C. Reed, “Differential Regulation of Bax and Bak by Anti-apoptotic Bcl-2 Family Proteins Bcl-B and Mcl-1,” *J Biol Chem*, vol. 283, no. 15, p. 9580, Apr. 2008, doi: 10.1074/JBC.M708426200.

[239] E. T. Schmid *et al.*, “AXL receptor tyrosine kinase is required for t cell priming and antiviral immunity,” *Elife*, vol. 5, no. JUNE2016, Jun. 2016, doi: 10.7554/ELIFE.12414.001.

[240] L. Fourgeaud *et al.*, “TAM receptors regulate multiple features of microglial physiology,” *Nature 2016 532:7598*, vol. 532, no. 7598, pp. 240–244, Apr. 2016, doi: 10.1038/nature17630.

[241] S. A. Nance, L. Muir, and C. Lumeng, “Adipose tissue macrophages: Regulators of adipose tissue immunometabolism during obesity,” *Mol Metab*, vol. 66, p. 101642, Dec. 2022, doi: 10.1016/J.MOLMET.2022.101642.

[242] J. M. Wentworth *et al.*, “Pro-Inflammatory CD11c+CD206+ Adipose Tissue Macrophages Are Associated With Insulin Resistance in Human Obesity,” *Diabetes*, vol. 59, no. 7, pp. 1648–1656, Jul. 2010, doi: 10.2337/DB09-0287.

[243] S. Virtue and A. Vidal-Puig, “Assessment of brown adipose tissue function,” *Front Physiol*, vol. 4, p. 128, 2013, doi: 10.3389/FPHYS.2013.00128.

[244] A. W. Fischer, J. M. A. de Jong, F. Sass, C. Schlein, J. Heeren, and N. Petrovic, “Thermoneutrality-Induced Macrophage Accumulation in Brown Adipose Tissue Does Not Impair the Tissue’s Competence for Cold-Induced Thermogenic Recruitment,” *Front Endocrinol (Lausanne)*, vol. 11, p. 568682, Oct. 2020, doi: 10.3389/FENDO.2020.568682/BIBTEX.

[245] C. Fryklund, M. Neuhaus, B. Morén, A. Borreguero-Muñoz, R. Lundmark, and K. G. Stenkula, “Expansion of the Inguinal Adipose Tissue Depot Correlates With Systemic Insulin Resistance in C57BL/6J Mice,” *Front Cell Dev Biol*, vol. 10, p. 942374, Sep. 2022, doi: 10.3389/FCELL.2022.942374/BIBTEX.

[246] C. Xiao, M. Goldgof, O. Gavrilova, and M. L. Reitman, “Anti-obesity and metabolic efficacy of the β3-adrenergic agonist, CL316243, in mice at thermoneutrality compared to 22°C,” *Obesity (Silver Spring)*, vol. 23, no. 7, pp. 1450–1459, Jul. 2015, doi: 10.1002/OBY.21124.

[247] T. Umekawa, T. Yoshida, N. Sakane, and M. Kondo, “Effect of CL316,243, a highly specific beta(3)-adrenoceptor agonist, on lipolysis of epididymal, mesenteric and subcutaneous adipocytes in rats,” *Endocr J*, vol. 44, no. 1, pp. 181–185, 1997, doi: 10.1507/ENDOCRJ.44.181.

[248] T. J. Bartness, Y. Liu, Y. B. Shrestha, and V. Ryu, “Neural Innervation of White Adipose Tissue and the Control of Lipolysis,” *Front Neuroendocrinol*, vol. 35, no. 4, p. 473, Oct. 2014, doi: 10.1016/J.YFRNE.2014.04.001.

[249] S. Chen *et al.*, “Macrophages in immunoregulation and therapeutics,” *Signal Transduct Target Ther*, vol. 8, no. 1, p. 207, Dec. 2023, doi: 10.1038/S41392-023-01452-1.

[250] M. Azuma *et al.*, “B70 antigen is a second ligand for CTLA-4 and CD28,” *Nature*, vol. 366, no. 6450, pp. 76–79, 1993, doi: 10.1038/366076A0.

[251] J. M. Valentine *et al.*, “β3-Adrenergic receptor downregulation leads to adipocyte catecholamine resistance in obesity,” *J Clin Invest*, vol. 132, no. 2, Jan. 2022, doi: 10.1172/JCI153357.

[252] L. Dowal *et al.*, “Intrinsic Properties of Brown and White Adipocytes Have Differential Effects on Macrophage Inflammatory Responses,” *Mediators Inflamm*, vol. 2017, p. 9067049, 2017, doi: 10.1155/2017/9067049.

[253] F. Omran and M. Christian, “Inflammatory Signaling and Brown Fat Activity,” *Front Endocrinol (Lausanne)*, vol. 11, p. 156, Mar. 2020, doi: 10.3389/FENDO.2020.00156.

[254] T. P. Fitzgibbons, S. Kogan, M. Aouadi, G. M. Hendricks, J. Straubhaar, and M. P. Czech, “Similarity of mouse perivascular and brown adipose tissues and their resistance to diet-induced inflammation,” *Am J Physiol Heart Circ Physiol*, vol. 301, no. 4, p. H1425, Oct. 2011, doi: 10.1152/AJPHEART.00376.2011.

[255] B. Cai, G. Fredman, and I. Tabas, “MerTK receptor cleavage promotes plaque necrosis and defective resolution in atherosclerosis The Journal of Clinical Investigation,” *J Clin Invest*, vol. 127, no. 2, 2017, doi: 10.1172/JCI90520.

[256] A. L. Law *et al.*, “Cleavage of Mer Tyrosine Kinase (MerTK) from the Cell Surface Contributes to the Regulation of Retinal Phagocytosis,” *J Biol Chem*, vol. 290, no. 8, p. 4941, Feb. 2014, doi: 10.1074/JBC.M114.628297.

[257] B. M. Freire, F. M. De Melo, and A. S. Basso, “Adrenergic signaling regulation of macrophage function: do we understand it yet?,” *Immunotherapy Advances*, vol. 2, no. 1, Jan. 2022, doi: 10.1093/IMMADV/LTAC010.

[258] K. Petkevicius *et al.*, “Macrophage beta2-adrenergic receptor is dispensable for the adipose tissue inflammation and function,” *Mol Metab*, vol. 48, p. 101220, Jun. 2021, doi: 10.1016/J.MOLMET.2021.101220.

[259] V. Ryuid and C. Buettner, “Fat cells gobbling up norepinephrine?,” *PLoS Biol*, vol. 17, no. 2, p. e3000138, Feb. 2019, doi: 10.1371/JOURNAL.PBIO.3000138.

[260] C. REINHART, H. M. WEISS, and H. REILÄNDER, “Purification of an Affinity-Epitope Tagged G-Protein Coupled Receptor,” *Membrane Protein Purification and Crystallization*, pp. 167–178, 2003, doi: 10.1016/B978-012361776-7/50010-3.

[261] C. Nishi, S. Toda, K. Segawa, and S. Nagata, “Tim4- and MerTK-Mediated Engulfment of Apoptotic Cells by Mouse Resident Peritoneal Macrophages,” *Mol Cell Biol*, vol. 34, no. 8, p. 1512, Apr. 2014, doi: 10.1128/MCB.01394-13.

[262] W. S. Driscoll, T. Vaisar, J. Tang, C. L. Wilson, and E. W. Raines, “Macrophage ADAM17 Deficiency Augments CD36-Dependent Apoptotic Cell Uptake and the Linked Anti-Inflammatory Phenotype,” *Circ Res*, vol. 113, no. 1, p. 52, Jun. 2013, doi: 10.1161/CIRCRESAHA.112.300683.

[263] S. Koda *et al.*, “β2-Adrenergic Receptor Enhances the Alternatively Activated Macrophages and Promotes Biliary Injuries Caused by Helminth Infection,” *Front Immunol*, vol. 12, p. 754208, Oct. 2021, doi: 10.3389/FIMMU.2021.754208/BIBTEX.

[264] D. Korns, S. C. Frasch, R. Fernandez-Boyanapalli, P. M. Henson, and D. L. Bratton, “Modulation of macrophage efferocytosis in inflammation,” *Front Immunol*, vol. 2, no. NOV, p. 12942, Nov. 2011, doi: 10.3389/FIMMU.2011.00057/BIBTEX.

[265] K. Petkevicius *et al.*, “Norepinephrine promotes triglyceride storage in macrophages via beta2-adrenergic receptor activation,” *The FASEB Journal*, vol. 35, no. 2, p. e21266, Feb. 2021, doi: 10.1096/FJ.202001101R.

[266] A. Venkateswaran *et al.*, “Control of cellular cholesterol efflux by the nuclear oxysterol receptor LXRα,” *Proc Natl Acad Sci U S A*, vol. 97, no. 22, p. 12097, Oct. 2000, doi: 10.1073/PNAS.200367697.

[267] S. Yoshida *et al.*, “Annexin V decreases PS-mediated macrophage efferocytosis and deteriorates elastase-induced pulmonary emphysema in mice,” *Am J Physiol Lung Cell Mol Physiol*, vol. 303, no. 10, Nov. 2012, doi: 10.1152/AJPLUNG.00066.2012.

[268] M. Burgess, K. Wicks, M. Gardasevic, and K. A. Mace, “Cx3CR1 Expression Identifies Distinct Macrophage Populations That Contribute Differentially to Inflammation and Repair,” *Immunohorizons*, vol. 3, no. 7, pp. 262–273, Jul. 2019, doi: 10.4049/IMMUNOHORIZONS.1900038.

[269] R. S. Scott *et al.*, “Phagocytosis and clearance of apoptotic cells is mediated by MER,” *Nature*, vol. 411, no. 6834, pp. 207–211, May 2001, doi: 10.1038/35075603.

[270] F. R. Maxfield, V. C. Barbosa-Lorenzi, and R. K. Singh, “Digestive exophagy: Phagocyte digestion of objects too large for phagocytosis,” *Traffic*, vol. 21, no. 1, pp. 6–12, Jan. 2020, doi: 10.1111/TRA.12712/.

[271] A. S. Haka *et al.*, “Exocytosis of macrophage lysosomes leads to digestion of apoptotic adipocytes and foam cell formation,” *J Lipid Res*, vol. 57, no. 6, p. 980, Jun. 2016, doi: 10.1194/JLR.M064089.

[272] M. Rosina *et al.*, “Ejection of damaged mitochondria and their removal by macrophages ensure efficient thermogenesis in brown adipose tissue,” *Cell Metab*, vol. 34, no. 4, pp. 533-548.e12, Apr. 2022, doi: 10.1016/J.CMET.2022.02.016.

[273] K. Kulaj *et al.*, “Adipocyte-derived extracellular vesicles increase insulin secretion through transport of insulinotropic protein cargo,” *Nature Communications 2023 14:1*, vol. 14, no. 1, pp. 1–13, Feb. 2023, doi: 10.1038/s41467-023-36148-1.

[274] R. M. Pirzgalska *et al.*, “Sympathetic neuron-associated macrophages contribute to obesity by importing and metabolizing norepinephrine,” *Nat Med*, vol. 23, no. 11, Nov. 2017, doi: 10.1038/NM.4422.

[275] D. E. Akinyemi, R. Chevre, and O. Soehnlein, “Neuro-immune crosstalk in hematopoiesis, inflammation, and repair,” vol. 45, no. 8, pp. 597–608, Aug. 2024, Accessed: May 01, 2025. [Online]. Available: https://pubmed.ncbi.nlm.nih.gov/39030115/

[276] D. M. Lamkin *et al.*, “β-Adrenergic-stimulated macrophages: Comprehensive localization in the M1-M2 spectrum,” *Brain Behav Immun*, vol. 57, pp. 338–346, Oct. 2016, doi: 10.1016/J.BBI.2016.07.162.

[277] T. Tanaka *et al.*, “Neuroendocrine Signaling Via the Serotonin Transporter Regulates Clearance of Apoptotic Cells,” *J Biol Chem*, vol. 289, no. 15, p. 10466, Apr. 2014, doi: 10.1074/JBC.M113.482299.

[278] J. Zhao *et al.*, “Efferocytosis in the Central Nervous System,” *Front Cell Dev Biol*, vol. 9, p. 773344, Dec. 2021, doi: 10.3389/FCELL.2021.773344.

[279] A. Körner *et al.*, “Sympathetic nervous system controls resolution of inflammation via regulation of repulsive guidance molecule A,” *Nature Communications 2019 10:1*, vol. 10, no. 1, pp. 1–15, Feb. 2019, doi: 10.1038/s41467-019-08328-5.

[280] H. Urakami *et al.*, “Stress-experienced monocytes/macrophages lose anti-inflammatory function via β2-adrenergic receptor in skin allergic inflammation,” *Journal of Allergy and Clinical Immunology*, vol. 155, no. 3, pp. 865–879, Mar. 2025, doi: 10.1016/J.JACI.2024.10.038.

[281] Y. Xiao *et al.*, “The reduction of microglial efferocytosis is concomitant with depressive-like behavior in CUMS-treated mice,” *J Affect Disord*, vol. 352, pp. 76–86, May 2024, doi: 10.1016/J.JAD.2024.02.045.

[282] L. Li *et al.*, “IL-25–induced shifts in macrophage polarization promote development of beige fat and improve metabolic homeostasis in mice,” *PLoS Biol*, vol. 19, no. 8, p. e3001348, Aug. 2021, doi: 10.1371/JOURNAL.PBIO.3001348.

[283] A. P. Weetman, “Autoimmune thyroid disease: propagation and progression,” *Eur J Endocrinol*, vol. 148, no. 1, pp. 1–9, Jan. 2003, doi: 10.1530/EJE.0.1480001.

[284] P. L. Cohen *et al.*, “Delayed apoptotic cell clearance and lupus-like autoimmunity in mice lacking the c-mer membrane tyrosine kinase,” *J Exp Med*, vol. 196, no. 1, pp. 135–140, Jul. 2002, doi: 10.1084/JEM.20012094.

[285] S. P. Wang *et al.*, “The Adipose Tissue Phenotype of Hormone-Sensitive Lipase Deficiency in Mice,” *Obes Res*, vol. 9, no. 2, pp. 119–128, Feb. 2001, doi: 10.1038/OBY.2001.15.

[286] Y. Kawano and D. E. Cohen, “Mechanisms of hepatic triglyceride accumulation in non-alcoholic fatty liver disease,” *J Gastroenterol*, vol. 48, no. 4, pp. 434–441, Apr. 2013, doi: 10.1007/S00535-013-0758-5.

[287] Y. Choi *et al.*, “Adipose Lipolysis Regulates Cardiac Glucose Uptake and Function in Mice under Cold Stress,” *Int J Mol Sci*, vol. 22, no. 24, Dec. 2021, doi: 10.3390/IJMS222413361.

[288] E. Nisoli *et al.*, “Tumor necrosis factor α mediates apoptosis of brown adipocytes and defective brown adipocyte function in obesity,” *Proc Natl Acad Sci U S A*, vol. 97, no. 14, p. 8033, Jul. 2000, doi: 10.1073/PNAS.97.14.8033.

[289] S. H. Chiang *et al.*, “The protein kinase IKKε regulates energy expenditure, insulin sensitivity and chronic inflammation in obese mice,” *Cell*, vol. 138, no. 5, p. 961, Sep. 2009, doi: 10.1016/J.CELL.2009.06.046.

[290] Y. Onogi *et al.*, “Pro-inflammatory macrophages coupled with glycolysis remodel adipose vasculature by producing platelet-derived growth factor-B in obesity,” *Scientific Reports 2020 10:1*, vol. 10, no. 1, pp. 1–13, Jan. 2020, doi: 10.1038/s41598-019-57368-w.

[291] A. Hernandez, B. Morte, M. M. Belinchón, A. Ceballos, and J. Bernal, “Critical Role of Types 2 and 3 Deiodinases in the Negative Regulation of Gene Expression by T3 in the Mouse Cerebral Cortex,” *Endocrinology*, vol. 153, no. 6, p. 2919, Jun. 2012, doi: 10.1210/EN.2011-1905.

[292] J. H. Oppenheimer, H. L. Schwartz, J. T. Lane, and M. P. Thompson, “Functional relationship of thyroid hormone-induced lipogenesis, lipolysis, and thermogenesis in the rat,” *Journal of Clinical Investigation*, vol. 87, no. 1, p. 125, 1991, doi: 10.1172/JCI114961.

[293] F. Villarroya, R. Cereijo, A. Gavaldà-Navarro, J. Villarroya, and M. Giralt, “Inflammation of brown/beige adipose tissues in obesity and metabolic disease,” *J Intern Med*, vol. 284, no. 5, pp. 492–504, Nov. 2018, doi: 10.1111/JOIM.12803.

[294] B. M. Freire, F. M. De Melo, and A. S. Basso, “Adrenergic signaling regulation of macrophage function: do we understand it yet?,” *Immunotherapy Advances*, vol. 2, no. 1, p. ltac010, 2022, doi: 10.1093/IMMADV/LTAC010.

[295] B. Cai *et al.*, “Macrophage MerTK Promotes Liver Fibrosis in Nonalcoholic Steatohepatitis,” *Cell Metab*, vol. 31, no. 2, p. 406, Feb. 2019, doi: 10.1016/J.CMET.2019.11.013.

[296] V. Efthymiou *et al.*, “Inhibition of AXL receptor tyrosine kinase enhances brown adipose tissue functionality in mice,” *Nature Communications 2023 14:1*, vol. 14, no. 1, pp. 1–22, Jul. 2023, doi: 10.1038/s41467-023-39715-8.

[297] K. Köröskényi *et al.*, “Loss of MER Tyrosine Kinase Attenuates Adipocyte Hypertrophy and Leads to Enhanced Thermogenesis in Mice Exposed to High-Fat Diet,” *Cells*, vol. 13, no. 22, Nov. 2024, doi: 10.3390/CELLS13221902.

[298] M. Haldar and K. M. Murphy, “Origin, Development, and Homeostasis of Tissue-resident Macrophages,” *Immunol Rev*, vol. 262, no. 1, p. 25, Nov. 2014, doi: 10.1111/IMR.12215.

[299] F. Guan *et al.*, “Tissue macrophages: origin, heterogenity, biological functions, diseases and therapeutic targets,” *Signal Transduction and Targeted Therapy 2025 10:1*, vol. 10, no. 1, pp. 1–67, Mar. 2025, doi: 10.1038/s41392-025-02124-y.

[300] “Hypertension,” *Pocket Companion to Brenner and Rector’s The Kidney*, pp. 439–467, 2011, doi: 10.1016/B978-1-4160-6640-8.00022-1.

[301] J. R. H. Raiko *et al.*, “Changes in electrocardiogram parameters during acute nonshivering cold exposure and associations with brown adipose tissue activity, plasma catecholamine levels, and brachial blood pressure in healthy adults,” *Physiol Rep*, vol. 9, no. 3, p. e14718, Feb. 2021, doi: 10.14814/PHY2.14718.

[302] J. Wortsman, S. Frank, and P. E. Cryer, “Adrenomedullary response to maximal stress in humans,” *Am J Med*, vol. 77, no. 5, pp. 779–784, Nov. 1984, doi: 10.1016/0002-9343(84)90512-6.

[303] F. Matheis *et al.*, “Adrenergic signaling in muscularis macrophages limits infection-induced neuronal loss,” *Cell*, vol. 180, no. 1, p. 64, Jan. 2020, doi: 10.1016/J.CELL.2019.12.002.

[304] S. Hasegawa *et al.*, “Activation of sympathetic signaling in macrophages blocks systemic inflammation and protects against renal ischemia-reperfusion injury,” *Journal of the American Society of Nephrology*, vol. 32, no. 7, pp. 1599–1615, Jul. 2021, doi: 10.1681/ASN.2020121723/-/DCSUPPLEMENTAL.

[305] L. A. Grisanti *et al.*, “Leukocyte-Expressed β2-Adrenergic Receptors Are Essential for Survival After Acute Myocardial Injury,” *Circulation*, vol. 134, no. 2, pp. 153–167, Jul. 2016, doi: 10.1161/CIRCULATIONAHA.116.022304.

[306] A. Schömig and G. Richardt, “Cardiac sympathetic activity in myocardial ischemia: release and effects of noradrenaline.,” *Basic Res Cardiol*, vol. 85 Suppl 1, pp. 9–30, 1990, doi: 10.1007/978-3-662-11038-6_2.

[307] V. Leroy *et al.*, “MerTK-dependent efferocytosis by monocytic-MDSCs mediates resolution of post-lung transplant ischemia-reperfusion injury,” *JCI Insight*, Oct. 2024, doi: 10.1172/JCI.INSIGHT.179876.

[308] J. F. Qin *et al.*, “Adrenergic receptor β2 activation by stress promotes breast cancer progression through macrophages M2 polarization in tumor microenvironment,” *BMB Rep*, vol. 48, no. 5, p. 295, 2015, doi: 10.5483/BMBREP.2015.48.5.008.

[309] N. Wu *et al.*, “MerTK+ macrophages promote melanoma progression and immunotherapy resistance through AhR-ALKAL1 activation,” *Sci Adv*, vol. 10, no. 40, p. eado8366, Oct. 2024, doi: 10.1126/SCIADV.ADO8366/SUPPL_FILE/SCIADV.ADO8366_TABLES_S1_TO_S7.ZIP.

[310] C. B. Overgaard and V. Džavík, “Inotropes and vasopressors:Review of physiology and clinical use in cardiovascular disease,” *Circulation*, vol. 118, no. 10, pp. 1047–1056, Sep. 2008, doi: 10.1161/CIRCULATIONAHA.107.728840/ASSET/C118B9D9-DDDA-4E51-B688-44C1A61B63F2/ASSETS/GRAPHIC/16FF4.JPEG.

[311] M. Cazzola, C. P. Page, P. Rogliani, and M. G. Matera, “β2-Agonist Therapy in Lung Disease,” *https://doi.org/10.1164/rccm.201209-1739PP*, vol. 187, no. 7, pp. 690–696, Jan. 2013, doi: 10.1164/RCCM.201209-1739PP.

[312] S. M. M. van Beek *et al.*, “Effect of β2-agonist treatment on insulin-stimulated peripheral glucose disposal in healthy men in a randomised placebo-controlled trial,” *Nat Commun*, vol. 14, no. 1, p. 173, Dec. 2023, doi: 10.1038/S41467-023-35798-5.

[313] L. Evans *et al.*, “Surviving Sepsis Campaign: International Guidelines for Management of Sepsis and Septic Shock 2021,” *Crit Care Med*, vol. 49, no. 11, pp. E1063–E1143, Nov. 2021, doi: 10.1097/CCM.0000000000005337.

[314] M. Cazzola, L. Calzetta, and M. G. Matera, “β2-adrenoceptor agonists: current and future direction,” *Br J Pharmacol*, vol. 163, no. 1, p. 4, May 2011, doi: 10.1111/J.1476-5381.2011.01216.X.

[315] S. G. Wendell, H. Fan, and C. Zhang, “G Protein–Coupled Receptors in Asthma Therapy: Pharmacology and Drug Action,” *Pharmacol Rev*, vol. 72, no. 1, p. 1, Jan. 2020, doi: 10.1124/PR.118.016899.

[316] B. Thyagarajan and M. T. Foster, “Beiging of white adipose tissue as a therapeutic strategy for weight loss in humans,” *Horm Mol Biol Clin Investig*, vol. 31, no. 2, Aug. 2017, doi: 10.1515/HMBCI-2017-0016.

[317] A. Kosteli *et al.*, “Weight loss and lipolysis promote a dynamic immune response in murine adipose tissue,” *J Clin Invest*, vol. 120, no. 10, pp. 3466–3479, Oct. 2010, doi: 10.1172/JCI42845.

[318] A. Jürets *et al.*, “Upregulated TNF Expression 1 Year After Bariatric Surgery Reflects a Cachexia-Like State in Subcutaneous Adipose Tissue,” *Obes Surg*, vol. 27, no. 6, p. 1514, Jun. 2016, doi: 10.1007/S11695-016-2477-5.

[319] Y. Xia *et al.*, “Tirzepatide’s role in targeting adipose tissue macrophages to reduce obesity-related inflammation and improve insulin resistance,” *Int Immunopharmacol*, vol. 143, p. 113499, Dec. 2024, doi: 10.1016/J.INTIMP.2024.113499.

[320] D. Jahn *et al.*, “Increased β2-adrenergic signaling promotes fracture healing through callus neovascularization in mice,” *Sci Transl Med*, vol. 16, no. 743, 2024, doi: 10.1126/SCITRANSLMED.ADK9129.

[321] “Axl<tm1.1Cvro> Targeted Allele Detail MGI Mouse (MGI:6147861).” Accessed: Jun. 19, 2025. [Online]. Available: https://www.informatics.jax.org/allele/MGI:6147861

[322] T. Tian *et al.*, “The P2X7 ion channel is dispensable for energy and metabolic homeostasis of white and brown adipose tissues,” *Purinergic Signal*, vol. 16, no. 4, pp. 529–542, Dec. 2020, doi: 10.1007/S11302-020-09738-7.

[323] R. E. Heap *et al.*, “Proteomics characterisation of the L929 cell supernatant and its role in BMDM differentiation,” *Life Sci Alliance*, vol. 4, no. 6, Jun. 2021, doi: 10.26508/LSA.202000957.

[324] M. Y. Jaeckstein *et al.*, “CD73-dependent generation of extracellular adenosine by vascular endothelial cells modulates de novo lipogenesis in adipose tissue,” *Front Immunol*, vol. 14, p. 1308456, 2023, doi: 10.3389/FIMMU.2023.1308456/FULL.

[325] F. Sass *et al.*, “TFEB deficiency attenuates mitochondrial degradation upon brown adipose tissue whitening at thermoneutrality,” *Mol Metab*, vol. 47, p. 101173, May 2021, doi: 10.1016/J.MOLMET.2021.101173.

7. Attachments

Table 9: List of hazardous substances according to GHS

Chemical	Manufacturer	Purity	GHS Symbol	Hazard Statement H	Precaution Statement P
40% Acrylamide/Bis Solution 37.5:1	Bio-Rad Laboratories, CA, USA	99.9 %	GHS07, GHS08	H302, H315, H317, H319, H332, H340, H350, H361f, H372, H412	P260, P264, P312, P501
Dimethyl sulfoxide	Carl Roth, Karlsruhe, Germany	≥ 99.5 %	GHS07	H227, H315, H319	P264, P280, P305, P351, P338, P332, P313, P337, P313, P362
Chloroform	Merck	99.9 %	GHS06 GHS08 GHS07	H302, H315, H319, H331, H336, H351, H361d, H372	P201, P202, P260, P261, P264, P270, P271, P280, P304, P340, P305, P351, P338, P311, P403, P233, P405, P501
CL316,243	Tocris Biosciences, Bristol, UK	≥97%		H401	P273, P501
Collagenase 2	Merck, Darmstadt, Germany	< =100%	GHS08	H334	P261
Collagenase D	Miltenyi Biotec, Bergisch Gladbach	230 U/g	GHS08	H334	P261
Dispase	Thermo Fisher Scientific Waltham, USA	1810 U/g	GHS07	H315, H319	P280
EDTA	Sigma-Aldrich, Taufkirchen, Germany	≥ 98.5%	GHS08	H319	P305, P35, P338
Ethanol	Merck, Darmstadt, Germany	≥ 99.9%	GHS02, GHS07	H225, H319	P210, P233, P240, P241, P242, P305, P351, P338, P403, P233
Formoterol	Sigma-Aldrich, Taufkirchen, Germany	>98%	GHS07, GHS08	H302, H332, H351, H361, H370, H373	P201, P202, P260
Formaldehyde	Carl Roth, Karlsruhe, Germany	≥37%	GHS02, GHS05, GHS06, GHS07, GHS08	H302-H314-H317-H330-H341-H350-H370-EUH071	P260 P280 P303+P361+P353 P304+P340 P305+P351+P338 P308+P31

Isoprotenerol	Sigma-Aldrich, Taufkirchen, Germany	-	GHS07	H302, H315, H319	P280
Ketamine	Albrecht, Aulendorf, Germany	10 mg/ml	GHS07	H301, H315, H319, H335	P261-P306-P351- P338
NAOH	Sigma-Aldrich, Taufkirchen, Germany	≥ 97 %	GHS05	H290, H314	P234, P260, P280, P301, P330, P331, P303, P361, P353, P305, P351, P338
Norepinephrine	Cayman Chemicals, Ann Arbor, USA	≥95%	GHS06	H300, H310, H330	P260, P262, P264, P270, P280, P301, P310, P302, P352, P304, P340, P321, P330, P405, P501
Paraformaldehyde	Electron Microscopy Sciences, Hatfield, USA	20%	GHS02, GHS07, GHS08	H228, H301, H302, H311, H315, H317, H319, H332, H334, H335, H341, H350,	P210, P261, P264, P270, P271, P272, P273, P280, P301, P310, P302, P352, P304, P340, P305, P351, P338, P308, P313, P312, P321, P330, P333, P313, P337, P342, P311, P362, P364, P403, P233, P405, P501
Rompun (Xylazine)	Bayer, Leverkusen, Germany	0.2%	GHS06	H301	P301, P310
Rosiglitazone	Cayman Chemicals, Ann Arbor, USA	≥98%	GHS08	H361	P201
TRIZOL REAGENT	Thermo Fisher Scientific	-	GHS05, GHS07, GHS08	**H227, H301, H311, H331, H314, H318, H335, H341, H373, H411, H302, H312, H332,**	**P201, P202, P210, P260, P264, P270, P280**

SDS ultra-pure	Carl Roth, Karlsruhe, Germany	≥ 99%	GHS02, GHS05, GHS07	H228, H302, H332, H315, H318, H335, H412	P210, P261, P280, P302, P352, P305, P351, P33 8, P312
Sodium azide	Fulka	≥ 99.0%	GHS06, GHS08, GHS09	H300, H310, H330, H373, H410	P262, P273, P280, P302, P352, P310, P304, P340, P310, P314

Table 10: Kits

Product/Kit	**Manufacturer**
Cholesterol FS	DiaSys Diagnostic Systems GmbH, Holzheim, Germany
CellTrace CFSE Cell proliferation kit	Thermo Fisher Scientific no. C34554
Eukitt® Quick-hardening mounting medium	Sigma-Aldrich, Taufkirchen, Germany
FITC Annexin V Apoptosis Detection Kit	BioLegend no. 640914, San Diego, California
High Capacity cDNA Reverse Transcription Kit	Applied Biosystems Inc., USA
LIVE/DEAD™ Fixable Blue Dead Cell Stain Kit	Thermo Fisher Scientific, Waltham, USA, L23105
NEFA-HR(2) Assay	FUJIFILM Wako, Neuss, Germany
NucleoSpin RNA II	Macherey & Nagel, Düren, Germany
SuperSignal™ West Femto Maximum Sensitivity Substrate kit	Thermo Fisher Scientific, Waltham, USA
SYBR™ Green PCR Master Mix	Applied Biosystems Inc., USA
TaqMan™ Universal Master Mix II	Applied Biosystems Inc., USA
Triglycerides FS	DiaSys Diagnostic Systems GmbH, Holzheim, Germany
Universal PCR MasterMix	Applied Biosystems Inc., USA

Table 11: Buffers and solutions

Buffer/Solution	**Manufacturer/Composition**
Anesthesia	Ketamine (100 mg/ml)/Rompun (2 %)/NaCl (0.9 %); 2.3/1.0/6.7, v/v/v; 15 µL/g bodyweight
Adipocyte isolation buffer	• NaCl 123 mM 7.188 g • KCl 5 mM 372.8 mg • CaCl2 1.3 mM 191.1 mg • Glucose 5 mM 991 mg • HEPES 100 mM 23.8 g Wasser ad 1000 ml
Blocking buffer milk 5%	• 2.5 g Milk Skim Powder in final 50 mL with TBST

Blotting buffer	• 56.2 g Glycine • 12.1 g Tris-base • 1 L Methanol in final 5 L with H_2O dest.
BSA 5 % with NaAzid 0.02%	• 2.5 g BSA • 50 µL Sodium azide 20% in final 50 mL with TBST
Citric acid buffer pH 6.0	• 1.92 g Citric acid • Adjust pH with 2M NaOH • 0.5 mL Tween20 in final volume of 1 L of H2O dest.
cOmplete™, Mini, EDTA-free Protease Inhibitor Cocktail	Roche Diagonstics®, Mannheim, Germany
EDTA solution 0.5M	Sigma-Aldrich, Taufkirchen, Germany
Eukitt® Quick-hardening mounting medium	Sigma-Aldrich, Taufkirchen, Germany
Formaldehyde solution 37%	Sigma-Aldrich, Taufkirchen, Germany
GeneRuler™ DNA Ladder Mix	Thermo Fisher Scientific, Waltham, USA
Hematoxylin Solution, Mayer's	Sigma-Aldrich, Taufkirchen, Germany
MACS buffer	• 744 mg EDTA • 5 g BSA • 37mg D-Glucose in final volume of 1 L of PBS
NaCl, 0,9 w/v %	Braun, Melsungen, Germany
NaOH 0.1M	• 3.99 g NaOH in final 1 L with H_2O dest.
NuPAGE™ LDS Sample Buffer (4X)	• Thermo Fisher Scientific, Waltham, USA
NuPAGE™ Sample Reducing Agent (10X)	• Thermo Fisher Scientific, Waltham, USA
PageRuler™ Prestained Protein Ladder	• Thermo Fisher Scientific, Waltham, USA
Perm/wash	BD Biosciences Perm/Wash no. 554723
Phosphatase Inhibitor Cocktail	• Biotool (bimake.com), Texas, USA
Pierce™ Bovine Serum Albumin Standard	• Thermo Fisher Scientific, Waltham, USA
Ponceau S solution	• Sigma-Aldrich, Taufkirchen, Germany
Proteinase K, recombinant	• Thermo Fisher Scientific, Waltham, USA
RIPA buffer	• 50 mM Tris-HCl pH 7.4 • 5 mM EDTA • 150 mM sodium chloride • 1 mM sodium pyrophosphate • 1 mM sodium fluoride • 1 mM sodium orthovanadate • 1 % NP-40
ROTI®Block	• Carl Roth, Karlsruhe, Germany

ROTI®-GelStain	• Carl Roth, Karlsruhe, Germany
Running buffer (10X)	• 54 g Tris-Base • 144 g Glycine • 10 g SDS • in final 1 L with H_2O dest.
SDS 10 %	• 10 g SDS • in final 100 mL with H_2O dest.
STE buffer (1X)	• 2,92 g NaCl • 1.21 g Tris-Base • 5 g SDS • 3.72 g EDTA • Adjust pH 7,4 • in final 1 L with H_2O dest.
TBE-buffer (5X)	• 54 g Tris-Base • 27.5 g Boric acid • 3.7 g EDTA • in final 1 L with H_2O dest.
TBS - Tween 0.1%	• 100 mL TBS 10X • 1 mL TWEEN® 20 • in final 1 L with H_2O dest.
TBS buffer (10X)	• 0.2M Tris-Base • 1.37M NaCl • in final 1 L with H_2O dest., pH7.4

Summary

Upon exposure to cold temperatures or during times of energy shortage, the body initiates complex adaptive responses to maintain thermal and energy homeostasis. A critical component of these responses is the activation of the sympathetic nervous system, which leads to the local release of norepinephrine (NE) in adipose tissue. NE, in turn, acts on adrenergic receptors on adipocytes to stimulate thermogenesis and lipolysis. In particular, brown adipose tissue (BAT) is well known for its thermogenic capacity, but also subcutaneous white adipose tissue (WAT) can adopt a thermogenic (beige) phenotype upon prolonged cold stimulation.

Activation of brown and beige adipose tissue is actively explored as a therapeutic strategy for obesity and metabolic syndrome, due to their roles in enhancing energy expenditure and improving insulin sensitivity. Sustained thermogenic activity thereby requires significant structural remodeling of adipose tissue, including changes to the extracellular matrix and expansion of tissue innervation and vascularization. Macrophages play a central role in these remodeling processes through their ability to perform *efferocytosis* - the clearance of dying cells. This process can induce a specialized, anti-inflammatory/tissue-remodeling profile in the efferocytic macrophages, mainly driven by the engagement of the two efferocytic receptors AXL and MERTK. Interestingly, impaired efferocytic function of adipose tissue macrophages has been linked to metabolic disorders such as type 2 diabetes, but its role in thermogenic activation of adipose tissue remains unexplored. In this study, we used cold exposure to induce thermogenic remodeling of adipose tissue and explored the role of macrophage efferocytosis during this process.

We found that F4/80^{+}CD11b^{+} macrophages isolated from the interscapular iBAT (iBAT) and inguinal WAT (ingWAT) of cold-housed C57BL/6 mice exhibited significantly higher efferocytic capacity compared to those from thermoneutral-housed controls. This enhanced efferocytosis was associated with the accumulation of ATMs expressing efferocytic receptors, particularly in BAT, suggesting that enhanced efferocytosis may contribute to the high remodelling potential and resistance to inflammation observed in BAT.

Interestingly, the cold-induced efferocytic response as well as increased *Mertk* expression were recapitulated in bone marrow-derived macrophages treated with NE or β2-adrenergic agonists *in vitro* and by injection of NE *in vivo*. Notably, β2 stimulation failed to induce efferocytosis in *Axl/Mertk*-deficient BMDMs, indicating that these receptors are essential for NE-induced uptake of dying cells. While immune modulatory effects of β2-adrenergic activation on macrophages have been reported previously, so far we are the first to show direct effects of NE on macrophage efferocytosis.

Next, we investigated the contribution of AXL/MERTK-dependent efferocytosis to thermogenic activation in brown and white adipose tissue, by using a mouse model lacking the expression of *Axl* and *Mertk* specifically in macrophages (*Csf1r-Cre*$^{+}$-*Axl*$^{f/f}$*Mertk*$^{f/f}$ mice). These mice showed lower thermogenic gene expression in iBAT and especially ingWAT when fed a high fat diet followed by repeated cold exposure. Moreover, under these conditions, mice lacking macrophage *Axl* and *Mertk* expression, exhibited lower signs of lipolytic activity in adipose tissues as shown by decreased levels of phosphorylated (active) hormone sensitive lipase and lower NE stimulated release of non-esterified fatty acids by BAT explants. Impairment in lipolysis was associated with reduced fasting plasma triglyceride and glucose levels, suggesting potential systemic metabolic consequences.

Consistent with the known role of efferocytosis in maintaining macrophage anti-inflammatory polarization, the observed reduction in thermogenic gene expression and lipolysis in *Csf1r-Cre*$^{+}$-*Axl*$^{f/f}$*Mertk*$^{f/f}$ mice were accompanied by increased inflammation in ingWAT. This included elevated levels of macrophage markers in adipose tissue, higher mRNA expression of pro-inflammatory cytokines such as TNFα and IL6, as well as the accumulation of Ly6C^{+} and iNOS^{+} inflammatory macrophages. Of note, TNFα has been shown to suppress adrenergic activation of adipose tissue, suggesting a potential mechanism by which *Axl/Mertk* deficiency in macrophages might impair adipose thermogenic and lipolytic function.

Altogether our findings identify a novel NE–AXL/MERTK axis that enhances macrophage efferocytic activity in response to adrenergic stimuli. Moreover, this effect appears to facilitate effective tissue thermogenic and lipolytic activation in adipose tissue, possibly by preventing excessive inflammation. These insights have important implications for the neuroendocrine regulation of immune function as well as for understanding adipose tissue health and disease.

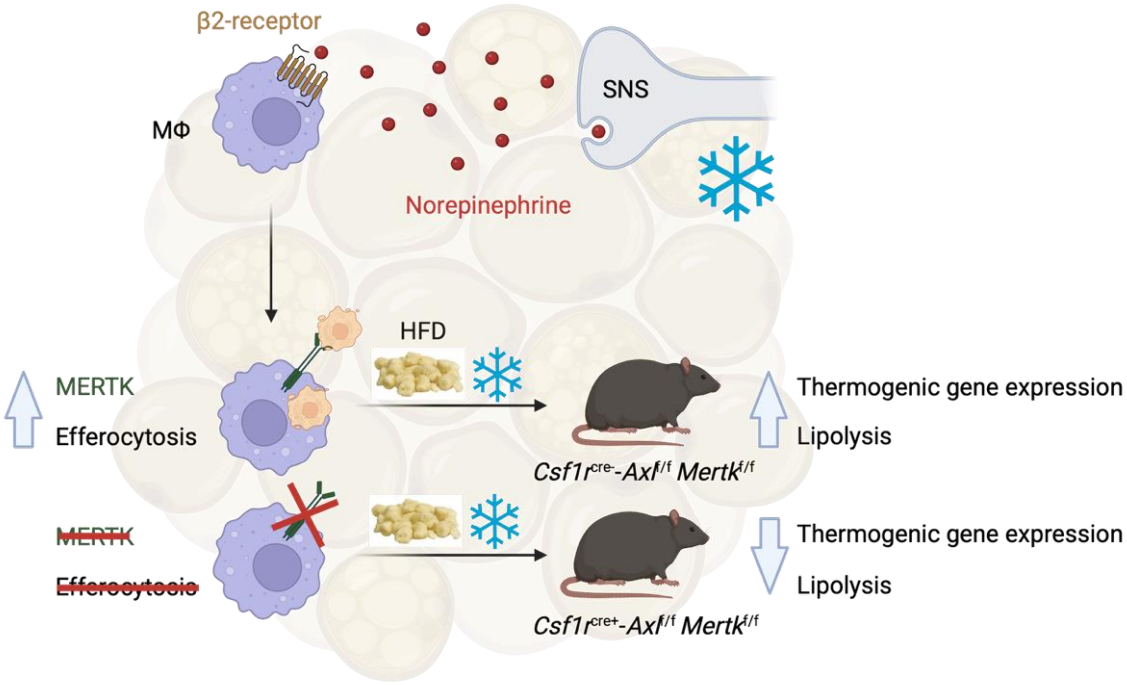

Figure 35: Graphical Abstract
SNS, sympathetic nervous system; MERTK, Mer-Tyrosine kinase; HFD, High fat diet; Csf1r, Colony-stimulating factor 1 receptor;

Zusammenfassung

Während kalter Temperaturen oder während eines Energiedefizits, leitet der menschliche Körper komplexe Anpassungsreaktionen ein, um seine thermische und energetische Homöostase aufrechtzuerhalten. Eine entscheidende Komponente dieser Reaktionen ist die Aktivierung des sympathischen Nervensystems, die zu einer lokalen Freisetzung von Norepinephrin (NE) im Fettgewebe führt. NE wiederum wirkt auf adrenerge Rezeptoren und stimuliert sowohl Thermogenese als auch Lipolyse in Adipozyten. Diese Prozesse sind besonders ausgeprägt im braunen Fettgewebe (BAT), das für seine thermogene Kapazität und seine Reaktionsfähigkeit auf Kältereize bekannt ist, und im subkutanen weißen Fettgewebe (WAT), welches einen thermogenen (beigen) Phänotyp annehmen kann.

Die Aktivierung des braunen und beigen Fettgewebes wird aktiv als therapeutische Strategie zur Behandlung von Fettleibigkeit und metabolischem Syndrom erforscht, da sie zur Steigerung des Energieverbrauchs und zur Verbesserung der Insulinempfindlichkeit beitragen kann. Eine anhaltende thermogene Aktivität erfordert dabei einen erheblichen strukturellen Umbau des Fettgewebes. Makrophagen spielen in solchen Umbauprozessen eine zentrale Rolle, indem sie durch Efferozytose - die Aufnahme und Beseitigung sterbender Zellen - einen spezialisierten

entzündungshemmenden und gewebeumgestaltenden Makrophagen-Phänotyp annehmen. Dabei hängt Efferozytose entscheidend von Rezeptoren wie AXL und MERTK ab.

Besonders Fettgewebsmakrophagen (ATMs) werden zunehmend als entscheidende Regulatoren der metabolischen Gesundheit und der Gewebeanpassung anerkannt. Eine gestörte Efferozytosefunktion in ATMs wird dabei mit Stoffwechselstörungen wie Typ-2-Diabetes in Verbindung gebracht. In dieser Studie nutzten wir Kälteexposition, um eine thermogene Aktivierung sowie einen Gewebeumbau im Fettgewebe zu induzieren. Dabei untersuchten wir die Rolle der Makrophagen-Efferozytose während dieses Prozesses.

Wir fanden heraus, dass F4/80^{+}CD11b^{+}-Makrophagen, die aus der interskapulären BAT (iBAT) und der inguinalen WAT (ingWAT) von kalt gehaltenen C57BL/6-Mäusen isoliert wurden, eine signifikant höhere Efferozytose-Kapazität aufwiesen als die Makrophagen von thermoneutral gehaltenen Kontrollen. Diese erhöhte Efferozytose war mit einem höheren Anteil von ATMs verbunden, die Efferozytose-Rezeptoren wie MERTK an ihrer Oberfläche exprimieren. Die stärksten Auswirkungen der Kälteexposition wurden in iBAT-Makrophagen beobachtet, die auch die höchsten absoluten Werte der Efferozytose aufwiesen. Dies unterstützt die Hypothese, dass das hohe Umbaupotenzial und die Resistenz gegen Entzündungen, die im BAT beobachtet werden, auf eine verstärkte lokale Efferozytose zurückzuführen sein könnten.

Interessanterweise konnte die kälteinduzierte Efferozytose-Reaktion sowie die erhöhte *Mertk*-Expression in Makrophagen aus dem Knochenmark (BMDMs) rekapituliert werden, wenn man diese mit β2-adrenergen Agonisten behandelt. Außerdem erhöhte eine NE-Injektion in Wildtyp-Mäusen, die bei Raumtemperatur gehalten wurden, die Efferozytose in CX3CR1^{+}Ly6C^{-} ATMs im iBAT signifikant.

Auswirkungen der β2-adrenergen Aktivierung auf die Immunfunktion von Makrophagen wurden bereits in vorigen Studien gezeigt, jedoch ist ein solch direkter Effekt auf die Makrophagen-Efferozytose noch nie zuvor berichtet worden. Bemerkenswert ist dabei, dass die β2-Stimulation in *Axl*/*Mertk*-defizienten BMDMs nicht dieselbe Efferozytose Antwort auslöste, was darauf hindeutet, dass diese Rezeptoren für die NE-induzierte Efferozytose wesentlich sind.

Als nächstes untersuchten wir den Beitrag der AXL/MERTK-abhängigen Efferozytose zur thermogenen Aktivierung des braunen und weißen Fettgewebes. Dazu wurde ein Mausmodell verwendet, bei dem die Expression von *Axl* und *Mertk* speziell in Makrophagen fehlt (*Csf1r*-Cre^{+}-*Axl*$^{f/f}$*Mertk*$^{f/f}$ Mäuse). Diese Mäuse zeigten eine geringere thermogene Genexpression im iBAT und insbesondere im ingWAT, wenn sie mit einer fettreichen Diät gefüttert wurden, gefolgt von wiederholter Kälteexposition. Darüber hinaus wiesen Mäuse, denen die *Axl*- und *Mertk*-Expression der Makrophagen fehlte, unter diesen Bedingungen deutlich geringere Anzeichen einer lipolytischen Aktivierung

im Fettgewebe *in vivo* auf, was sich in verminderten Spiegeln der phosphorylierten (aktiven) hormonsensitiven Lipase zeigte. Die beeinträchtigte Lipolyse in *Csf1r*-Cre^{+}-*Axl*$^{f/f}$*Mertk*$^{f/f}$ Mäusen wurde auch durch eine geringere NE induzierte Freisetzung nicht veresterter Fettsäuren aus BAT-Explantaten bestätigt. Die Beeinträchtigung der Lipolyse ging mit einer Verringerung der Triglycerid- und -Glukosespiegel im Blutplasma einher, was auf mögliche systemische metabolische Folgen hindeutet.

Im Einklang mit der bekannten Rolle der Efferozytose in der Aufrechterhaltung einer entzündungshemmenden Polarisierung in Makrophagen zeigten *Csf1r*-Cre^{+}-*Axl*$^{f/f}$*Mertk*$^{f/f}$ Mäuse erhöhte Entzündungszeichen im ingWAT. Diese Zeichen bestanden aus erhöhten Werte von Makrophagenmarkern im Fettgewebe, einer höheren Expression von pro-inflammatorischen Zytokinen wie TNFα und IL6 und aus einer Ansammlung von Ly6C^{+} und iNOS^{+} entzündlichen Makrophagen. Entzündungszytokine, insbesondere TNFα, unterdrücken nachweislich die adrenerge Aktivierung des Fettgewebes, was auf einen möglichen Mechanismus hindeutet, durch den ein *Axl/Mertk*-Mangel in Makrophagen möglicherweise die thermogene und lipolytische Funktion des Fettgewebes beeinträchtigen kann.

Insgesamt weisen unsere Ergebnisse auf eine neuartige NE-AXL/MERTK-Achse hin, welche die Efferozytenaktivität von Makrophagen als Reaktion auf adrenerge Reize steigert. Darüber hinaus scheint dieser Effekte die thermogene und lipolytische Aktivierung im Fettgewebe zu unterstützen, möglicherweise durch die Hemmung überschießender Entzündungsreaktionen. Diese Erkenntnisse haben Implikationen für die neuroendokrine Kontrolle von Immunfunktionen und dessen Einfluss auf die Gesundheit und Funktionalität des Fettgewebes.

Abbreviations

ABCA1	adenine triphosphate-binding cassette transporter A1
ACC	acetyl-CoA carboxylase
ACLY	adenine triphosphate Citrate Lyase
ANOVA	analysis of variance
Apo	apolipoprotein
ATGL	adipose triglyceride lipase
ATMs	adipose tissue macrophages
ATP	adenine triphosphate
BAT	brown adipose tissue
BMDMs	bone marrow–derived macrophages
BSA	bovine serum albumin
cAMP	cyclic adenosine monophosphate
CD36	cluster of differentiation 36
ChREBP	carbohydrate response element-binding protein
CREB	cyclic adenosine monophosphate response element-binding protein
DAGs	diacylglycerols
Dio2	deiodinase type 2
DMEM	Dulbecco's Modified Eagle Medium
DMSO	dimethylsulfoxid
DNL	de novo lipogenesis
ECP	extracorporeal photopheresis
ER	endoplasmic reticulum
FASN	fatty acid synthase
FFAs	free fatty acids
gWAT	gonadal WAT
h	hours
HFD	high-fat diet
HSL	hormone-sensitive lipase
iBAT	interscapular brown adipose tissue
IL1β	interleukin-1β
IL6	interleukin-6
ingWAT	inguinal WAT
iWAT	subcutaneous white adipose tissue in mice
LAM	lipid-associated macrophage
MAGs	monoacylglycerols
min	minutes
NE	norepinephrine
NEFAs	non-esterified fatty acids
NST	non-shivering thermogenesis
OXPHOS	oxidative phosphorylation
pHSL	phosphorylated hormone-sensitive lipase
PKA	protein kinase A
PPAR	peroxisome proliferator-activated receptor
RPMI	Roswell Park Memorial Institute
RT	room temperature
SNS	sympathetic nervous system

SVF	stromal vascular fraction
TAG/TAGs	triacylglycerol/triglycerides
T3	triiodothyronine
TH	tyrosine hydroxylase
TN	thermoneutrality
TNF-α	tumor necrosis factor-alpha
UCP1	uncoupling protein 1
VEGF	vascular endothelial growth factor
WAT	white adipose tissue

List of figures

List of tables

SPublications, presentations and abstracts at national and international congresses

Publications

1. Liebold I, **Meyer S**, Heine M, Kuhl A, Witt J, Eissing L, Fischer AW, Koop AC, Kluwe J, Wiesch JSZ, Wehmeyer M, Knippschild U, Scheja L, Heeren J, Bosurgi L, Worthmann A. TREM2 Regulates the Removal of Apoptotic Cells and Inflammatory Processes during the Progression of NAFLD. Cells. 2023 Jan 17;12(3):341. doi: 10.3390/cells12030341. PMID: 36766683; PMCID: PMC9913311.

2. Stephany Leyk, Imke Liebold, Clarissa Lanzloth, Ulrike Richardt, Johan M. Kux, Christoph Kilian, Manuela Moritz, Antonia Gocke, **Simon Meyer**, Katharina Höhn, Barbara Honecker, Helmut Hass, Marius Böttcher, Sören Weidemann, Simon Kind, Hartmut Schlüter, Nahla Galal Metwally, Lorenz Adlung, Pablo J. Sáez, Thomas Jacobs, Klaus Ruckdeschel, Lidia Bosurgi. Extraceccular versicle properties and functions defined by the originatings cell´s fitness status. Journal of Extraceullular biology. (**Submitted**)

Manuscripts in preparation

1. **Meyer S**, Liebold I, Witt J, Adlung L, Bosurgi L, Worthmann A. A norepinephrine-MERTK axis stimulates efferocytosis in adipose tissue macrophages.

Presentations at national and international congresses

1. **2021**, 44th European Lipoprotein Club (ELC), Tutzing, Germany

   -"TREM2-dependent internalization of lipoprotein particles in brown adipose tissuse macrophages in response to cold exposure" (Short talk)

Posters at national and international congresses

1. **2023**, 45th European Lipoprotein Club (ELC), Tutzing, Germany
   -"*Brown adipose tissue activation induces an efferocytic phenotype in local macrophages"*

2. **2023**, 1st BATenergy Conference, Hamburg, Germany
   -" Norepinephrine increases efferocytic capacity of macrophages in a direct manner*"*

3. **2025**, 2nd BATenergy Conference, Bonn, Germany
   -"A norepinephrine-MERTK axis stimulates efferocytosis in adipose tissue macrophages."

Journal permissions

For the composition of the current thesis, texts, parts and figures where reused, adapted or changed from my following first-author publications.

Meyer S, Liebold I, Witt J, Adlung L, Bosurgi L, Worthmann A. A norepinephrine-MERTK axis stimulates efferocytosis in adipose tissue macrophages. (**In preparation**)

Author's Contribution Statement

All experiments or analysis presented in this thesis were made by the author (**Simon Meyer**) unless explicitly stated otherwise. To reiterate in order of appearance:

1. The experiments underlying results presented in **Figure 12** and **Figure 20** and **Figure 31** were caried out by the author, including planning, mice handling and cell isolation. Cell staining, FACS analysis and data analysis were carried out by **Dr. Imke Liebold**.

2. The experiments underlying results presented in **Figure 13** were conducted by **Jenniffer Witt** with help of the author. The Gene expression analysis on the obtained $Cd11b^+$ cell fraction was carried out by the author.

3. The experiments and sample preparation steps underlying the RNA sequencing results presented in **Figure 15** were conducted by the author while data preparation was carried out by **Dr. Lorenz Adlung**. Further analysis was carried out by the author.

4. The experiments underlying results presented in **Figure 16** were conducted by the author while the readout of cytokine concentrations in the media (LEGENDplex™) was done by **Dr. Stephany Leyk**.

Acknowledgements

I extend my deepest gratitude to **Dr. Anna Worthmann** and **Dr. Lidia Bosurgi** for their outstanding supervision, trust, guidance, and unwavering patience. Their professional and personal excellence made this journey not only more pleasant but also far more successful.

I am also profoundly grateful to **Prof. Dr. Jörg Heeren** for warmly welcoming me into his lab and for kindly serving as the chair of my PhD thesis committee. His expertise and the supportive work culture he fosters are truly inspiring to all who have had the privilege of working with him. My sincere thanks also go to **Prof. Dr. Nicola Gagliani** and **Prof. Dr. Hartmut Schlüter** for serving as evaluators of this thesis.

I would like to express my heartfelt thanks to **Dr. Imke Liebold**, **Jenniffer Witt**, **Dr. Stephany Leyk**, and **Dr. Lorenz Adlung** for their invaluable assistance with data collection and analysis. Your support was instrumental, and it was a pleasure to work alongside you.
Special thanks to **Dr. Anke Baranowski** for her help with the β2-deficient mice experiments.

I am also grateful to the members of AG Worthmann, particularly **Laura Ehlen** and **Johanna Hiefner**, and to both past and present members of AG Heeren: **Janina Behrens**, **Jennifer Brieger**, **Sandra Ehret**, **Dr. Sebastian Graute**, **Karthik Gunasekaran, Dr. Markus Heine**, **Birgit Henkel**, **Dr. Kim Hurkmans**, **Dr. Michelle Jäckstein**, **David McGrath**, **Sabrina Pilz**, **Vivian Rutchek**, **Dr. Ludger Sheja**, **Peter Stenzel**, **Martin Vargek**. This thesis is the result of a truly collaborative effort, and I deeply appreciate the many hours you dedicated to supporting my experiments and the countless insightful discussions we shared. Most of all, I truly enjoyed working with you. I would also like to thank **Laura Mitsching**, the always helpful secretary of the IBMZ, for her invaluable support behind the scenes.

Finally, I want to thank my **family** and **friends** for their constant encouragement and for providing a welcome distraction from academia when I needed it — which was more often than I'd like to admit.

Most importantly, my heartfelt thanks go to **Judith Dehn**. Thank you for standing by me through long days, late nights, and moments of doubt and frustration. Especially in the final days before submission, you proved that I could not wish for a more supportive partner. Your love and belief in me made this possible.

Eidesstattliche Versicherung

Ich versichere ausdrücklich, dass ich die Arbeit selbständig und ohne fremde Hilfe, insbesondere ohne entgeltliche Hilfe von Vermittlungs- und Beratungsdiensten, verfasst, andere als die von mir angegebenen Quellen und Hilfsmittel nicht benutzt und die aus den benutzten Werken wörtlich oder inhaltlich entnommenen Stellen einzeln nach Ausgabe (Auflage und Jahr des Erscheinens), Band und Seite des benutzten Werkes kenntlich gemacht habe. Das gilt insbesondere auch für alle Informationen aus Internetquellen.

Soweit beim Verfassen der Dissertation KI-basierte Tools („Chatbots“) verwendet wurden, versichere ich ausdrücklich, den daraus generierten Anteil deutlich kenntlich gemacht zu haben. Die „Stellungnahme des Präsidiums der Deutschen Forschungsgemeinschaft (DFG) zum Einfluss generativer Modelle für die Text- und Bilderstellung auf die Wissenschaften und das Förderhandeln der DFG“ aus September 2023 wurde dabei beachtet.

Ferner versichere ich, dass ich die Dissertation bisher nicht einem Fachvertreter an einer anderen Hochschule zur Überprüfung vorgelegt oder mich anderweitig um Zulassung zur Promotion beworben habe.

Ich erkläre mich damit einverstanden, dass meine Dissertation vom Dekanat der Medizinischen Fakultät mit einer gängigen Software zur Erkennung von Plagiaten überprüft werden kann.

Datum: 30.06.2025 Unterschrift